Conformational changes in ezrin analyzed by Förster resonance energy transfer

Dissertation

am Fachbereich Biologie der Universität Münster

Victoria Shabardina

2015

Biologie

Conformational changes in ezrin analyzed by Förster resonance energy transfer

Inaugural-Dissertation

zur Erlangung des Doktorgrades

der Naturwissenschaften im Fachbereich Biologie

der Mathematisch-Naturwissenschaftlichen Fakultät

der Westfälischen Wilhelms-Universität Münster

vorgelegt von

Victoria Shabardina

Aus Kirov

2015

Dekan:	**Prof. Dr. Wolf-Michael Weber**
Erster Gutachter:	**Prof. Dr. Volker Gerke**
Zweiter Gutachter:	**Prof. Dr. Martin Bähler**
Tag der mündlichen Prüfung:	**8.12.2015**
Tag der Promotion:	**18.12.2015**

Contents

Summary

Ezrin, a member of the ERM (Ezrin-Radixin-Moesin) protein family, serves as a linker between cell membrane and cytoskeleton in the cells of all protozoans. Thereby, it is involved in cell motility, cell division, cell-cell adhesion and the maintainance of cell polarity. Ezrin comprises two functionally important domains, the N-ERMAD (N-terminal ERM association domain) that contains binding sites for the membrane lipid PIP_2 (phosphatidylinositol-4,5-bisphosphate) and several membrane proteins and the C-ERMAD (C-terminal ERM association domain) that contains an actin binding site (ABS). In resting cells ezrin exists in a so-called dormant state, where most of its binding sites, including the ABS, are masked by an autoinhibitory association between N-ERMAD and C-ERMAD. Cell stimulation can lead to an activation of ezrin's membrane-actin crosslinking function. This is achieved by a disruption of the N-ERMAD/C-ERMAD association and the unmasking of the membrane protein and F-actin binding sites. Ezrin activation is thought to be triggered by interaction with PIP_2 and phosphorylation of a conservative threonine at position 567 in the C-ERMAD, but the contribution of the each activation factor is not fully understood yet. In this study we probed ezrin's conformational state by FRET (Förster resonance energy transfer) and showed that disruption of the N-ERMAD/C-ERMAD association occurs through a combination of the action of both activating factors.

FRET on solid supported lipid bilayers (SSLB) was used here for the first time to detect conformational changes in ezrin upon its activation. Ezrin fluorescent constructs containing a C-terminal eGFP tag and an N-terminally crosslinked Cy3 dye were generated and employed in FRET experiments following binding to SSLB. The SSLB contained either PIP_2 or DOGS-Ni-NTA which allowed an interaction with a His tag present in all constructs. In addition to wild type ezrin, a Cy3-ezrinT567D-eGFP construct, mimicking ezrin's phosphorylated state, was employed in the FRET experiments. Both double-labeled constructs, the wild type and phosphomimicking mutant, were shown to produce FRET signals when bound to DOGS-Ni-NTA-containing SSLB indicating a close proximity of Cy3 and the eGFP tag in the dormant conformation of ezrin. Upon binding to PIP_2-containing SSLB, the efficiency of FRET decreased, suggesting that the Cy3 and eGFP had moved apart most likely due to a disruption of the N-C association in the protein. The strongest FRET efficiency drop was observed for the phosphomimicking ezrin construct Cy3-ezrinT567D-eGFP bound to PIP_2-containing SSLB. These findings demonstrate that, although PIP_2-binding alone appears to induce some change in the ezrin conformation, phosphorylation at threonine 567 is necessary for a complete disruption of the N-ERMAD–C-ERMAD association. Together, these findings are in line with a two-step ezrin activation model that requires 1) PIP_2 binding to unmask threonine 567 and 2) subsequent threonine 567 phosphorylation.

1 Introduction

1.1 The ERM protein family

Ezrin is a member of the ERM (Ezrin, Radixin, Moesin) protein group which belong to the band 4.1 protein superfamily. The first protein discovered in this superfamily was isolated from erythrocytes membrane and named protein 4.1, referring to the relative mobility of the protein band resulting from SDS-PAGE (sodium dodecyl sulfate polyacrylamide gel electrophoresis) separation (Yu, Fischman, and Steck 1973). It was shown to provide mechanical stability to the membrane. Later, other related proteins were identified, constituting a larger superfamily of 5 gene families, including tyrosine phosphatase PTPH1, the tumor suppressor merlin, ezrin, radixin, moesin – cytoskeleton-cell membrane linker proteins, and others. Despite their functional diversity band 4.1 superfamily members share a common feature, the conserved FERM-domain (4.1 ERM domain) that provides binding to membrane proteins and the phospholipid PIP_2, suggesting that all superfamily members perform their functions in association with the membrane (K Takeuchi et al. 1994). The FERM-domain of ezrin, radixin and moesin has binding activity also towards their own C-terminal region. This interaction causes an auto-inhibited conformational state, preventing the ERMs from binding to their interaction partners.

Ezrin (less known as cytovillin or p81) was the first protein identified with homology to the 4.1 protein, it's FERM domain has 30% sequence similarity with the FERM domain of 4.1 protein (Conboy et al. 1986; Gould et al. 1989). Ezrin was found in intestinal epithelial cells as a major protein of microvilli of the intestinal brush border (A Bretscher 1983; Pakkanen et al. 1987). Later radixin was discovered in adherens junctions isolated from rat liver cells, moesin was first isolated from bovine uteri and characterized as a heparin-binding protein (W. Lankes, Griesmacher, Grünwald, Schwartz-Albiez, & Keller, 1988; Tsukita & Hieda, 1989).

1.2 ERM proteins and their conservative features

ERM proteins are present in all sequenced metazoans, but are not found in unicellular organisms, such as yeasts. This implies that ERM evolved in animal cells for maintaining multi-cellularity and regulating cell-cell interaction. Invertebrates express only one isoform, vertebrates have three: ezrin, radixin, moesin. These three proteins are 75% homologous in the whole sequence with 85% homology in the FERM domain (Funayama et al. 1991; W. T. Lankes and Furthmayr 1991). Furthermore, comparisons of ERM sequence among vertebrates and invertebrates yield striking results: the ERM homologues in *Drosophila melanogaster* (Dmoesin) and *Caenorhabditis elegans* (ERM-1) share 76% sequence

homology with human ezrin (Monique Arpin et al. 2011) and are thought to be evolutionary progenitors of the human ERM (Van Fürden et al. 2004). In general, ERM proteins branched from a common ancestor protein for the whole 4.1 superfamily late in evolutionary history of the band 4.1 group (see Fig.1) (K Takeuchi et al. 1994). Ezrin, radixin and moesin emerged by gene duplication (Verena Niggli and Rossy 2008); their genes are located on chromosomes 6, 11 and 10, respectively. The three isoforms are found in most tissues, although ezrin is preferably expressed in epithelial cells, moesin in endothelial cells and leucocytes, and radixin shows high expression levels in liver. At the same time the localization in near-membrane regions rich in associated actin (i.e. microvilli, ruffling membranes, adhesion sites, cleavage furrow) is characteristic for all three proteins (Sato et al. 1992). The main function of ERM proteins is serving as membrane-cytoskeleton linkages: the N-terminal ERM association domain (N-ERMAD), which corresponds to the FERM domain, can interact with several membrane proteins, while the C-terminal ERM association domain (C-ERMAD) carries an actin binding site (Algrain, Turunen, Vaheri, Louvard, & Arpin, 1993; M Arpin, Algrain, & Louvard, 1994; Yao, Cheng, Forte, & Cell, 1996). In the autoinhibited or dormant form of ezrin its N-ERMAD and C-ERMAD are bound to each other, masking most of the other proteins binding sites (Pearson et al. 2000). The transition to the activated or open conformation, according to the most prevalent of existing hypotheses, is facilitated by an interaction with membrane PIP_2 via a PIP_2-binding site in the N-ERMAD and phosphorylation of a C-terminal threonine (Nakamura et al. 1999). The phenomenon of ezrin activation is central in this work and will be discussed in details further.

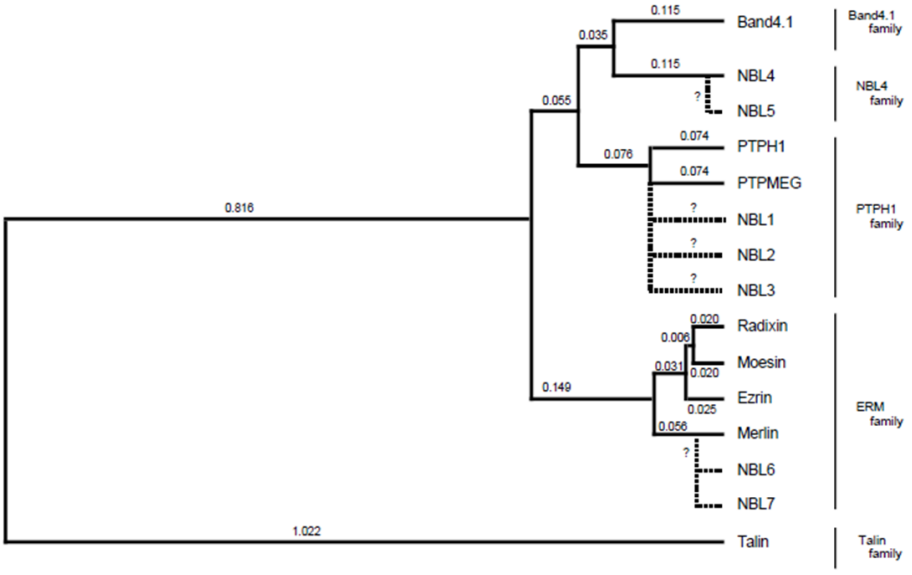

Fig. 1. Band 4.1 superfamily phylogenetic tree according to (K Takeuchi et al. 1994)**.**

Although ERM have some differences in expression pattern, they are considered as redundant proteins (Anthony Bretscher, Edwards, and Fehon 2002; Fiévet, Louvard, and Arpin 2007). This feature is most likely the precaution of nature against the loss of viable cell functions. Thus, in experiments with retinal pigment epithelium cells only the combination of antisense RNA for ezrin, radixin and moesin resulted in a pronounced inhibition of cells' adhesion and microvilli formation, whereas knock-out of only one of the proteins showed mild changes in the cells' normal behavior (Kosei Takeuchi et al. 1994). Similarly, knock-out experiments in mice showed a strong effect only in those tissues where only one particular isoform was expressed. For example, radixin is solely expressed in stereoscilia of hair cells in the cochlea (the part of the inner ear), correspondingly, radixin knockdown mice exhibited hearing loss. Interestingly, the vestibular stereoscilia did not reveal any distortion, apparently because of the small amount of ezrin which is also expressed in vestibular ear part (Kitajiri et al. 2004). Unlike ezrin and moesin, radixin interacts with α5 subunit of $GABA_A$ receptor, therefore, the lack of radixin, in particular, affects $GABA_A$ clustering in mice hippocampus (Loebrich et al. 2006). Radixin is a dominant ERM protein in hepatocytes, it organizes MRP2 (multidrug resistant protein 2) in the bile canalicular membrane and attenuation of radixin results in disturbance of bilirubin secretion in bile (Kikuchi et al. 2002).

Knock-out of ezrin in mice results in a disarrangement of the brush border structure, disrupted microvilli formation and a disarrayed configuration of adhesion complexes in intestinal epithelium. Such mice die in neonatal age when they switch to the adult diet (Saotome, Curto, and McClatchey 2004). Gastric epithelial (parietal) cells provide acid secretion into the stomach, and ezrin mediates the fusion of HCl-containing vesicles with the apical part of the cells. In the parietal cells of ezrin deficient mice these vesicles accumulate in the cytoplasm, which causes achlorhydria disease (Tamura et al. 2005). Furthermore, retinal pigment epithelium cells deficient in ezrin show a reduction in microvilli formation that causes defects in photoreceptors (Vera L Bonilha et al. 2006). The specificity of ezrin among other ERM was shown by the identification of the phosphorylation sites, not present in radixin or moesin, such as Y145 phosphorylated by Src kinase in proliferating epithelial cells and by Lck kinase in T lymphocytes (Autero et al. 2003; Srivastava et al. 2005).

Moesin knock-out mice showed a normal phenotype, although it is the most distinct in sequence protein among ERMs, also differing in some phosphorylation sites (Doi et al. 1999) and minor structural features. For example, it reveals stability against calpain in stimulated lymphocytes unlikely ezrin and radixin (Shcherbina et al. 1999).

The knock-out studies underscore the role of ezrin as a founder of the group playing a crucial role in the normal function of several animal cells types and tissues, as the most

profound effect are seen in ezrin knock-out mice, while radixin and moesin mostly play redundant roles. Therefore studying ezrin can help to elucidate the functional and structural features of the whole ERM group.

1.3 Ezrin is involved in cell cortex organization and signaling cascades

Multiple studies of ERM activities in the cells have provided contradictory data. For example, in moving T lymphocytes ERM accumulate at the rear end of the cell to mediate the retraction process, but in T lymphoma cells phosphorylated form of ERM together with ICAM-2 participate in uropod expanding (Charrin & Alcover, 2006; Lee et al., 2004; Helander et al., 1996). More precise analysis of different data suggests that the functions and regulation of ERM depends on the cell type (Verena Niggli and Rossy 2008) and particular developmental stages. This, probably, can be explained by various regulatory factors such as interactions between ezrin, radixin, moesin and their binding partners and particular signaling ways in different cell types. ERM proteins interact with the number of proteins in the cell; in most cases these interactions are mediated via the FERM domain – either directly or through intermediate proteins (EBP50, PDZK1). Most FERM domain binding partners can be classified as transmembrane proteins (CD43/44, ICAM1/2) and cytosolic signalling molecules (phosphatidylinositol 3-kinase, Rho-specific guanine nucleotide dissociation Inhibitor GDI) (Anthony Bretscher et al., 2002; Ivetic & Ridley, 2004; Loebrich et al., 2006). The high number of the diverse binding partners suggests that ezrin and other ERM can be bound to more than one protein at a time, indicating its involvement in complex scaffolding and signalling processes. Anyway, all the processes in which ERM participate are centered at the cell membrane and related to the regulation of morphology and mechanical properties of it. The key processes include arrangement of apical membranes of epithelia, such as microvilli assembly and stereocilia formation, participation in parietal cells secretion, contribution to immunological synapse function, leucocyte rolling and migration of cancer cells, cell division and polarity, junction assembly and Rho GTPase signaling.

An experiment demonstrating the importance of ezrin in the cell cortex was performed on rat fibroblasts transformed with v-fos. Ezrin overexpression and phosphorylation in such cells led to pseudopodia formation. Use of micro-scale chromophore-assisted laser inactivation (micro-CALI) allowed functional destruction of ezrin precisely in pseudopodia and resulted in a complete decomposition of the formations (Lamb et al. 1997). Ezrin is responsible for microvilli arrangement in most epithelia (Berryman, Franck, and Bretscher 1993) and elimination of ezrin leads to disturbance of microvilli formation and, consequently, brush borders, the common structure of the apical domain of epithelial cells (A Bretscher, 1983; Bonilha et al., 2006; Saotome et al., 2004). The dependance of microvilli formation on ezrin was confirmed in a study of apoptotic events in the cells during which microvilli normally disassemble: during this restructurization ezrin and also other ERM

proteins were shown to change their membrane localization and undergo dephosphorylation in the cytoplasm – the likely reason of microvilli disassembly (J. Chen, Cohn, and Mandel 1995). A recent publication demonstrated that repeated cycles of ezrin phosphorylation by LOK (lymphocyte oriented kinase) and SLK (STE20-like kinase) allowed microvilli in the brush border acting as dynamic, self reorganizing structures (Viswanatha et al. 2012). Ezrin, noted to act together with its binding partner NHERF1, was claimed to be a key element to regulate and modify the complex system of apical microvilli (Garbett and Bretscher 2012). In ezrin -/- intestinal epithelial cells not only the microvilli were short and irregular, altogether the cortical web structure was documented to be thicker and deformed, as compared to wild type cells, suggesting that ezrin is enlolved in structuring the underlying actin apical terminal web, from where microvilli emerge (Saotome, Curto, and McClatchey 2004). A specific form of epithelial microvilli is found in the retinal pigment epithelium, which expresses only ezrin, but not other ERM. Its highly specialized cells have very long microvilli which supply photoreceptors with nutrients (Bok 1993). The knock-down of ezrin in this cell line leads to a great decrease in the number and length of microvilli; ezrin disregulation in these cells has been suggested as a reason of retinal degenerations (Kivelä et al. 2000). Moreover, moesin and radixin overexpression experiments fail to compensate for the lack of ezrin in retinal pigment epitelium (Vera Lúcia Bonilha, Finnemann, and Rodriguez-Boulan 1999). This phenomenon of selective usage of a particular ERM protein in some cells' types implies the mechanisms that orchestrate the circulation of ERM proteins remain ambiguous.

As a linker between membrane and cytoskeleton, ezrin is an important member in the complexes of cell-cell adhesion and cell-surface contact. In MTD-1A cells, attenuation of ERM expression caused abnormality in the formation of these complexes (K Takeuchi et al. 1994). In particular, knock-down of all ERM together caused cells to deattach from the plate; single protein knock-down showed that cells continue to grow normally but failed to reattach after trypsinizationg in case of ezrin or radixin, but not moesin knock-down. In mamalian epithelial cells overexpressing the T567D mutant of ezrin, mimicking the protein active form, led to inability of cysts formation in a collagen matrix, which was caused by disrupting and preventing the formation of cell-cell junctions (Monique Arpin et al. 2011). Stimulation of epithelial cells with HGF (hepathocyte growth factor) similarly led to dissociation of cell-cell junctions following phosphorylation of tyrosine 477 in ezrin and to relocalization of ezrin to the front membrane of migrating cells (Naba et al. 2008). Processes involved in establishing cell contacts depend on activation-deactivation cycles of Rho and Rac GTPases (D'Angelo et al., 2007, Hatzoglou et al., 2007). ERM can be found as participants in GTPase cascades, for example, in A431 EGF-stimulated cells, ezrin interacts with PLEKHG6 (Rho guanine nucleotide exchange factor) that activates RhoG and the RhoG effector ELMA, showing the ezrin ability to regulate upstream and downstream effectors in Rho-cascades (D'Angelo et al., 2007; Ivetic & Ridley, 2004).

Ezrin participates in assocition of T cells and antigen presenting cells (APC) during immune responce: after activation of T cell receptor (TCR) ezrin accumulates together with CD43 at the perifery of the immunological synapse (IS), facilitating contact between the two cells; the relocation of ezrin to the perifery coincides with actin polimerization at the distal parts of the IS (Cullinan, Sperling, and Burkhardt 2002; Roumier et al. 2001). The relocation of ezrin requires its dephosphorylation-rephosphorylation which might be ensured via some Rho-GTPase regulation. The reported interaction of ezrin with Rho-GDI at the IS supports this hypothesis (Delon, Kaibuchi, and Germain 2001). At the IS perifery ezrin recruits the TCR to the T cell-APC contact area arranging the clustering of the receptors that is required for the maturation of immunological synapses (Grakoui et al. 1999).

The role of ezrin during leucocytes rolling is linked to microvilli formation which ensures thethering of leucocytes to blood vessels endothelium. The process requires interaction of PSGL-1 (P-selectin glycoprotein ligand-1) on leucocyte membrane with P-selectin on the membrane of endotelial cells and is mediated by binding of ERM to PSGL-1. Disruption of ezrin/PSGL-1 complex results in unstable microvilli in leucocytes (Spertini, Baïsse, and Spertini 2012). Microvilli retraction allows cell rolling and ezrin phosphorylation-dephosphorylation cycles are required for this event (Ivetic and Ridley 2004). The regulation of ezrin phosphorylation in this process is thought to be conducted by Rho-kinases (Oshiro, Fukata, and Kaibuchi 1998).

Ezrin also performs an important role in dividing cells. In mammalian colonic epithelial cells (Caco2), grown in matrigel, ezrin undergoes spacial redistribution during the mitotic cycle (Hebert et al. 2012). From equal cortical distribution in G1-phase, in S-phase ezrin changes to uni-polar distribution arranging one of the centrosome, thereby setting the spindle orientation; in telophase ezrin concentrates in the cleavage furrow (Hebert et al. 2012). In eight-cell mouse embryos ezrin relocates from junctions to epical parts of the cells, which on one hand allows them to divide and form the developing embryo and also to establish mitotic spindle orientation (Louvet et al. 1996). Similar observations of ezrin relocation were made during development of the outer layer in mouse blastocysts (Louvet et al. 1996). ERM-1 also undergoes a redistribution from junctions to apical parts of the cells during initial tissue differentiation in C.elegance embryo (Van Fürden et al. 2004). This function in polarity establishment was also observed during formation of lumina in intestines, in particular, during arranging of the apical junctions. Apical junctions ensure normal development of lumina by coordinating the cells division. In ezrin deficient intestinal cells the lumina was deformed and the apical junctions had abnormal elongated shape (Saotome, Curto, and McClatchey 2004).

The previous examples demonstrate that ERM proteins and ezrin, in particular, are major components in cell adhesion and mobility, also being involved in Rho-cascades. These

features obviuosly makes them important participants in cancer cells migration. Ezrin distribution in the cell can be characteristic for some type of cancers. Thus, in breast cancer metastases ezrin favours the cytoplasmic localization or accumulates at membrane in non-polarized way, whilst in normal breast epithelium and in non-malignant breast tumor ezrin localization is apical (Monique Arpin et al. 2011). These data are in agreement with a recent study (Hoskin et al., 2015), which suggested that ezrin has more influence on metastatic development rather than on primary breast cancer, mostly by regulating focal adhesions and invadopodia dynamics in processes controlled by Rho GTPases. It was also shown that ezrin is involved in metastasis formation in osteosarcoma and its knock-down in osteosarcoma cell lines leads to reduced cell growth (Lo Vasco et al. 2013); ezrin silencing in mice with osteosarcoma decreased its dissemination (Khanna et al. 2004). The possible regulatory mechanism can involve phosphoinositide-specific phospholipase PI-PLC, wich regulates the concentration of PIP_2, an ERM activator, and is colocolized with ezrin in osteosacroma cell line (Lo Vasco et al. 2013). In EGF stimulated HeLa cells ezrin was shown to increase cells invasion properties, probably due to activation of PI3-kinase and SK2 (sphingosine kinase) via MAPK-pathway (Adada et al. 2015). Although, the mechanisms of ezrin participation in cancer progression revealed up to date are dependent on the cancer type in animal models and the way of stimulation in cell lines, the fact that the cancerogenic function of ezrin is based on remodelling of cell membrane morphology and requires the active state of the protein is commonly accepted.

1.4 Dormant and activated states of ezrin

In the cell ezrin undergoes a switch between the active and dormant state. The dormant state is charachterized by an autoinhibitory interaction between N-ERMAD and C-ERMAD (Gary and Bretscher 1995) that can be disrupted by interaction of ezrin with membrane PIP_2 (phosphatydilinositol 4,5-bisphosphate) and phosphorylation of the conserved threonine 567 (Verena Niggli and Rossy 2008). In radixin and moesin, these are threonine 564 and threonine 558, respectively (Matsui et al. 1998). The sequences around these threonines are preserved to such extent that phosphorylated threonine can be recognized in all three ERM proteins by the same antibodies generated against only one phosphorylated ERM protein (Matsui et al. 1998).

Although both, PIP_2-binding and threonine phosphorylation, are aknowledged as factors modulating ezrin behaviour in the cell, different models on ezrin activation excist: 1) only PIP_2 binding at the cell membrane is crucial during the process (Shigenobu Yonemura et al. 2002), 2) phosphorylation of C-terminal threonine is the key event during activation (Matsui et al. 1998; Simons et al. 1998), 3) initial PIP_2 binding, then stabilizing threonine 567 phosphorylation are required for full activation (Hughes & Fehon, 2007; Niggli & Rossy, 2008). To elucidate the question, researchers use different well established means, such as,

mutants analysis, binding to artificial lipid structures decorated with PIP_2 lipids, binding assays using interaction partners. Mutants analysis includes binding sites deletions or their modifications, as well as mutants at the C-terminal threonine: phosphomimicking mutants, ezrin T567D or T567E that imitates partly activated protein due to introducing by aspartic acid or glutamic acid as negative charge similar to the phosphate group; un-phosphorylable mutant ezrin T567A that cannot be modified by kinases in the cells and is concidered as constituitively inactive form.

As phosphatidylinositol-4,5-bisphosphate and specific phosphorylation have a critical effect on ezrin function, it is useful, firstly, to review the role of these two factor in general in the cell.

1.4.1 Role of PIP_2 in the cell

Phosphotidylinositol 4,5-bisphosphate PIP_2 is well known as important bioregulator in the cell. Its cleavage results in release of phosphotidylinositol, IP_3, which increases Ca^{2+} concentration in the cell, and diacylglycerol DAG, which regulates phospholipase C activity. PIP_2 is incorporated in the plasma membrane of the cell and comprises 1% of all phospholipids (Gillooly and Stenmark 2001) and 99% of those with two phosphate groups (Vanhaesebroeck et al. 2001). PIP_2 acts as the second messenger in many processes including membrane trafficking, enzyme activation, membrane-cytoskeleton connection, microvilli formation. The multitude and diversity of its functions can be explained by the existance of the different PIP_2 pools in the membrane (Martin 2001; Simonsen et al. 2001). It is not yet clear what regulates PIP_2 clustering, although some works showed that PIP_2 accumulates in cholesterol rafts (D. A. Brown and London 2000) and that MARKCS protein can sequester PIP_2 in the membrane using electrostatical forces and, therefore, does not perturb its interaction with other molecules, like PH domain of PLCδ (McLaughlin et al. 2002). The important role in PIP_2 sequestering was recently ascribed to Annexin A2 which was shown to induce PIP_2 clusters formation in Ca^{2+}-dependet manner, moreover the complex with S100A10 protein was suggested to increase the properties of Annexin A2 to organize the lipid rafts (Drucker et al. 2013). The distinctive physical feature of PIP_2 is its negative charge provided by the phosphate groups and, depending on pH and binding partners can be -3, -4 and -5. This feature of PIP_2 and other phospholipids makes the plasma membrane the most negatively charged comparment of the cell (its electric field equals to 10^5 V/cm) and enables electrostatic interactions with many proteins (Goldenberg and Steinberg 2010). For example, 37 proteins were identified within the Rho, Ras, Arf and Arb families of small GTPases that electrostatically interact with cell membrane PIP_2 (Shi et al. 2013). Another characteristic of PIP_2 is its big head group that allows protruding in the aqueous phase further than other phospholipids of the plasma membrane (Fig. 2).

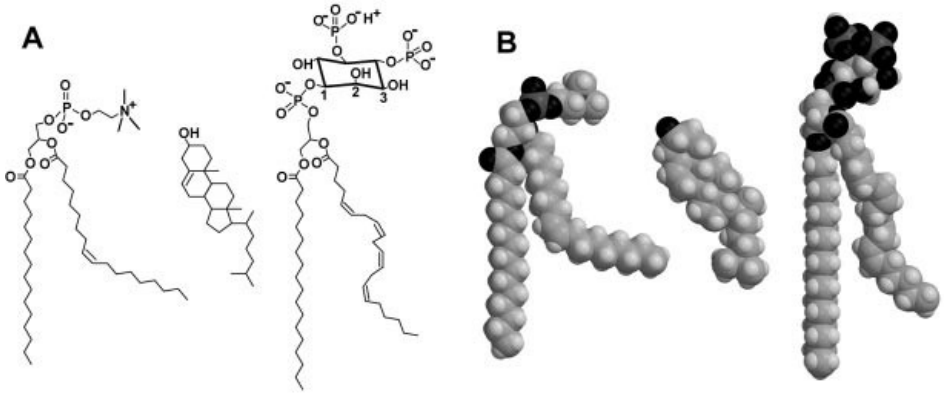

Fig. 2. Comparing schematical structures of POPC, cholesterol and PIP_2. A – chemical structures, B – molecular models. POPC (1-palmitoyl-2-oleoyl-3-phosphatidylcholine) is the most common phospholipid in the cells. Figure is taken from publication (McLaughlin et al. 2002).

There are several known protein domains that specifically bind PIP_2, among them the PH domain (PLC-δ), ENTH domain (CALM protein), FERM domain and the PX domain (NADPH oxidase, PI3-kinase). The presence of basic and/or aromatic amino acids is important for the binding to negatively-charged PIP_2, as well a conformational factor, providing a binding "pocket" with hydrogen-bonds (Prehoda et al. 2000).

The interactions with FERM domains of ERM proteins, as well as with α-actinin, spectrin, and vinculin (Czech 2000), indicated that PIP_2 is one of the essential regulators of cytoskeleton assembly during microvilli and membrane raft formation and cell adhesion. A charachteristic experiment employing laser tweezers showed that a change in PIP_2 concentration is a sensitive tool to adjust the strength of membrane/cytoskeleton interactions, i.e., higher PIP_2 concentration in the membrane corresponds to a higher adhesion energy of ezrin/actin interaction (Raucher et al. 2000). Similar findings were obtained by analysing with AFM technique MDCK cells injected with PIP_2 : the membrane tension increased by 50% after the injection. At the same time ezrin deficient cells with unchanged PIP_2 levels showed a 40% drop in the membrane rigidity, too (Braunger et al. 2014). Enrichemt of PIP_2 in membrane ruffles was detected in EGF stimulated HeLa cells and in NIH-3T3 fibroblasts (Honda et al. 1999; Tall et al. 2000). High concentrations of PIP_2 in the membrane can induce activation of PIP kinases, which are responsible for the synthesis of different phosphatidylinositols (Czech 2000). Up-regulation of phosphatidylinositol 4-phosphate 5-kinase, resulting in PIP_2 synthesis, recruited ezrin to the membrane in HeLa cells and mouse fibroblasts (Auvinen, Kivi, & Vaheri, 2007; Matsui, Yonemura, & Tsukita,

1999). In contrast, phospholipase C inactivated ezrin via decreasing PIP_2 levels in the membrane (Hao et al. 2009).

Not all PIP_2 binding domains have strong affinity to this phospholipid: sometimes the result of the interaction is only anchoring of multidomain proteins or protein complexes to the membrane and requires further membrane interaction for stabilization. For example, WASP proteins become active only when they bind to membrane PIP_2 and Cdc42 at the same time (F. Chen et al. 2000) and dynamin can stably bind to membrane only in all oligomeric form when its several PH domains bind several neighbouring PIP_2 molecules (Lemmon and Ferguson 2000). This aspect of different modes of PIP_2/proteins interaction is interesting in respect to this study, too, as the feature of PIP_2/ezrin binding is one of the phenomenons questioned here. In this regard it is important to recall that ezrin was shown to accumulate in membrane ruffles and microvilli, following the PIP_2 distribution (A Bretscher, 1983; A Bretscher, Reczek, & Berryman, 1997; Menager, Vassy, Doliger, Legrand, & Karniguian, 1999).

1.4.2 Protein phosphorylation as one of the main regulators of cell functioning

The attention to the importance of enzymatic phosphorylation of proteins in the cells arose in 1950s by Fischer and Krebs, who first demonstrated that enzyme activity can be regulated by reversible phosphorylation (FISCHER and KREBS 1955). The specific features of the phosphate group are dianionic nature (not inherent for any amino acids) and the ability of phosphoryl oxygens to form hydrogen bonds (Louise N Johnson 2009), therefore the addition of negatively charged phosphate group induces subsequent conformational changes in proteins. Tyrosine, threonine and serine are the most common phosphorylated amino acids; in different species in homologous proteins they can be substituted by negatively charged aspartic or glutamic acids. In modern research proteins with phosphorylated amino acids are commonly substituted with mutants bearing aspartic or glutamic acids instead of the original phosphorylatable residue.

The phenomenon of enzymatic phosphorylation had appeared early in the evolution of life and phosphorylation of specific residues is important for both eukaryotic and bacterial cells. For example, CheY, a bacterial chemotaxis protein, transits to the active conformation due to electrostatic repulsion caused by phosphorylation (L N Johnson and Barford 1993). Eukaryotic phosphorylation can lead to association of proteins, like in STAT (signal transducer and activator of transcription), but also to protein dissociations as in case of serine and threonine phosphorylation in the complex between pRb (retinoblastoma protein) and transcription factors E2F/DP1 (X. Chen et al. 1998; Rubin et al. 2005). Phosphorylation-dephosphorylation events modulate MARCKS membrane attachment/reattachment modes, together with PIP_2 that mediates correct protein targeting to the membrane (Kim et al. 1994). The modification of proteins with phosphate group influences such processes as

protein transport within the cell, ability to interact with other cell components, marking proteins as targets for degradation. Monitoring phosphorylation of particular proteins can help in disease diagnosis (Cohen 2001).

There are many known examples of how addition of phosphate group influences proteins and enzymes states, but, as evolution studies show that the genes of kinases became diverse even between different species, the conservation of phosphorylation sites in proteins between species is not too common (Louise N Johnson 2009). Therefore to understand a particular process, in the case of this thesis – ezrin activation by phosphorylation, the specific protein structure has to be taken into consideration.

1.4.3 Structure and conformations of ezrin

As already mentioned, the ezrin molecule is composed of the highly conserved N-terminal FERM domain, also known as N-ERMAD, the central α-helical domain, and C-ERMAD. N-ERMAD of human ezrin consists of 297 amino acids (Smith et al. 2003) and is subdivided into 3 lobes, F1, F2 and F3 that are shaped in a clove-like manner and contain the PIP_2-binding site and binding sites for membrane proteins. The crystal structure of full length ezrin is not yet available, but the N-ERMAD structures of all three ERM have been solved: each lobe has a certain structure, i.e. F1 (2-82 amino acids) maintains a ubiquitin-like folding, F2 (83-195 amino acids) shows structural characteristic of acyl-CoA-binding proteins, F3 (196-297 amino acids) is similar to a PH (pleckstrin homology) domain (Smith et al. 2003). N-ERMAD of radixin has the following dimensions, according to its crystalized form (K Hamada et al. 2000): the surface projection equals to 70*70 Å, the height is 40 Å.

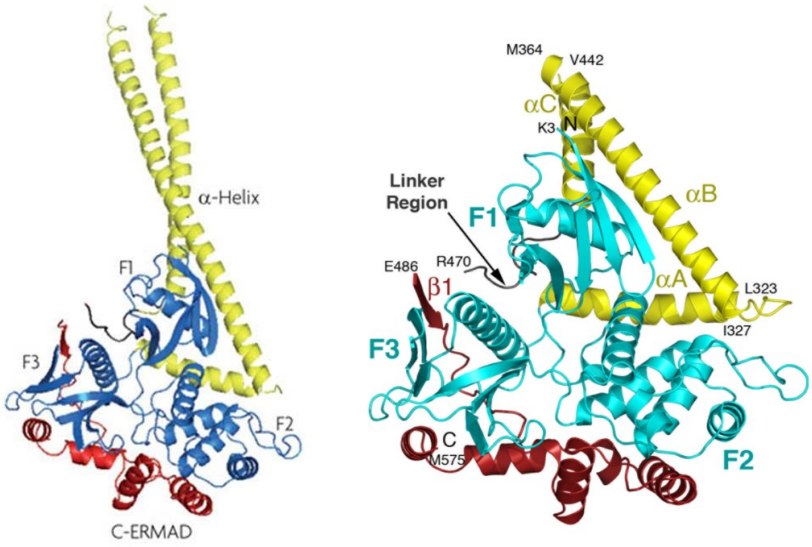

Fig. 3. Models of intra-molecular interaction of N-ERMAD with C-ERMAD of insect moesin (Spodoptera frugiperda). C-ERMAD is depicted in red, F1, F2, F3 domains of N-ERMAD are in blue color, central α-helical domains is in yellow. The right figure depicts the contact zones of α-helical domain. Taken from Fehon, McClatchey, and Bretscher 2010; Li et al. 2007.

The PIP_2 binding site was identified in the N-ERMAD, using different generated mutants, and most likely comprises regions between the F1 and the F3 lobes: residues 12-115 and 233-310. The characteristic feature of this regions are sequences $KK(X)_nK$ or $KK(X)_nRK$, i.e. basic amino acids sequences, where X - any amino acid (Barret, Roy, Montcourrier, Mangeat, & Niggli, 2000; Hamada, Shimizu, Matsui, Tsukita, & Hakoshima, 2000). The most important residues are thought to be the lysines 253, 254, 262, 263, and also 63 and 64; the simultaneous mutation of all of these lysines led to substantial decrease in binding to PIP_2–containing liposomes (Barret et al. 2000). The study of the crystalized radixin complex with inositol triphosphate IP_3 confirmed the presence of basic amino acids in the area of contact with IP_3/PIP_2 head and suggested that phosphate groups might imply pressure on the F3 lobe to complete binding. This in turn pushes the C-terminal part and therefore mediates unmasking of N-ERMAD (Keisuke Hamada et al., 2003; K Hamada et al., 2000). Because there are no evidences that IP_3 can activate any of ERM proteins, the structures with IP_3 should be considered with caution.

N-ERMAD has strong binding activity towards C-ERMAD that consists of a β-strand and four α-helices (A-D), C-ERMAD bears a conserved actin binding site. The C-N association of ezrin was shown in FRET studies with the use of YFP-ezrin-CFP construct expressed in HeLa cells (Zhu, Liu, and Forte 2005). The crystal structure of the moesin N-ERMAD/C-ERMAD complex (Pearson et al. 2000) revealed that in the inactive state of the protein, the A and D helices of the C-ERMAD stretch along the F2 and F3 N-terminal lobes and cover their binding sites. The particular residues that might contribute to this intra-molecular interaction were

identified by comparison of the crystal structures of the sole N-ERMAD, i.e. the active state, and the inactive N-ERMAD/C-ERMAD complex (Fig. 3, 4). These residues are 135–150 and 155–180 in the F2 subdomain and 210–214 and 235–267 in the F3 subdomain (Smith et al. 2003). It was noticed that the degree of disorder (characterized by B factor which is the measure of relative vibrational motion of different protein structures) of the F2 and F3 lobes in crystalized N-ERMAD is higher as compared to that in N-ERMAD bound to C-ERMAD (inactive state), suggesting that these subdomains are mobile structures and require C-ERMAD or other proteins to stabilize their conformation. It is also higher than the B factor of the F1 lobe alone (Smith et al. 2003). Such conformational mode was named keystone interaction, i.e. the mode of binding between several proteins or domains to stabilize the existing connection. Indeed, the ezrin binding partner EBP50 was shown to interact with moesin N-ERMAD in the way to mimic the D-helix interaction with F3 in the N-terminal part of ezrin, particularly interacting with residues 210, 212, 214 and 244 (Finnerty et al. 2004). Similarly, ICAM-2 binds to the F3 lobe interacting with amino acids 260, 281, 285, 288 (K Hamada et al. 2000). ERM mutants in the hydrophobic region of the D helix fail to mask N-ERMAD interaction sites (Gary and Bretscher 1995). The actin binding site (ABS) that is contained in the last 30 amino acids of C-ERMAD (Anthony Bretscher, Edwards, and Fehon 2002) is also masked in the N-ERMAD/C-ERMAD complex. ABS of ezrin has a conservative sequence: it has 30% similarity, for example, to glycophorin, another member of the band 4.1 protein family that connects membrane proteins and actin filaments (Gould et al., 1989; Algrain et al., 1993; Chishti et al., 1998); it includes the amino acid region KYKXL that is also found in other actin binding proteins, for example, in myosin heavy chain (Turunen, Wahlström, and Vaheri 1994). The X is represented in ERM proteins by the threonine and its phosphorylation does not affect the binding efficiency of recombinant radixin C-terminal to actin (Matsui et al. 1998), underscoring the exclusive conformational role of the residue.

Some studies suggest that PIP_2 binding to N-ERMAD of ezrin can unmask the threonine 567 in the C-terminal to allow its phosphorylation (Fievet et al. 2004). Phosphorylation, in turn, brings the whole protein to a less folded conformation. A number of kinases were reported to phosphorylate this residue, including Rho kinase, SLK family, PKCθ (Monique Arpin et al. 2011). According to the crystal structure of inactive moesin the C-terminal threonine is placed in between bound N-ERMAD and C-ERMAD, therefore introducing a negative phosphate group at this threonine induces electrostatic and steric changes which weaken the bond between the C- and N-terminal domains (Pearson et al., 2000; Matsui et al., 1998; Nakamura et al., 1999).

The α-helical domain has the structure of a coiled-coil and can be subdivided into 3 helices: αA, αB and αC. It is the least studied part of the ERM molecule but when the crystal structure of full length moesin from *Spodoptera frugiperda* was solved (Li et al. 2007), its role in N-ERMAD masking and, in particular, masking of the PIP_2-binding site was unraveled. The analysis of the structure revealed several interaction sites of the α-helical domain with

the F1 and F2 lobes of moesin N-ERMAD (Fig. 3), especially important for these interactions are the 70 Å anti-parallel coiled-coil region on the border between the αB and αC helices which contains a heptad repeat, a characteristic feature of all coiled-coils. This coiled-coil region relaxes its condense structure during the activation process (Li et al. 2007). The biochemical experiments and sequence comparison with the other ERM proteins and merlin showed that the loop between the αB and αC helices interacts with N-ERMAD and the interaction sites are conserved sequences within the ERM family (Hoeflich et al., 2003; Edwards & Keep, 2001). Interestingly, limited enzymatic digestion of inactive monomers and homodimers of ezrin yielded different proteolysis patterns (A Bretscher, Gary, and Berryman 1995). A possible explanation is the formation of the heptad repeat that occurs not only within the coiled-coil of one ezrin molecule but also between two helices of different ezrin molecules in the case when ezrin is the dimer. Moreover, it was noticed that stimulation of the HeLa and gastric parietal cells with histamine resulted in the increased monomeric pull of ezrin and decreased fraction of the oligomeric protein form, suggesting that inactive ezrin is represented mostly by dimers and oligomers while active ezrin form is monomeric (Zhu, Liu, and Forte 2005).

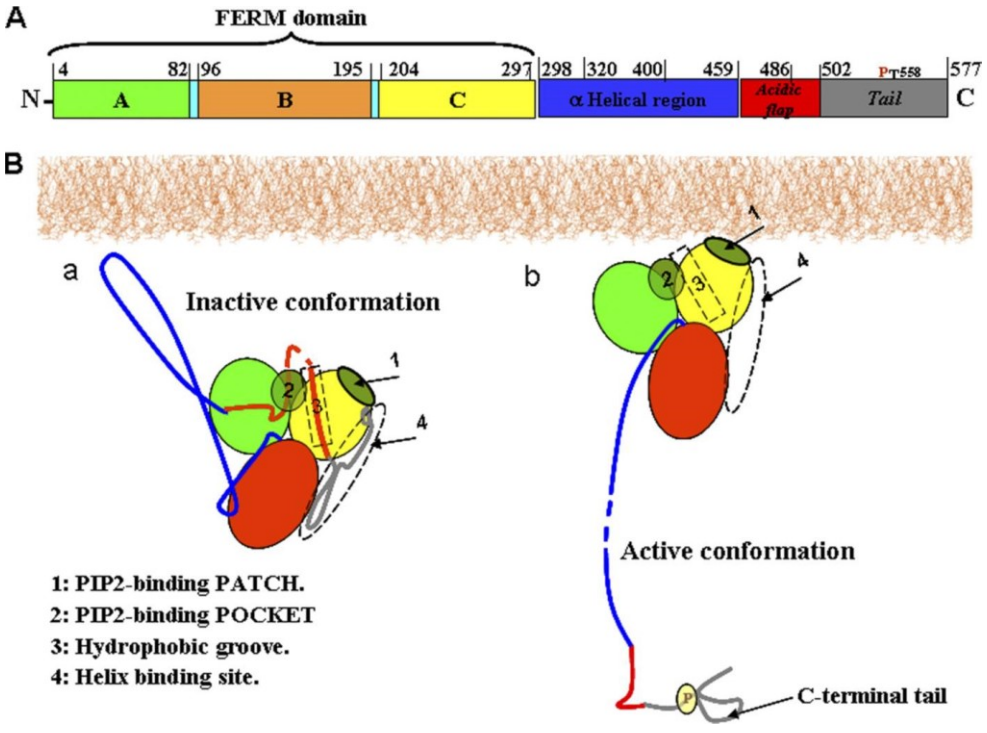

Fig. 4. Schematic structure of an ERM molecule. Illustration source (Ben-Aissa et al. 2012).

It is thought, in general, five interacting sites between N-ERMAD and C-ERMAD support the closed conformation of ERM proteins, also three sites are exist in the α-helical domain folding around N-ERMAD and also masking N-ERMAD binding sites (Pearson et al., 2000; Li et al., 2007). The multitude of masking structures suggests flexibility and sensitivity in the regulation of ezrin functions. Little known about mechanisms of ERM interaction with their binding partners, but many of those have been identified. Interaction studies with unphosphorylatable ezrin T567A, ezrin-wt, phosphomimicking ezrin T567E and the N-ERMAD part expressed in Jeg-3 cells (Viswanatha et al. 2013) revealed that every represented form of the ezrin molecule has its own prefered binding partners. For example, proteins FHOD1 (formin-diaphanous family), SCYL3 (Ezrin-Binding protein PACE-1) bind to ezrin T567A as efficiently as to ezrin-wt; about 50% of ezrin-wt was phosphorylated in the cells, therefore it was considered as active or partially active form while ezrin T567A represents the inactive state of the protein. DAG1 and EBP50, in turn, bind more efficiently to ezrin T567D, considered the fully open form by Viswanatha, and still better to N-ERMAD which lacks the C-terminal part and, therefore, has all its binding sites fully accessible. This finding supports the theory that ezrin may adopt at least three conformational states, each performing certain functions in the cell, and confirms that the C-terminal part of ezrin indeed prevents some protein interactions even in the fully opened ezrin T567E mutant. Most of the binding partners of ezrin interact with regions located within N-ERMAD (CD43/44, ICAM1/2, Dlg1, NHE1/3, Ras, S100P, ect.), some with the coil-coiled structure of the α-helical domain (Fes, Eps8, WWOX), and only few with the C-ERMAD (CLIC3, SCYL3, actin) (Viswanatha et al. 2013). Of course, the strongest binding partner of inactive ezrin is PIP_2 (V Niggli et al. 1995).

Well analyzed binding partners of ezrin, CD43/44 and ICAM 1/2, can unveil some details of the binding mechanism. These proteins interact with N-ERMAD via their cytoplasmic domains. No certain binding sequences were yet identified within these proteins, but some rules seem to exist, i.e. these cytoplasmic tails are rich in basic residues, and the interaction mode depends on ionic strength and is favored by the acidic environment within the interaction area. Therefore, the cleft between lobes F2 and F3 in the N-terminal domain, which is rich in glutamate and aspartate, could constitute a preferable interaction site (K Hamada et al., 2000; S Yonemura et al., 1998). Other proteins that interact with FERM-like domains are also characterized by positively charged residues and fit in the acidic groove between the F2 and F3 lobes. For example, kinesin-like-protein KIF1C interacts with the FERM domain of tyrosine phosphatase PTP-D1 (Dorner et al. 1998), CD44 binds band 4.1 protein (Nunomura et al. 1997), and the α-interferon receptor 1 subunit interacts with the FERM-like domain of JAK kinase (Yan et al. 1996). These findings infer the universal nature of the binding model of ERM and band 4.1 superfamily proteins with their membrane interacting partners.

1.5 Ezrin activation hypothesis

All existing studies are in agreement that ezrin's activation is essential for its functioning in the cell and that the activation of the protein is facilitated by certain factors: PIP_2 binding and C-terminal threonine phosphorylation, but the effect and contribution of each of these events are not fully understood. In the dormant, "closed" conformation ezrin and other ERM proteins reside in cytoplasm and their protein binding sites and actin binding site are masked. Transition to the activated state, according to the most widely accepted hypothesis is mediated, first, by binding to PIP_2 in the plasma membrane at ERM's conserved PIP_2-binding site. This subsequently unmasks the C-terminal threonine (T567 in ezrin) and allows its phosphorylation by Rho-kinase, protein kinase C (Hughes & Fehon, 2007; Niggli & Rossy, 2008) and some other kinases. Activated ezrin is localized at the membrane, especially in actin rich membrane structures, and able to bind to cytoplasmic tails of membrane proteins via its N-ERMAD and to actin filaments via its C-terminal actin binding site (Nakamura et al., 1999; Matsui et al., 1998; Huang, Wong, Lin, & Furthmayr, 1999; Pearson et al., 2000). First experiments in this direction showed that the PIP_2-binding mutant, generated by mutation of lysines in PIP_2-binding sites, showed impaired PIP_2 binding in vitro. In vivo this ezrin mutant failed to localize at the membrane and showed a diffuse cytoplasmic distribution (Barret et al. 2000). Liposome binding experiments demonstrated that ezrin binds specifically to PIP_2 incorporated in POPC liposomes (Herrig et al., 2006; Blin et al., 2008), and in combination with an actin filaments binding assay revealed that moesin binds F-actin in presence of PIP_2 but not in presence of phosphatidylinositol PI (Huang et al. 1999). More works demonstrated that PIP_2 can also modulate the binding behavior of ERM proteins. For example, in vitro binding studies showed that the binding of moesin to CD44, a known interaction partner of ERMs, was possible only in presence of PIP_2 (K Hamada et al. 2000). Analysis of ezrin binding to PIP_2-containing solid supported lipid bilayers (SSLB) by quartz crystal microbalance (QCM) and fluorescence microscopy suggested that the binding occurs in cooperative manner resulting in ezrin accumulation in distinct patches on the surface (Herrig et al. 2006; Bosk et al. 2011). Probably PIP_2 not only attaches ezrin to the membrane and introduces changes in its conformation but also is involved in localizing the protein along the membrane in an ordered manner. These findings promote the idea of PIP_2 as the main factor of ERM activation and phosphorylation as a facultative event.

For further discussion it is important to note that it was shown in activation studies with ezrin, radixin and moesin that they behave similarly (Shigenobu Yonemura et al. 2002), therefore findings about other members of ERM group can be attributed to ezrin too.

There are evidences that overexpression of phosphomimicking mutants of ezrin (T567D) and moesin (T558D) can increase the ERM fraction bound to the membrane and induce formation of microvilli and lamellipodia (Hao et al. 2009; Oshiro et al., 1998; S Yonemura & Tsukita, 1999; Gautreau, Louvard, & Arpin, 2000). Overexpression of the phosphomimicking mutant in HTB-58 cells increased their spontaneous migration (Austermann et al. 2008).

Phosphorylated at the C-terminal moesin, purified from platelets, was shown to bind F-actin filaments in co-sedimentation assay more efficient than non-phosphorylated protein (Nakamura et al. 1999). Such findings promoted the idea that PIP_2 binding is only optional for activation or specifically involved in certain processes. Several kinases can phosphorylate the conserved C-terminal threonine of ERMs: protein kinase C α and θ, Rho-kinase, Nck-interactin kinase (NIK) were reported to bind ezrin (Fiévet et al., 2007; Ivetic & Ridley, 2004; Baumgartner et al., 2006), as well as mentioned before (LOK (Simons et al. 1998) and SLK kinases (McClatchey 2014). Existence of the enzyme diversity means that, depending on cell type and the cell process, different pathways can activate ezrin, and probably also radixin, moesin.

Several other residues in ezrin can be phosphorylated, for example, tyrosine 477 can be phosphorylated by Src kinase (Heiska and Carpén 2005). Although this residue does not contribute to the activation process it is thought to participate in signal transduction; also tyrosine 477 phosphorylation site is not present in other ERM (Monique Arpin et al. 2011). The conserved tyrosine 145 is phosphorylated downstream of EGF stimulation of epidermal cells (Krieg and Hunter 1992), and in T lymphocytes this tyrosine is the substrate for kinases of the Src family (Autero et al. 2003). Tyrosine kinases activation can also lead to the formation of homotypic and heterotypic (between members of ERM family) oligomers in the cells (Shcherbina et al. 1999). Although the function of these oligomers is not clear yet, their formation might be a tool to modulate and structure the cell cortex.

It is important to mention that regulation of ERM activity can be modulated by phosphatases, thus, protein phosphatase 2C and myosine phosphatase are known to dephosphorylate ezrin in vitro (M. J. Brown et al. 2003) (Parameswaran, Matsui, and Gupta 2011). Based on this knowledge, the C-terminal threonine phosphorylation seems to be an important factor regulating ERM behavior.

Biophysical studies were also employed to clarify the ezrin activation theory and they revealed that synergystic actions of the known activating factors might occur. For example, another F-actin binding assay employing His-tagged ezrin, bound to supported membranes either via PIP_2 or via DOGS-Ni-NTA, showed that ezrin interacts with actin when it is bound to PIP_2–containing membranes, but not when it is bound via the His-tag to DOGS-Ni-NTA lipids incorporated in the lipid bilayer (Janke et al. 2008). The scheme of the experiments is depicted on Fig. 5A. Hao et al. (Hao et al., 2009) in their experiments with phosphomimicking moesin T558D showed that either mutation in PIP_2-binding site or depletion of PIP_2 by neomycin caused inability of moesin to localize at the membrane. Further experiments with different ezrin constructs expressed in epithelial cells revealed that a function of PIP_2 is not only in accumulating ERM at the membrane but also its binding is required for threonine phosphorylation: when ezrin was anchored to the membrane via a fused PH domain it could not undergo C-terminal threonine phosphorylation if the PIP_2-binding site was defective. In contrast, ezrin-wt, also fused to a PH domain, could be

phosphorylated at the membrane as it was detected with antibodies against T567 phosphorylated ERM (Fievet et al. 2004).

A

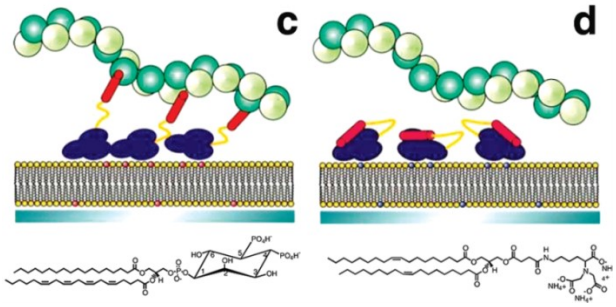

B

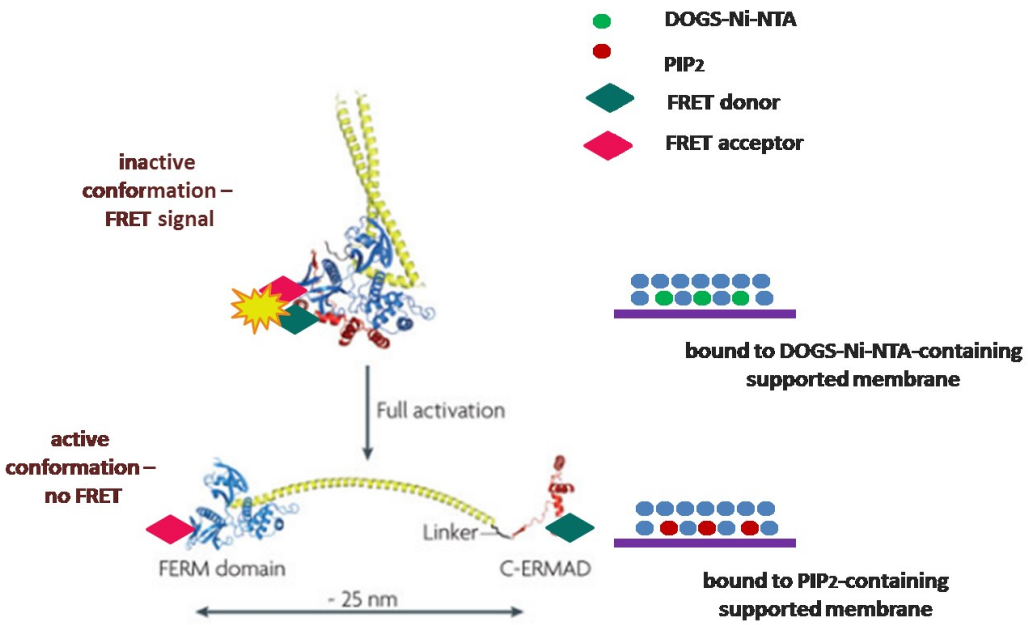

Fig. 5. Scheme of experiments. A – The model employed in the work of Janke et al. in the actin binding experiments. Ezrin was bound to (c) PIP_2- or (d) DOGS-Ni-NTA-containing SSLB, actin filaments were attached to the cantilever of AFM. In the situation (c) ezrin was partially activated by the interaction with PIP_2 and was capable of actin binding. Figure was adapted from Janke et al. 2008. B – The model used in this thesis. Fluorescently labeled ezrin molecule is thought to be in the closed conformation when bound to DOGS-Ni-NTA-containing SSLB, therefore FRET is expected to occur. In the case of ezrin bound to PIP_2-containing SSLB the conformational changes occur and FRET could not be possible anymore. The figure from Fehon, McClatchey, and Bretscher 2010 was used for this scheme.

A third activation factor of ezrin is known and by now it is the less studied one. S100P was identified as an ezrin binding protein and shown to facilitate actin binding of ezrin (Koltzscher et al. 2003). S100P binds to the N-ERMAD (82-173 residues) in Ca^{2+} dependent manner and competes with PIP_2 in ezrin binding in vitro (Austermann et al. 2008). Co-localization with ezrin at the membrane together with the evidences of overexpression of both, ezrin and S100P, in cancer cells (Austermann et al., 2008; Curto & McClatchey, 2004; Diederichs et al., 2004) suggest the participation of the two proteins in metastatic events.

Two recent studies in the field of ezrin activation developed new experimental system for biochemical and biophysical analysis of the protein, which presented evidence supporting a synergystic mode in the ezrin activation process. Interactions in a three component system "membrane–ezrin–actin" were investigated in vitro. Experiments using ezrin in the system similar to described in Fig. 5A showed differences in actin binding to ezrin and its threonine-mutants (Bosk et al. 2011). Ezrin doped membranes of the two types were incubated with actin filaments and the actin binding of ezrin wild type protein was compared to the binding of its mutants, ezrin T567A and ezrin T567D. The ezrin-actin binding was then analyzed by fluorescent microscopy detecting signal of fluorescently labeled F-actin. The most efficient interaction with F-actin was seen for the phosphomimicking ezrin T567D bound to PIP_2-containing membranes, the least efficient for the un-phosphorylatable ezrin T567A. Ezrin-wt and ezrin T567D anchored to the membrane via His-tag show similar intermediate actin binding. In contrast, PIP_2 binding strikingly enhanced the interaction with actin for both of them. This first in vitro F-actin/ezrin/membrane interaction thus showed that ezrin activation, characterized here by efficiency of actin binding, was dependent strongly on PIP_2, and threonine 567 phosphorylation was suggested as a secondary process which stabilizes the connection between ezrin and the membrane. Later, more detailed findings were obtained by the same group with the use of colloidal probe microscopy in a similar experimental system with ezrin attached to the two types of lipid bilayers. Measured by AFM binding forces between ezrin and F-actin revealed that a singular ezrin-actin bond has the same characteristics in all the experimental conditions, but the cumulative binding is much stronger for the protein bound to the membrane via its PIP_2-binding site than via the His-tag. Moreover only a slight increase in cumulative binding force for the T567D mutant was observed as compared to ezrin-wt (Braunger et al. 2014). These works unraveled important details about conditions of the ezrin activation and its binding to F-actin, showing the characteristics of the singular bond and confirming the synergism of the activation factors. But the question, whether phopshoprylation has only a minor influence in the process, is still not answered clearly.

1.6 Aim of the study and general experimental approach

The aim of this work was to directly reveal conformational changes associated with ezrin activation with the use of in vitro system and purified proteins. The demonstration of the N-ERMAD–C-ERMAD complex dissociation upon action of the activating factors will be the first experiment of such type in the field of ezrin studies. Förster Resonance Energy Transfer (FRET) technique was chosen as a method to confirm the conformational changes of the fluorescently labeled ezrin constructs bound to solid supported membranes. A designed here ezrin chimera with Cy3 label on N-terminus and eGFP at C-terminus was expected to produce a FRET signal when bound to the DOGS-Ni-NTA-containing SSLB via its His-tag representing the inactive form of ezrin. Binding to the PIP_2-containing SSLB was considered as activating, therefore decreasing FRET, conditions. The samples were monitored using the laser scanning microscope. Phopsphomimicking ezrin mutant ezrinT567D was employed to imitate the second activating factor – C-terminal phosphorylation. Such a model was designed to elucidate the question of the synergism between PIP_2-binding and C-terminal phosphorylation (Fig. 5B).

Forster Resonance Energy Transfer (described by Theodor Förster in 1940s) is a very sensitive method for measuring distances between molecules and between parts of a single molecule and can distinguish molecular units within the distance of several nanometers. Thus, it is used in co-localization and conformational studies. The phenomenon of FRET represents the non-radiative transfer of energy from an excited donor fluorophore to a nearby acceptor fluorophore. FRET does not depend on photon transfer and the acceptor is not required to possess properties of a chromophore, but in biological applications FRET is commonly when used with two fluorophore molecules. The phenomenon can be explained best in terms of the interaction between two dipoles: the electronically excited donor dipole oscillates and can pass its energy to the acceptor dipole if it has similar oscillating frequency. Thus, the emission spectrum of the donor should in part overlap with excitation spectrum of the acceptor. Energy transfer is possible only within short distances of 1 to 10 nm and 50% transfer efficiency corresponds to the so called Forster radius. This Forster radius is specific for each FRET pair (Fig. 6). A typical and often used FRET pair is CFP (donor) and YFP (acceptor), its Forster radius is 4.9 nm (http://zeiss-campus.magnet.fsu.edu/articles/spectralimaging/spectralfret.html), i.e. if YFP is placed within 4.9 nm from CFP Forster transfer can occur and YFP emission can be recorded following excitation of CFP.

1

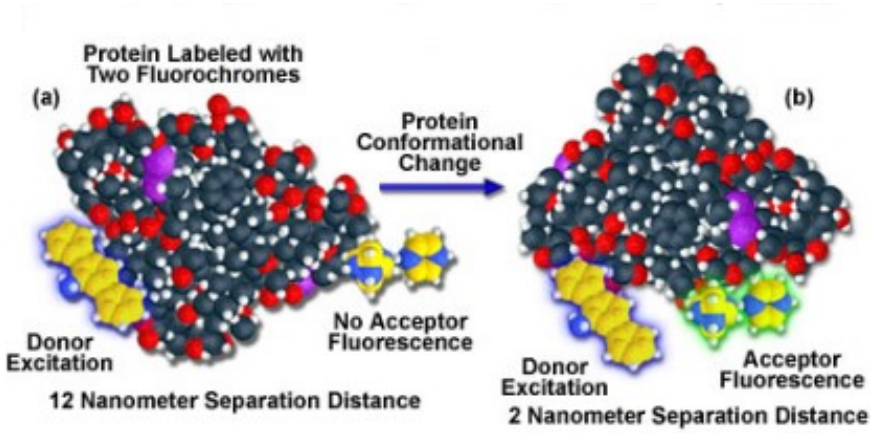

2

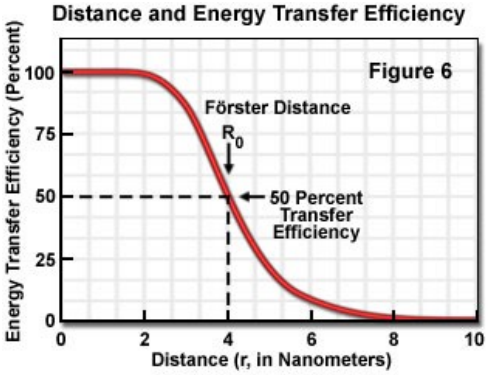

Fig. 6. Forster Resonance Energy Transfer. A: scheme of intramolecular FRET, (a) No FRET occurs due to the large distance between the donor and the acceptor fluorophores (>10 nm), (b) FRET is possible as the distance between the two fluorophores is short enough (<10 nm). B: FRET efficiency as a function of the distance between donor and acceptor fluorophores. FRET efficiency equals 50% at the Fortser radius or Forster distance.
Images source - http://www.olympusmicro.com/primer/techniques/fluorescence/fret/fretintro.html.

The Forster radius is determined by the overlap interval of the FRET pair spectra, the quantum yield of the donor, the refractive index of the solution and the orientation of fluorophores relative each other, more specifically the orientation factor of dipole moments κ. All the mentioned parameters can be measured and calculated, except for the orientation parameter. Typically, it is considered to be 2/3 for freely rotating fluorophores, but is hard to estimate when the FRET donor and acceptor are attached to macromolecules. Therefore, every fluorophore couple should be tested in each particular case to be assigned as a FRET pair. In this work, the GFP-Cy3 pair was used for FRET experiments, GFP being the donor and Cy3 the acceptor. The fluorescent spectra of GFP and Cy3 are depicted in Fig. 7.

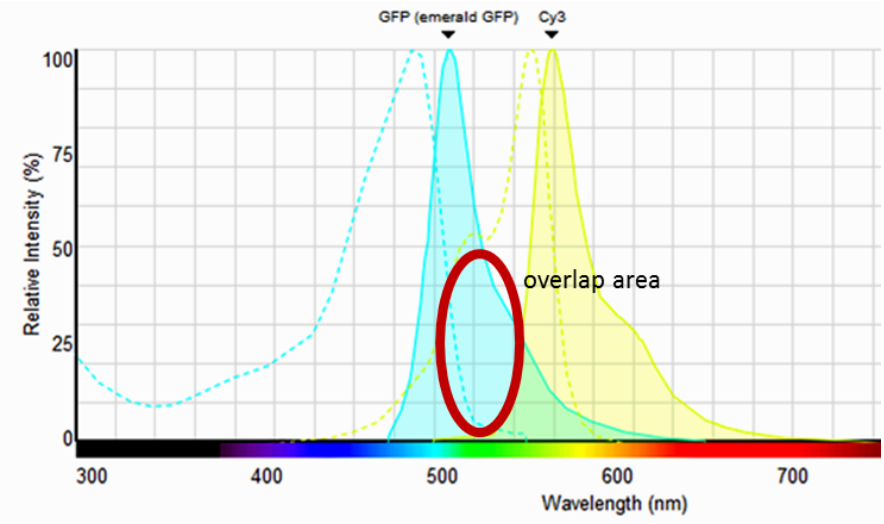

Fig. 7. The overlap in fluorescency spectra of eGFP and Cy3 demonstrates that the fluorophores' spectral characteristics meet FRET requirements. Data obtained from Fluorescence SpectraWiever, ThermoFisher Scientific.

The FRET signal usually is comprised of some part of the donor emission signal and a signal from the direct excitation of the acceptor, they are called the donor spectral bleed-through and acceptor spectral bleed-through, respectively. These noise signals must be taken into account during estimation of the FRET efficiency because they can lead to false positive FRET estimations. There are several methods in use to calculate the FRET efficiency (a ratio between photons accepted by the acceptor and photons emitted by the donor) and account for the mentioned background signals. The most used techniques include sensitized emission, acceptor photobleaching, Fluorescence Life Time Microscopy (FLIM) and spectral imaging. **Sensitized emission** or ratiometric imaging is usually applied to measure FRET occurring during fast events in the cell. The cell expressing a FRET construct is being excited at the donor excitation wave length and emission of the donor and the acceptor are recorded. The ratio of the acceptor/donor fluorescence signal is calculated then to estimate the energy transfer efficiency. The controls with only donor and only acceptor samples are required to subtract the bleed-through signals. The most precise method that does not need controls is **acceptor bleaching** or donor dequenching. FRET between a pair of fluorophores results in the quenching of the donor fluorescence due to the resonance energy transfer to the acceptor, therefore the destruction of the acceptor fluorescence by the high laser intensity leads to de-quenching of the donor, i.e. the donor recovers its quality of emitting fluorescent light. The difference in donor emission, in presence of the functioning acceptor

and of the bleached acceptor, is calculated and ascribed as FRET efficiency. The bleaching time for some acceptors can take up to several minutes and this should be taken in consideration when planning experiments. The **FLIM** technique is another way of determining FRET in a precise manner and independent of noise signals. All fluorophores can be characterized by decay time in their fluorescence emission, also called fluorescence lifetime. During FRET the fluorescence lifetime of the donor is decreased due to the presence of the acceptor. Thus, measuring of the donor fluorescence lifetime in the presence and the absence of the acceptor can estimate the efficiency of the resonance energy transfer. Moreover, this method depends only on the donor features, therefore no controls are required. FLIM also can be applied when the acceptor does not possess chromophore qualities. The two previous methods require fluorescent microscopes; the FLIM is conducted using specifically designed equipment comprising pulsed lasers and single photon counting detectors. **Spectral imagine** of FRET can be performed on spectrophotometers in solution or in cells using the specially designed confocal microscopes with acousto-optic tunable filters. Emission of the donor and the acceptor is recorded in one spectrum following the donor excitation. The spectra of the control samples (only donor, only acceptor) should be taken at the identical conditions. The FRET efficiency is then determined as $E_{FRET} = 1 - (I_{DA}/I_D)$, where I_{DA} is the intensity of the donor emission in the presence of the acceptor and I_D – in the absence of the acceptor. The spectra of the acceptor only are needed to calculate the normalized emission intensity of the FRET sample, i.e. to correct for the bleed-through signal.

New application of FRET-acceptor bleaching technique on solid supported bilayers were applied to directly demonstrate the conformational activation of ezrin induced by PIP_2 binding and C-terminal phosphorylation and to elucidate the question of correlation between these two activation factors. The knowledge of this activation can help us to understand the dynamic regulation of the connection between membranes and the underlying cytoskeleton.

2 Materials

2.1 Chemicals and reagents

Acetic acid (mol. biol. grade)	AppliChem
Acrylamide mix	Roth
Agar-Agar	AppliChem
Agarose LE	Biozym
Ammoniumhydroxyd	Sigma
Beta-Mercaptoethanol	Roth
Boric acid, buffer grade	AppliChem
Bovine serum albumin	Serva
Bromophenol blue	Sigma
Coomassie Billiant Blue	AppliChem
Cy3 mono-reactive NHS ester	GE Healthcare
Dinatriumhydrogenphosphate	Roth
Dimethyl sulfoxide (DMSO) (mol. biol. grade)	AppliChem
Dimethyl sulfoxide (DMSO) anhydrous	Life Technologies
Dithiothreitol (DTT)	AppliChem
DMEM 4500 mg glucose/l w/o L-glutamine	Sigma
DOGS-Ni-NTA (1,2-dioleoyl-*sn*-glycero-3-[(N-(5-amino-1-carboxypentyl)iminodiacetic acid)succinyl] Ni salt)	Avanti Polar Lipids, Inc.
DOPC (1,2-dioleoyl-*sn*-glycero-3-phosphocholine)	Avanti Polar Lipids, Inc.
DyLight405 maleimide	ThermoFischer Scientific
EDTA (mol. biol. grade)	AppliChem
Epidermal growth factor human >=97% SDS-PAGE (EGF)	Sigma
Ethanol (mol. biol. grade)	AppliChem
Ethidium bromide	Sigma
FCS	Biochrom
G418 sulphate	PAA
Glycerol (mol. biol. grade)	AppliChem
Hepes (cell culture grade)	AppliChem
Hydrochloric acid 37 % (analysis grade)	AppliChem
Hydrogen peroxide	Grüssing GmbH Analytika
IPTG	AppliChem
Isopropanol (mol. biol. grade)	AppliChem
Imidazole	Roth
Kalium chloride (mol. biol. grade)	Roth
Kanamycin sulphate	AppliChem
L-Glutamine 200 mM	Lonza

Lipofectamine 2000	Invitrogen
Loading Buffer 6x	Thermo Scientific
Low fat milk powder	AppliChem
Methanol (technical grade)	AppliChem
Mowiol 4-88	Calbiochem
Natriumdihydrogenphosphate	Roth
Opti-MEM	Invitrogen
PBS w/o Ca^{2+}, Mg^{2+}	PAN Biotech
Penicillin/Streptomycin	Lonza
Paraformaldehyde (PFA)	Sigma
Phalloidin-TRITC	Sigma
$PI(4,5)P_2$ (L-α-phosphatidylinositol-4,5-bisphosphate, purified from porcine brain with a fatty acid composition primarily composed of 18:0, 18:1, and 20:4 acyl chains)	Avanti Polar Lipids, Inc.
PIPES (buffer quality)	AppliChem
Phenylmethanesulfonylfluoride PMSF	(Biochemica) AppliChem
POPC (1-palmitoyl-2-oleoyl-*sn*-glycero-3-phosphocholine)	Avanti Polar Lipids, Inc.
Protease inhibitor cocktail tablets	Roche
SDS pellets (biochem. grade)	Roth
Silicon wafers	Silicon materials
Sodium azide	AppliChem
Sodium chloride (mol. biol. grade)	AppliChem
Sodium Citrate	Roth
Tetramethylethylenediamine (TEMED)	AppliChem
Trichlormethan/Chloroform	Roth
Tris	AppliChem
Triton X-100	AppliChem
Trypsin-EDTA	PAA
Tween 20	AppliChem
Yeast extract BioChemica	AppliChem

2.2 Markers

1kb GeneRuler Plus DNA ladder	Thermo Scientific
Page Ruler Plus Prestained Protein Ladder	Thermo Scientific
Protein Marker lll, prestained	Peqlab

2.3 Kits

Copmassie Plus – The Better Bradford Assay Kit	Thermo Scientific

HiYield PCR Clean-up/Gel Extraction Kit	Sued-Laborbedarf GmbH
HiYield Plasmid Mini DNA-Kit	Sued-Laborbedarf GmbH
KAPAHifi PCR Kit with dNTP Mix	Peqlab
PureLink HiPure Plasmid Filter Maxiprep Kit	Invitrogen

2.4 Antibodies

2.4.1 Primary antibodies

	mAB/pAB	Species	Dilution	Manufacturer
anti-ezrin	pAB	Rabbit	WB 1:10000	Millipore
anti-ezrin	mAB	Mouse	IF 1:250	BD
anti-GFP	pAB	Rabbit	WB 1:10000	Invitrogen
anti-T7-tag	mAB	Mouse	WB 1:10000	Novagen

2.4.2 Secondary antibodies

	Target species	Dilution	Manufacturer
IRDye 680CW Conjugated Goat Anti-Mouse IgG	mouse	1:14000	Li-cor
IRDye 800CW Conjugated Goat Anti-Rabbit IgG	rabbit	1:14000	Li-cor
Alexa Fluor 647 Donkey Anti-Mouse IgG	mouse	1:250	Dianova

2.5 Enzymes

α-Chemotrypsin from bovine pancreas Grade 1	Applichem
KAPAHifi DNA polymerase	Peqlab
T4 DNA ligase	Fermantas
FastAP thermosensitive alkaline phosphotase	Thermo Scientific
Restriction enzymes: EcoR1, Sal1, Xba1, Dpn1	Fermentas

2.6 Cell lines

A431 cell line – adherent epithelial cells, derived from human epidermoid carcinoma. High espression level of EGFR.

HeLa cell line – adherent epithelial cells, derived from human cervical adenocarcinoma.

HEK293T cell line – adherent epithelial cell line, derived from human embryonic kidney cells, is a modification of HEK293 cell line. HEK293T express SV40 T-antigen gene what enhances the production of transfected plasmids.

2.7 Bacterial strains

E. coli BL21(DE3)pLysS
Genotype: F- *omp*T *hsd* SB (rB-mB-) *gal dcm* (DE3) pLysS (Camr) GE healthcare biosciences

E. coli DH5α
Genotype: F+, deoR, endA1, gyrA96, hsdR17, (rk-,mk+), glnV44, thi-1, recA1,relA1, supE44, Φ80ΔlacZΔM15, thi-1, Δ(lacZYA-argF)U169 Promega

Rosetta
Genotype: F- ompT hsdSB(rB- mB-) gal dcm (DE3) pRARE2 (CamR) Addgene

JM110
Genotype: rpsL thr leu thi-1 lacY galK galT ara tonA tsx dam dcm supE44 Δ(lac-proAB)
from prof. Prüfer AG, Istitute of Biology and Biotechnology of Plants, Muenster

2.8 DNA-constructs

2.8.1 Eukaryotic and bacterial expression vectors

pET28a(+) is a vector for protein expression in E. coli, under T7 promoter with N-terminal (His)6-tag and additional C-terminal (His)6-tag, carries kanamycin resistance gene, Clontech.

pET24b(+) is a vector for protein expression in E.coli, under T7 promoter with N-terminal (His)6-tag, also additional C-terminal (His)6-tag, carries kanamycin resistance gene, Clontech.
pEYFP-C1 is a vector for expression of proteins with N-terminal enhanced-YFP tag in eukaryotic cells, under CMV promoter, carries G418-resistance gene, Clontech.

pECFP-N1 is a vector for expression of proteins with C-terminal enhanced-CFP tag in eukaryotic cells, under CMV promoter, carries G418-resistance gene, Clontech.

pEGFP-N1 is a vector for expression of proteins with C-terminal enhanced-GFP tag in eukaryotic cells, under CMV promoter, carries G418-resistance gene, Clontech.

Construct	**Vector**	**Insert**	**Reference**
Ezrin-CFP	pECFP-N1	Ezrin	This thesis

His-YFP-Ezrin-CFP	pEYFP-C1	Ezrin-CFP, addition of (His)6-tag	This thesis
Ezrin-eGFP	pEGFP-N1	Ezrin	Annika Heil
Ezrin-eGFP	pET28a(+)ezrin	eGFP	This thesis
EzrinT567D-eGFP	pET28a(+)ezrinT567D	eGFP	This thesis
His-ezrin	pET28a(+)	Ezrin	M. Koltzscher
His-ezrinT567D	pET28a(+)	Mutation of the Threonine567 in Ezrin-wt	J. Austermann
eGFP	pET24b(+)eGFP	eGFP	A.Schmidt

2.8.2 Oligonucleotides

Restriction free cloning of pET24b(+)EzrGFP (van den Ent and Löwe 2006).
Forw: 5´- TCCGAGGCCCTGTTAAAGCTTGCGGATGGGTCGGGATCCAGTAAAGAAGA-3´ and
Rev: 5´- AGTGCGGCCGCAAGCTTCTCGACTTAGCCATGTGTAACCCCAGCAGCTG -3´

To introduce an 6xHis-tag for purification from eukaryotic cells following primers were used:
Forw: 5´ - GAGCCGCCATGCATCATCATCATCATCATGGAGGA and
Rev: 5` - TCCTCCATGATGATGATGATGATGATGCATGGCGGCTC.

2.9 Equipment

Amicon Ultra-4 Centrifugal Filter Unit 50k	Millipore
Cell scraper	Greiner
Coverslips 22 X 22 mm, Nr. 1	Diagonal
Cryo tubes, 2 ml	Greiner
Dialysis Slide-A-Lyser, 3 - 12 ml, 10 kD cutoff	Pierce
Illustra NAP 10 size exclusion columns	GE Healthcare
Quartz cuvettes	Hellma
Microscope slides	Diagonal
Microwell 96-well plates, flatbottom	Greiner
Nitrocellulose membrane Protan BA85, 0.45 µm	Diagonal
Parafilm	American Nat. Can
Tissue culture dishes (diff. sizes)	Greiner
Whatman paper	Diagonal

2.10 Devices

Bacteriological incubator	Memmert
Balances	Quintix Sartorius
Centrifuge Avanti J-25	Beckman
Centrifuge Optima TL Ultracentrifuge	Beckman
Centrifuge Optima L-70K Ultracentrifuge	Beckman
Centrifuge Megafuge 1.0R	Heraeus
Counting chamber	Roth
DMIL inverted microscope	Leica
EVOS digital inverted microscope	Peqlab
Fluorimeter FluoroMax-2	Instruments S.A.
French Pressure Cell Press	SLM-Aminco
Incubator Heracell 240 I CO_2	Thermo Scientific
Incubator-shaker refrigerated Innova 4230	New Brunswick Scientific
LSM 780/Axio Observer	Carl Zeiss Microscopy GmbH
LSM 710	Carl Zeiss Microscopy GmbH
Microwave oven	Panasonic
Minigel system	Peqlab
Minigel system	Biometra
Mini Trans-Blot	Cell Bio-Rad
NanoDrop ND-1000 UV/Vis-Spectrophotometer	Peqlab
Odyssey Infrared Imaging System LI-COR	Biosciences
pH meter 766	Calimatic Knick
Pipetboy Acu Integra	Biosciences
Plasma cleaner electronic diener	Plasma-Surface-Technology
Power Pack P25 power supply	Biometra
RIfS	Self-assembled in Claudia Steinem lab, Göttingen
RoboCycler gradient 96	Stratogene
Sonifier 250	Branson G.Heinemann
SpeedVac SC110	Omnilab
Spectrophotometer DU640	Beckman
Spectrophotometer UV-visible 50scan	Varian
Sterile work bench Herasafe HS12	Heraeus
Sterile work bench	BDK Luft und Reinraumtechnik GmbH
Table centrifuge Biofuge pico	Heraeus
Thermomixer 5436	Eppendorf
Vortex	Genie Scientific Industries
UV lamp Solo TS Imagine System	Biometra
Water bath 1008	GFL

3 Methods

3.1 Cell biology methods

3.1.1 Cultivation of adherent eukaryotic cells

HeLa, A431 and HEK293T were cultivated in high glucose DMEM (4.5 g/L) supplemented with 10% FCS, 2mM L-glutamine, 100 U/ml Penicillin and 10mg/ml Streptomycin at 37°C and 7% CO_2.

For passaging, the medium was aspirated and TE solution was added for 5 min for HeLa cells and 15-20 min for A431 cells, at 37°C. For HEK293T cells trypsinization was not needed, the cells could be detached with gentle medium flow through a pipette. Thereafter the cells were centrifuged at 800 rpm for 4 min at 20°C. Pelleted cells were re-suspended in the fresh medium and seeded at a required density.

3.1.2 Cryo-stocks

Cells were grown in 10-cm Petri dishes up to 90% confluency, trypsinized and pelleted. The pellet was suspended in 1 ml of fresh medium containing 10% DMSO. Then the cells were frozen in freezers at -80°C and placed for storage in liquid nitrogen.

3.1.3 EGF stimulation experiments

A431 cells were starved for 5-7 hours in DMEM medium without FCS in 24-well dishes at a confluency of 50-70%. After stimulation with 33 nM EGF for 10 min at 37°C cells were fixed with PFA (see 3.1.4.1). For each experiment 3 samples were generated: 1-non starved cells, 2-starved, not stimulated cells, 3-starved and then stimulated cells.

3.1.4 Confocal immunofluorescence imaging

3.1.4.1 PFA fixation of cells

Cells were seeded in 24-well plates, on cover slips for confocal microscopy. Medium was aspirated and 4% PFA in PBS solution was immediately added to the cells for 5 min. Subsequently, the cells were permeabilized with 0.5% Triton X-100 in PBS for 15 min and incubated with glycin buffer for 10 min 3 times. Then blocking buffer was then added for 30 min. After every new step the cells were washed with PBS twice. All steps were carried out at RT.

4% PFA in PBS:

Four grams of PFA was heated in 100 ml of $PBS^{+/+}$, with 1mM NaOH, at 70°C for 2-3 hrs with constant stirring. After the solution turned transparent it was cooled down to room temperature and the pH was adjusted to 7.4 with HCl. Storage at -20°C.

Glycin buffer:
130 mM NaCl
7 mM Na_2HPO_4
3.5 mM NaH_2PO_4
100 mM glycin
Store at 4°C.

Blocking buffer:
130 mM NaCl
7 mM Na_2HPO_4
3.5 mM of NaH_2PO_4
7.7 mM NaN_3
0.02% BSA
0.2% TritonX100
0.05% Tween20
0.1% FCS
Store at 4°C.

3.1.4.2 Staining with antibodies

Cells were incubated with primary antibodies in blocking buffer for 1 hour at RT or overnight at 4°C, washed twice with PBS for 15 min and subsequently stained with secondary antibodies for 1 hour at RT, then washed for 20 min with PBS. For actin staining TRITS-Phalloidin was added simultaneously with the secondary antibodies.

At the end the cells were washed 2 times with water. Thereafter the cover-slips with the cells were mounted on a drop of Moviol 4-88 (1% N-propyl-gallat and 2 mM sodium azide added) on a glass slide. After drying overnight at 4°C the cells were inspected by microscopy.

3.1.4.3 Laser scanning microscopy

Preadjusted settings for eYFP, eCFP, eGFP, Alexa647 and Phalloidin were used on a LSM 780 (confocal laser scanning microscope, Zeiss) with x63 oil immersion objective. The LSM Image Browser was used to process the images.

3.1.5 Transient transfection

Transfections were performed with Lipofectamine 2000 according to the manufacturer's protocol. An important modification, antibiotics were not added to the cultivation medium before 24 hours after transfection to enhance cell survival.

3.1.6 Stable transfection

Cells were transfected as described above. Efficiency of transfection was analyzed using a fluorescence microscope EVOS (AMG), detecting fluorescence of the ectopically expressed YFP (or GFP)-fused protein in the cell. Sub-clones were selected in medium containing 1.4 µg/ml G418 antibiotic using series of dilutions in 96-well plates. Briefly, cells were diluted to a concentration 0.7 cells per well and grown for 2 weeks, changing medium every 4 days. Selected clones were grown in 20 cm dishes with the defined amount of G418 antibiotic in the medium.

3.2 Molecular biology methods

3.2.1 Plasmids cloning

Two cloning strategies were used.

3.2.1.1 Restriction free cloning (van den Ent and Löwe 2006)

Thirty-nucleotides primers were used to amplify a given region from a donor plasmid. This region, which is to be inserted into the acceptor vector, is used as "primer" for a second PCR reaction to amplify the whole acceptor vector with inserted region. Dpn1 digestion is then used to destroy the parent plasmid. To confirm the succesfull cloning the constructs were sequenced (using BigDye polymerase mix in the facility of Universitäts Klinikum Münster). Then the constructs obtained were transformated into DH5α strain of E.coli for further amplification and purification.

The final pET28a(+)EzrGFP construct was generated using the GFP sequence from an pET24b(+)GFP vector (donor vector) and pET28a(+)ezrin plasmid (acceptor vector), (Fig. 8). The following primers were used:
Forw: 5´- TCCGAGGCCCTGTTAAAGCTTGCGGATGGGTCGGGATCCAGTAAAGAAGA-3´ and
Rev: 5´- AGTGCGGCCGCAAGCTTCTCGACTTAGCCATGTGTAACCCCAGCAGCTG -3´

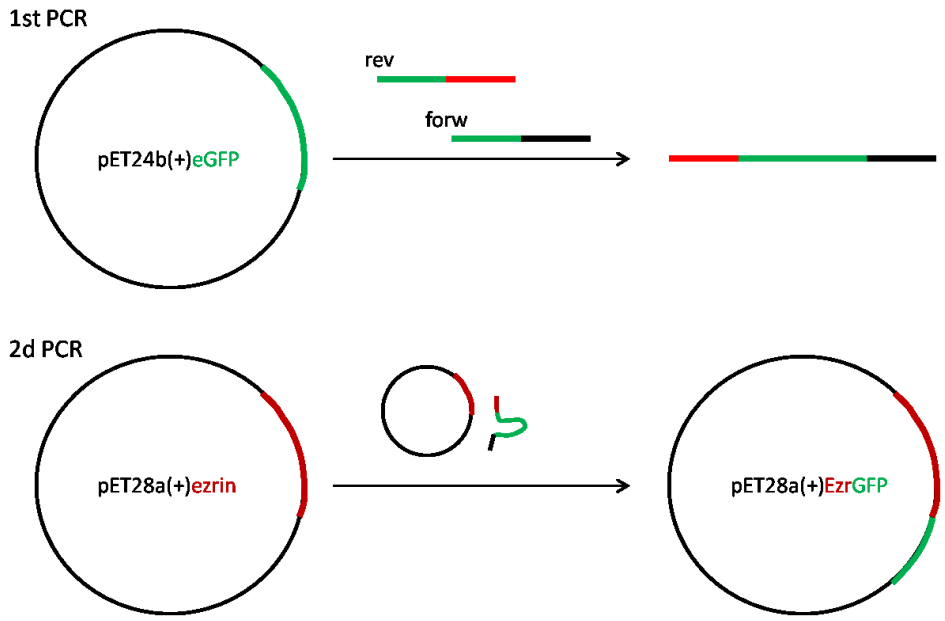

Fig. 8. Schematic representation of the restriction free cloning of ezrin-GFP and T567D-GFP constructs.

A plasmid for expressing the phosphomimicking mutant, DGFP, was generated with the same set of primers using the pET28a(+)EzrT567D as an acceptor plasmid (where Threonin 567 was changed to Aspartic acid) for inserting the eGFP sequence.
PCR conditions for clonning:

1st PCR

Denaturation	98°C	4min
30 cycles	Denaturation 98°C	30s
	Annealing 61°C	45s
	Extension 72°C	1min
Final Extension	72°C	6min

2nd PCR

Denaturation	98°C	4min
35 cycles	Denaturation 98°C	30s
	Annealing 54°C	30s
	Extension 72°C	4min
Final Extension	72°C	4min

HiYield PCR Clean-up/Gel Extraction Kit (SLG) was used to purify DNA after each step of amplification.

3.2.1.2 Cut-ligation method

Certain restriction enzymes were selected to remove an insert from a donor plasmid and T4 DNA ligase was used to fuse the insert with the accepting vector. All the manipulations were performed according to manufacturer's recommendations (see Materials).

EcoR1 and Sal1 restriction enzymes were used to remove the ezrin coding region from the pET28a(+)ezrin plasmid, ligated into the pECFP vector. EcoR1 and Xbal1 were then used to cut out the ezrinCFP part, which was then inserted in the pEYFP vector (Fig. 9). To introduce a 6xHis-tag for purification from eukaryotic cells following primers were used:
Forw: 5´ - GAGCCGCCATGCATCATCATCATCATCATGGAGGA and
Rev: 5` - TCCTCCATGATGATGATGATGATGATGCATGGCGGCTC.

<u>1 step of cut-ligation cloning: inserting ezrin sequence in pECFP-N1 vector</u>

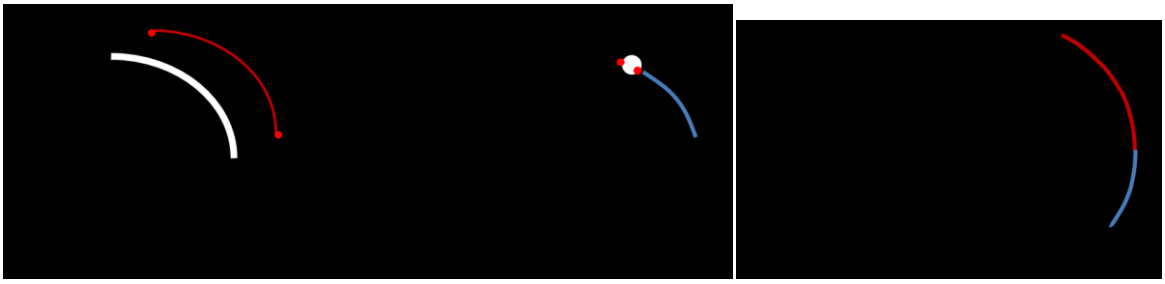

<u>2 step of cut-ligation cloning: inserting ezrin-CFP in pEYFP-C1 vector</u>

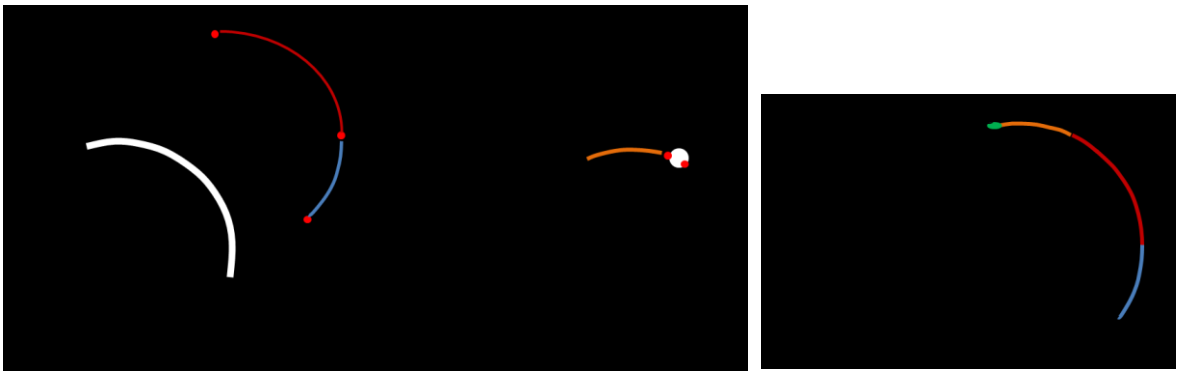

Fig. 9. Molecular cloning: two-steps scheme of cut-ligating method.

All the cloned constructs were verified by sequencing (using BigDye polymerase mix in the facility of Universitäts Klinikum Münster) and transformated into DH5α strain of E.coli for further amplification and purification.

The purification of the plasmid fragments after restriction digestion was performed using HiYield PCR Clean-up/Gel Extraction Kit (SLG) after separation of the fragments during DNA gel-electrophoresis (see. 3.3.3 of Methods).

3.2.2 Maxi-preps

3.2.2.1 E.coli transformation

Frozen (80°C) 50 µl aliqoutes of chemically competent DH5α (for plasmid prep) or BL21 (for protein expression) strains were thawed on ice. 50-300 ng of desired plasmid DNA was added and the bacteria left on ice for 30 min, followed by a heat-shock at 42°C for 1 min and 10 more min incubation on ice. The bacteria were then mixed with 1ml of LB medium without antibiotic and cultivated for 40 min at 37°C at 180 rpm. Bacteria were plated on agar plates with kanamycin (30 µg/ml).

3.2.2.2 Plasmid prep

E.coli DH5α were used for plasmid amplification. A chosen colony from a kanamycin agar plate was pre-cultured overnight at 37°C, 180 rpm in LB medium with 30 µg/ml of kanamycin. Bacteria were then harvested, lysed and the plasmid DNA purified using the maxi-prep kit according to the manufacturer (see Materials).

3.3 Biochemical methods

3.3.1 SDS-PAGE

Protein samples were boiled at 95°C for 5 min in SDS-SB and then separated in acrylamyd gels using a combination of 2 gel layers: stacking gel (5% acrylamid) and separating gel (10% acrylamid). 200mV current was applied to the electrophoresis chamber for 40-60 min.
Gels were stained in Coomassie solution for 30 min at RT and washed in destaining buffer for 2-3 hours.

Sample buffer (1x SDS-SB):
62.5 mM Tris ph 6.8
2% SDS
10% glycerine

300mM 2-mercaptoethanol
~ 0.1% (w/v) bromphenol blue

Stacking gel (5%):
17% acrylamid / bisacrylamid
125 mM Tris pH 8.8
0.1 % SDS
0.1 % APS
0.1 % TEMED

Separating gel (10%/12%):
10% or 12% acrylamide/bisacrylamid*
375 mM Tris pH 8.8
0.1 % SDS
0.1 % APS
0.04 % TEMED
*30 % acrylamide and bisacrylamide stock solution at a ratio of 37.5:1

Running buffer:
25 mM Tris
2% SDS
192 mM glycine

Coomassie staining buffer:
40% methanol
10% acetic acid (100% stock)
0,1% Coomassie Brilliant Blue R250
50% ddH_2O

Destain buffer:
45% methanol
10% acetic acid
45% ddH_2O

3.3.2 Western Blot analysis

3.3.2.1 Proteins transfer

Acrylamid gels were overlaid with nitro-cellulose membranes were placed between filter paper and fiber pads, put in gel holder cassettes and then inserted in a mini trans-blot tank system. An ice block was also placed in the tank to cool the system. Transfer was performed at 300 mA per tank for 1h in 4°C cold transfer buffer at RT.

Transfer-buffer:
0.5 M Tris
0.5 M Boric acid
In ddH2O

3.3.2.2 Immunodetection of proteins.

Blot membranes were blocked with 5% milk powder in TBS-T buffer for 30 min at RT. Primary antibodies were added for 30 min at RT or overnight at 4°C in the same solution. Secondary antibodies were added to the membranes in the milk solution after 10 min, 3 times washing with TBS-T buffer. Secondary antibodies linked to IR-dyes for IR-detection (LI-CORE system) were incubated with the membranes for 45 min at 1:10000 dilution. Blot membranes were washed again 3 times for 10 min in TBS-T and then processed in the LI-CORE detection system.

TBS-T: 20 mM Tris
150 mM NaCl
0.2 % (w/v) Tween 20
pH 7.5 with HCl
in ddH2O

3.3.2.3 Stripping of blot membranes

Primary and secondary antibodies can be stripped from Western blot membranes in stripping buffer for 30-50 min at 52°C. Following stripping membranes were then thoroughly washed with TBS-T and primary and secondary antibodies could then be applied to the membranes again as described above.

Stripping buffer:
625 µl Tris
2 ml SDS 10%
69 µl mercaptho-etanol
up to 10 ml with H_2O

3.3.3 DNA gel-electrophoresis

DNA gel-electrophoresis was used to separate plasmid fragments after enzymatic restriction. To prepare gels, the agarose LE (0.5%) was suspended with TAE buffer and dissolved upon heating in the microwave. Then it was cooled to 40-45°C, and ethidium bromide was added at ratio 1:10000 (v:v). The agarose solution was then poured into the gel chamber and left at RT to polymerase. The samples were mixed with the 6x Loading Buffer (ThermoScientific) and loaded in the gel pockets. Running time constituted 40-60 min at 100 mV.

Purification of the desired plasmid fragments were performed using the HiYield PCR Clean-up/Gel Extraction Kit (SLG) as described by manufacturer.

TAE buffer, pH 8.0:
40 mM Tris-HCl
0.1 % acetic acid
1 mM EDTA

3.3.4 Bacterial expression and purification of the proteins

The BL21 E.coli strain was used for expression of recombinant proteins. Bacteria were transformed with pET28a(+)Ezrin/D-GFP plasmids and plasmid selection was performed by addition of 30 μg/ml kanamycin to the medium. Pre-cultured bacteria were grown in LB medium at 37°C, in a bacterial shaker at 180rpm until ab OD of 0.6. Protein expression was induced with 1mM IPTG and the culture was cultivated at the same conditions for 3-5 hrs. Bacterial cells were harvested by 10 min centrifugation at 4krpm, 4°C and the pellet was resuspended in lysis buffer and homogenized in a French press. The cells debris was separated by 1h of ultra-centrifugation at 30krpm, 4°C and the supernatant incubated on a shaker for 30 min at 4°C with Ni-NTA agarose beads equilibrated in lysis buffer. The beads were transferred to a column, washed with wash-1 and wash-2 buffers and protein bound via the 6xHis-tg were eluted with elution buffer.

For the expression of untagged ezrin and ezrinT567D mutant the freeze-thaw method with subsequent ultrasonication (cycle duty=60%, output control=5) was used to disrupt bacterial cell walls and lysate cells.

The quality of the purified proteins was analyzed using SDS-PAGE and Western blot. For further experiments proteins were dialyzed against the buffer required.

LB-medium:
1 % Trypton
0.5 % yeast extract
1 % NaCl
30 μg /ml kanamycin

Lysate buffer:
1mM EDTA pH=8.0
10mM b-mercaptoethanol
20mM imidasol
300mM NaCl
40mM HEPES pH7.4
1mM PMSF

Wash-1 buffer:
40 mM HEPES, pH 7.4
25 mM imidasol, pH 7.4
150 mM NaCl

10 mM beta-mercaptoethanol
1mM PMSF
Wash-2 buffer:
40 mM HEPES, pH 7.4
35 mM imidasol, pH 7.4
150 mM NaCl
10 mM beta-mercaptoethanol
1 mM PMSF
Elution buffer:
500 mM imidasol, pH 7.4
150 mM NaCl
10 mM beta-mercaptoethanol
1 mM PMSF

3.3.5 Recombinant expression and purification of proteins from HEK293-T cells

HEK293T cells expressing His-tagged YFPezrinGFP were scratched from Petri dishes containing DMEM and pelleted at RT, 800 rpm for 4 min. All further manipulations were performed on ice. The cell pellet was resuspended in cold low salt buffer and cells were then lysed by pushing the suspension through a syringe needle Nr1 from BD Microlance™ 3. The lysis level was detected analyzing a drop of the suspension under the optical microscope. Cellular debris was removed by ultracentrifugation (40 min, 20000 rpm, 4°C). Supernatants containing proteins were then dialyzed against HEPES+ buffer and incubated with pre-equilibrated Ni-NTA agarose beads for 30 min at 4°C. Column purification was then performed as described above (see 3.3.4.).
10 ml of low salt buffer was required for cell pellets collected from 150 20cm-Petri dishes with cells grown to a confluency of 90-100%.
Low salt buffer pH7.4:
10 mM HEPES
0.5 mM EDTA
1 mM DTT
Protein inhibitor tablet
HEPES+ buffer pH7.4:
40 mM HEPES
150 mM NaCl
2 mM DTT
1 mM PMSF

3.3.6 Fluorescent labeling of proteins

3.3.6.1 Fluorescent labeling with Cy3™ Mono NHS ester

Cy3 NHS ester dye (1 mg of purchased powder dissolved in 200 µl of anhydrous DMSO) was used for labeling the N-terminal amino-group of C-terminal GFP-fused proteins. To achieve a preferred binding of the dye to the N-terminal α-amino group, the manufacturer's protocol was modified by conduction the labeling pH6.5 in 1:1 molar ratio at RT for 3-4 minutes. Removing of the excess dye was performed immediately on a Sephadex size exclusion column. Labeling efficiency was quantified by running the protein samples on SDS gel and visualizing labelled proteins using an UV-lamp UVsolo TS. For subsequent experiments the labeled proteins were dialyzed against the buffer required.

Labeling buffer – PIPES buffer pH6.5:
10 mM PIPES
150 mM NaCl

3.3.6.2 Fluorescent labeling with DyLight405-maleimide

One milligram of DyLight405-maleimide was dissolved in 100 µl of anhydrous DMF. Prior to the reaction proteins were reduced with a 100-molar excess of DTT for 30 min at RT and then dialyzed against labeling buffer. Alternatively, the TCEP reducing agent was used in the same molar ratio for 10 min at RT without subsequent dialysis. Dye and protein were mixed in a molar ratio 1:1 and incubated at 4°C overnight with slow shaking. Excess dye was removed on a Sephadex size excluding column.

Labeling buffer – HEPES, pH7.4:
10 mM HEPES
150 mM NaCl

3.3.6.3 UV-vis specta

Light absorbance of Cy3 labeled constructs was measured using a 50scan UV-visible spectrophotometer (Varian) at 280 nm (optimal absorbance of aromatic amino acids in proteins) and 550 nm (Cy3 absorbance maximum). Cy3 labeling efficiency was calculated using the formula:

$$\frac{D}{P} = \frac{A_{552}/E_{Cy3}}{(A_{280} - 0.08 * A_{552})/E_{protein}}$$

where D/P corresponds to the dye-protein ratio, i.e. the labeling efficiency, A_{280} and A_{552} are the maximum absorptions of the aromatic amino acids and the cross-linked Cy3 dye, respectively. Factor of 0.08 – the correction for the dye absorption at 280 nm. Extinction coefficients: $ex.c_{Cy3}$=150000 $M^{-1}cm^{-1}$, $E_{ezrin/ezrinT567D}$=64390 $M^{-1}cm^{-1}$, $E_{EzrGFP/DGFP}$=87710 $M^{-1}cm^{-1}$.

The extinction coefficient of ezrin was taken from the database (http://www.signaling-gateway.org/molecule/query?afcsid=A000892), the extinction coefficient for EzrGFP was calculated as described (Pace et al. 1995). The extinction coefficients of the mutants were taken as those of wild type, since exchange of threonine to aspartic acid does not influence spectral properties of proteins.

3.3.6.4 Fluorometric measurements

Fluorescence excitation and emission spectra were recorded with a fluorimeter FluoroMax-2 (Instruments S.A.) in quartz cuvettes (Hellma), light path 10 mm. Excitation scan and emission scan were read using the settings provided in the FlouroMax software.

3.3.7 Bradford assay

Protein concentrations were determined using the Coomassie Plus Bradford Protein Assay Reagent. An aliquot of a protein in water was mixed with Bradford Reagent at a ratio of 1:1, total volume 1 ml, and incubated 10 min at RT. Absorption was then measured at 595 nm using a spectrophotometer. Concentrations were calculated based on standard curve obtained using 0.1, 0.5, 1, 2, 4, 6, 8, 10 µg of BSA.

3.3.8 Liposomes preparation

Lipid mixtures were prepared from methanol:chloroform (1:1) lipid stocks. Briefly, solutions were dried in nitrogen flow and subsequently in a SpeedVac at 37°C for 4-5h. Dried lipids films were dissolved in the required buffer solution and incubated at 50°C (water bath) for 45 min, being thoroughly vortexed for 1 min every 15 min. In that way multi-lamellar liposomes were formed, which were used in liposomes pelleting assay.
For the FRET experiments employing solid supported membranes and for RIfS experiments lipid films were dissolved in the required buffer and incubated at RT for 30 min, vortexing after 20, then 5 and 5 min after the buffer had been added. Next, the suspension was treated in a sonicator at 60% of duty cycle, output control 4, for 15 min 2 times, changing heated water in the sonicator reservoir to cold water in between. This procedure resulted in the formation of SUVs (small uni-lamellar vesicles).

3.3.9 Liposomes pelleting assay

Three different types of multi-lamellar vesicles were prepared (3.3.8. of this manuscript): 1) 92:8 molar ratio POPC:PIP_2, 2) 92:8 molar ratio DPPC:DOGS-Ni-NTA. Total lipid concentration – 0.8 mg for 1ml of E1 buffer. 50 mg of protein of interest in E1 buffer was added to 100 µl of the vesicles suspension, filled with the buffer up to 200 µl and incubated

at RT for 1h. After ultra-centrifugation at 60 krpm at 4°C, pellet and supernatant fractions were collected and analyzed by SDS-PAGE.

E1 buffer pH7,4:
20 mM Tris
50 mM KCl
0.1 mM EDTA
0.1 mM NaN_3

3.3.10 Supported lipid bilayer preparation and protein binding

SUVs suspensions, prepared as described in 3.3.8. of this manuscript (total lipid concentration – 0.6 mg/ml), were applied to hydrophilized silicon substrates (or wafers, wafer size – 0.8cmx1cm), fixed in plastic chambers for 1h at RT, then carefully washed with a corresponding buffer. Spreading of SUVs on the surface leads to the formation of a continuous lipid bilayer. Defined amounts of protein were dropped on the wafer covered with the lipid bilayer, distributed gently via pipeting and left for binding at 4°C overnight. Thereafter, wafers were carefully washed with the respective buffer. Samples were then examined under the microscope.

Lipid films contained PIP_2/POPC or DOGS-Ni-NTA/DOPC, molar ratio given: 8% PIP_2 – 92% POPC, 8% DOGS-Ni-NTA – 92% DOPC, 4% PIP_2 – 96% POPC, 4% DOGS-Ni-NTA – 96% DOPC, 2% PIP_2 – 98% POPC, 2% DOGS-Ni-NTA – 98% DOPC.

For the PIP_2 containing liposomes low-pH citrate buffer is required to properly immobilize SUVs on the surface and spread the correct bilayer (Braunger et al. 2013). E1 buffer was then used as washing buffer. DOGS-Ni-NTA containing liposomes were immobilized and spread using E1-Ca^{2+} buffer for the 1st step, and E1-EDTA-free buffer for the second step.
Protein binding to PIP_2 containing lipid bilayers and subsequent washing was optimal in E1 buffer. For binding of protein to DOGS-Ni-NTA containing lipid bilayers E1-EDTA-free buffer was used.

To hydrophilize silicon substrates (100 nm SiO_2 layer for LSM experiments, 5000 nm oxide layer for RIfS) wafers were heated to 70°C in a solution containing H_2O_2(30%):NH_4OH(25%):H_2O 1:1:5 for 15 min, while stirring. Before using in experiments wafers were thoroughly washed with distilled water and dried under nitrogen. For the RIfS experiments the wafers were treated with oxygen plasma for 6 min in the ozonizer (electronic diener Plasma-Surface-Technology).

Citrate buffer pH4.8:
20 mM Na-Citrat
50 mM KCl
0.1 mM EDTA
0.1 mM NaN_3

E1-Ca^{2+} buffer, pH7.4 = E1 buffer with no EDTA and 2 mM $CaCl_2$ added.

E1-EDTA-free buffer = E1 with no EDTA

3.3.11 Reflectometric Interference Spectroscopy - RIfS

Reflectometric interference spectroscopy was used to observe protein binding to solid supported lipid bilayers. The RIfS device detects the interference of white light (500-600nm) at the protein layer bound to the solid supported lipid membrane.
The light source - tungsten halogen lamp - is connected through the illuminating optical fiber to the flow chamber which is supplied with a silicon wafer (prepared as described in 3.3.10.). The collecting optical fiber receives the reflected light. This signal is detected by the SpectraSuite software and is analyzed in MATLAB application giving the Optical Thickness-Time plot as the final result. The RIfS set-up was self-established in the laboratory of Claudia Steinem, University of Göttingen (Stephan et al. 2014).

The vial with liposomes solution was connected with the flow chamber via plastic tubes. Liposomes containing either PIP_2 or DOGS-Ni-NTA lipids were pumped through the flow chamber, where they bound to the hydrophilic wafer and fused into a lipid bilayer. Following washing the vial with a protein solution in E1 buffer was connected to the flow chamber and left circulating in the system until the equilibrium of the protein-lipid binding was reached.

3.3.12 Intra- and inter-molecular FRET on supported lipid bilayers

The sample preparation was described above (3.3.10. of Methods).

The FRET time-bleaching image series were conducted in the CLSM 710 confocal laser scanning microscope (Zeiss), using x63 oil immersion objective. To confirm FRET the acceptor fluorophore Cy3 was bleached and the fluorescence response of the FRET donor, GFP, was monitored. The bleaching and FRAP tool of the Zeiss software were applied. Bleaching of Cy3 in the indicated ROI (Regions Of Interest) was carried out at 561nm, 100% laser power, with 3 iterations, time series: interval = 0. Excitation wavelength for Cy3 and GFP are 561 and 488 nm respectively. The emission was recorded in the interval 493 – 550 nm for eGFP and 575 – 681 nm for Cy3. The bleaching and FRET efficiency were calculated using FRET_calc plugin in JmageJ.

The experiments were performed in the laboratory of Claudia Steinem, University of Göttingen.

3.3.12.1 Statistical analysis.

The collective data was analyzed in R-statistical program applying heteroskedasticity test, Shapiro test against normality; Anova type ll test for significance of differences between the experimental groups was run on *linear fixed effects model* (*lme*) of the data set.

3.3.13 Enzymatic protein digest

Chymotrypsin was used to cut Cy3-labeled proteins that were further analyzed by Western blot and UV-illumination of the same blot membranes. According to PeptideCutter ExPASy (http://web.expasy.org/peptide_cutter/) chymotrypsin can cut 68 times in EzrGFP, DGFP and 40 times in ezrin, ezrinT567D (at tryptophan, tyrosine, phenylalanine sites). Chymotrypsin powder was freshly dissolved in digestion buffer at a concentration of 1 mg/ml. To perform the digest this prepared enzyme solution was diluted in the same buffer 1:100 and 1 µl of the dilution was then mixed with 9 µl of the protein (concentration 3 mg/ml) in any buffer without EDTA. The reaction time was 5 min at RT. To stop the reaction SDS-PAGE sample buffer was added and the mixture was boiled at 95°C for 5 min, then SDS-PAGE and Western blot were performed.

Chymotrypsin digestion buffer, 10x, pH7.8:
80 mM Tris/HCl
100 $CaCl_2$

4 Results

C-ERMAD and N-ERMAD, in the closed conformation of ezrin, bound to one another in an autoinhibitory manner. Several studies have suggested that this association is disrupted upon ezrin activation and a resulting change in the conformation (Huang et al. 1999; Gautreau, Louvard, and Arpin 2000; Nakamura et al. 1999). Two goals were pursued in this project: 1) to demonstrate that the transition of ezrin into the active state involves an increase of the distance between C-ERMAD and N-ERMAD and 2) to elucidate the contribution of each of the ezrin activation factors in this process.

Förster Resonance Energy Transfer (FRET) between two fluorophores attached to C- and N-terminus of ezrin is a sensitive method for detecting the change in the distance within the protein molecule (intra-molecular FRET). Energy transfer from an excited donor fluorophore to an acceptor fluorophore in ground state is possible only when they are in the proximity of less than 10 nm and results in the fluorescence of the acceptor. For the FRET experiments with ezrin I designed the chimera of ezrin and C-terminal eGFP, chemically labeled with the Cy3 fluorophore at the N-terminal end of ezrin, as eGFP (donor) and Cy3 (acceptor) have been used as efficient FRET (Snapp and Hegde 2006). The attached Cy3 and eGFP are expected to give strong FRET signal in the close conformation of ezrin, since C-ERMAD and N-ERMAD are bound to each other (Zhu et al. 2007) and the fluorophores are expected to be in close proximity. In the activated state the FRET signal should weaken or disappear as the distance between the two domains potentially reaches 25 nm (Fehon, McClatchey, and Bretscher 2010). Measurements of the FRET efficiency were done using the laser scanning microscope LSM 710 (Zeiss) on recombinant proteins bound to solid supported lipid bilayers (SSLB).

To understand the mechanism of ezrin activation the combination of its activation factors – PIP_2 binding and phosphorylation of T567 threonine on CERMAD were exploited in the same experimental set up. I compared behavior of ezrin-wt and the ezrinT567D phosphomimicking mutant when the proteins were bound to SSLB either via the PIP_2-binding site or via an N-terminal His-tag. Ezrin binding to DOGS-Ni-NTA lipids via the His-tag represents the non-activating condition. The model with solid supported membranes has an advantage to experiments within cells, because it allows comparing protein states in activating and non-activating conditions without effects of secondary interactions which can occur in the cell.

The mixture of Cy3-labelled ezrin and GFP-fused ezrin were included as an inter-molecular FRET control. The different protein constructs will be further referred to as

following: GFP-fused ezrin – EzrGFP, GFP-fused phosphomimicking mutant of ezrin – DGFP, Cy3-labelled EzrGFP – Cy3EzrGFP, Cy3-labelled DGFP – Cy3DGFP, Cy3-labelled ezrin – Cy3Ezr, Cy3-labelled phosphomimicking mutant – Cy3D.

4.1 Expression and purification of the recombinant ezrin, ezrinT567D and their GFP-fused derivatives using the BL21 strain of E.coli and HEK293T cells

Ezrin and ezrinT567D were expressed in BL21 E.coli and purified via His-tag using affinity chromatography (3.2.4. of Methods) with the yield of 3-5 mg of the protein from 500 ml of bacterial culture. The expression plasmids pET28a(+)ezrin and pET28a(+)ezrinT567D enabled efficient expression of the stable proteins.

The first fluorescent construct designed for the FRET experiments was ezrin fused to YFP (N-terminal) and CFP (C-terminal), as the YFP-CFP FRET pair is widely used. Therefore, the pET28a(+)YFPEzrCFP plasmid was generated by cut-ligation molecular cloning (3.2.3.2. in Methods).

Attempts to purify YFPEzrCFP from different E.coli strains were not successful. The following strains were used: BL21, Rosetta (can use eukaryotic codons which may be misread in other E.coli strains), JM110 (Dam and Dcm negative, i.e. lacking metilation on ATC and C(A/T)GG), DH5α. It was possible to enrich a His-tagged protein on the Ni-NTA affinity column, but SDS-PAGE analysis revealed that it had the mass of 105 kDa, while the calculated size of YFPEzrinCFP is about 140 kDa. Western blot analysis of the bacterial samples taken 3 hours after expression induction, stained with antibodies against ezrin and GFP (suitable for YFP and CFP too), showed that the band of 105 kDa band reacted with both antibodies. This indicated that the protein was disrupted before the purification and had only CFP or only YFP attached to ezrin:

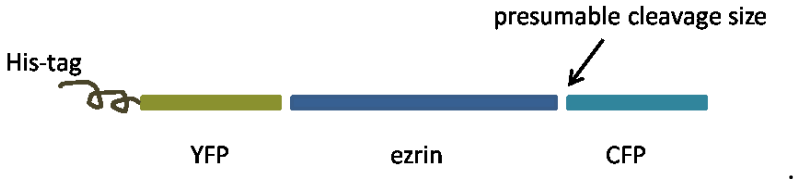

However, it was possible to obtain the desired protein upon recombinant expression in HEK293T eukaryotic cells. HEK293T cells are a popular cell line for protein expression due to the presence in their genome of the SV40 large T antigen from Simian Vacuolating virus 40. The product of the gene enhances the production of the transfected plasmid, therefore contributes to higher recombinant protein yield. To purify YFPEzrCFP from HEK293T cells I introduced a His-tag sequence (3.2.3.2. of Methods) into the pEYFPEzrCFP plasmid which I

obtained as an intermediate product during the cloning of pET28a(+)YFPEzrCFP for bacterial expression. The stably transfected cell line were established by selection with G418 antibiotic at concentration of 1.4 μg/ml.

YFPEzrCFP protein purified from HEK293T cells had the correct 140 kDa size as judged by SDS-PAGE and Western blot (Fig.10). But the amount of the protein which could be obtained from 100 confluent 20-cm plates ranged only from 0.5 to 1 mg. This amount turned out not to be not enough for the planned experiments.

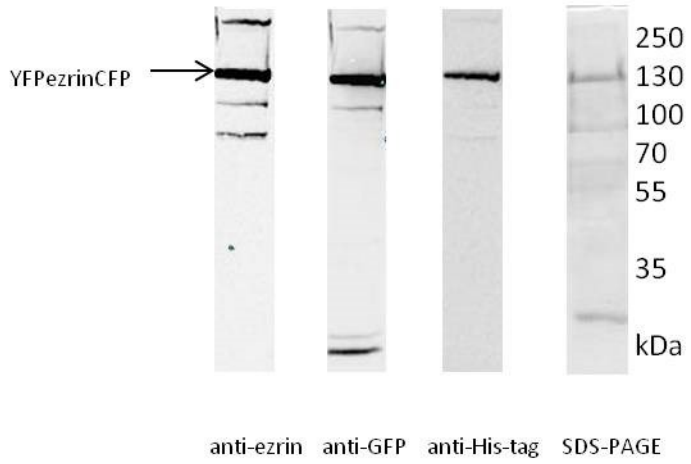

Fig. 10. Purification of recombinant YFPEzrCFP from HEK293T cells. Anti-ezrin, anti-GFP, anti-His-tag **–** immunodetection with antibodies against His-tag, ezrin and eGFP moieties, SDS-PAGE- coomassie staining of the elution fraction from the His-tag affinity column.

Due to these experimental limitations in obtaining sufficient amount of YFPEzrCFP I changed the strategy and generated differently labeled fluorescent ezrin protein. Specifically, I used C-terminally GFP-tagged ezrin that could be labeled with chemical fluorophore at the N-terminal end. High yields of ezrinGFP were obtained using the pET24b(+)EzrinGFP expression plasmid in BL21 E.coli cells. Three to five mg of EzrGFP and DGFP each could be purified from 0.5-1 L of bacterial culture as described in 3.3.4. of Methods. (Fig.11)

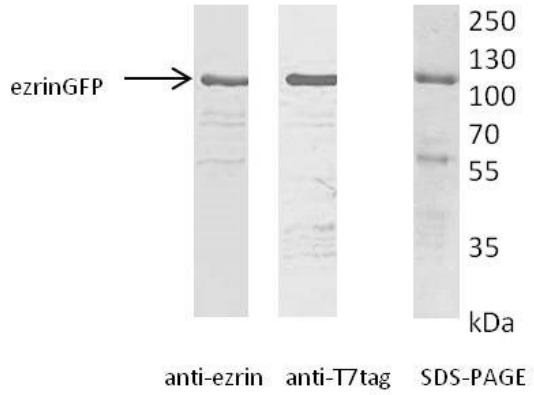

Fig.11. Purification of recombinant EzrGFP from E.coli. Anti-ezrin, anti-T7tag – immunodetection with antibodies against ezrin and T7-tag, SDS-PAGE- coomassie staining of the elution fraction from the His-tag affinity column.

4.2 Liposome pelleting assay: the fluorescent derivatives of ezrin bind to PIP_2 and DOGS-Ni-NTA containing liposomes like the wild type protein

EzrGFP and YFPEzrCFP were tested for binding to two types of liposomes: 1) POPC:PIP_2, molar ratio 92:8, 2) DOPC:DOGS-Ni-NTA, molar ratio 92:8. Proteins were incubated with the liposomes at RT for 1 hour and then the mixture was subjected to ultracentrifugation for 1 hour at 100krpm. The pellet and supernatant fractions were analyzed by SDS-PAGE. His-tagged ezrin-wt was included as the control, since it is known to specifically bind to PIP_2 (V Niggli et al. 1995). Fig. 12 illustrates that both fusion constructs bound to PIP_2- and DOGS-Ni-NTA-containing liposomes (pellet fraction) similar to ezrin-wt.

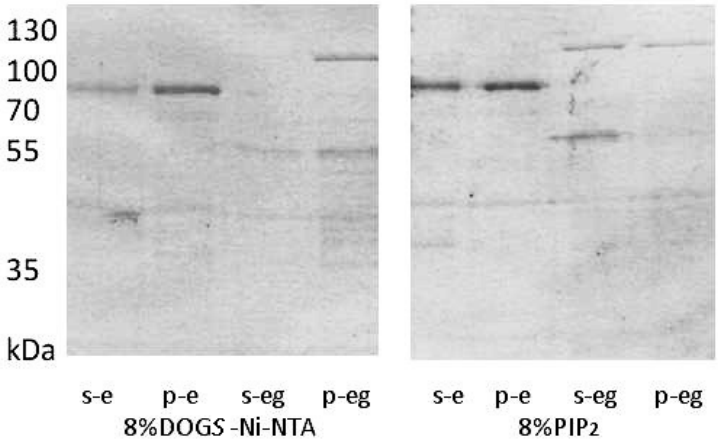

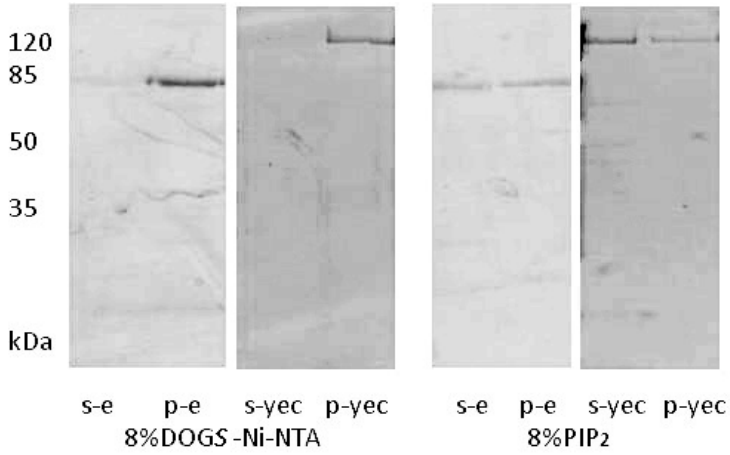

Fig.12. Liposomes pelleting assay, coomassie stained SDS-PAGE. Letters "s" and "p" stand for "supernatant" and "pellet", "e" – ezrin, "eg" – EzrGFP, "yec" – YFPEzrCFP.
The values in per cent estimating the amounts of the proteins in the supernatant fractions "s" and in the pellet fractions "p":

1st gel DOGS-Ni-NTA binding				1st gel PIP_2 binding			
ezrin		EzrGFP		Ezrin		EzrGFP	
s	36.40%	s	5.50%	s	50.60%	s	57.10%
p	63.60%	p	94.50%	p	49.40%	p	42.90%
2d gel DOGS-Ni-NTA binding				2d gel PIP_2 binding			
Ezrin		YFPEzrCFP		Ezrin		YFPEzrCFP	
S	9.75%	s	22%	S	50.90%	s	67.20%
P	90.25%	p	78%	P	49.10%	p	32.80%

Densitometry was performed using Image J analysis software (NIH) for this evaluation.

4.3 EzrGFP and DGFP are recruited to the cell membrane in EGF activated A431 cells similar to endogenous ezrin

A431 cells express high levels of the EGF receptor and, therefore, are a convenient model for EGF stimulation experiments. Moreover, ezrin recruitment to the membrane in EGF stimulated A431 cells was also reported earlier (A Bretscher 1989). Serum-starved cells, overexpressing EzrGFP or DGFP, were stimulated with EGF. The same procedure was carried out with non-transfected cells to compare the behavior of the GFP-fused proteins and endogenous ezrin.

Three cell samples were prepared for each protein: 1 - *non-starved:* here cells were cultured in serum rich medium (10% FCS), 2 – *starved:* here cells were maintained in serum-free medium, 3 - *starved-stimulated:* here cells were kept in serum free conditions and then stimulated with EGF. All experimental groups of cells were grown simultaneously on glass cover slips in 24-well plates, then fixed with PFA and examined under the microscope LSM 780 (Zeiss).

Non-starved and *starved* samples had few and small actin-positive cell protrusions and microvilli, the distribution of EzrGFP and DGFP was mostly cytosolic. The *starved-stimulated* cells revealed a phenotype with many long microvilli and protrusions, and EzrGFP, as well as DGFP, were recruited to the cell membrane and accumulated in the rpotrusions. Experiments with endogenous ezrin showed a similar results (Fig. 13-15), indicating that the C-terminal GFP tag does not affect the behavior of ezrin within the cells.
Differences between EzrGFP and DGFP were not observed.

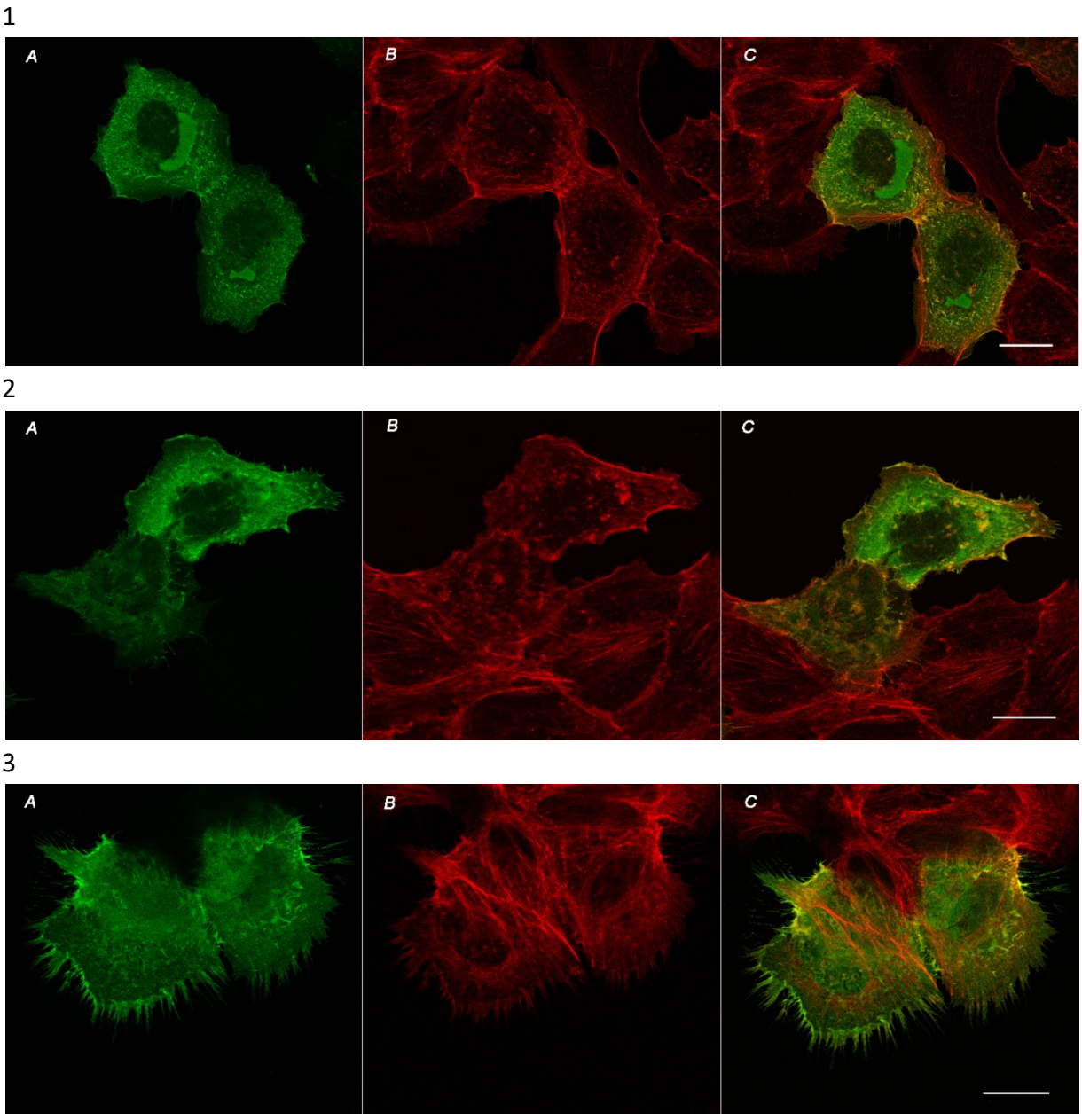

Fig. 13. EGF stimulation of A431 cells over-expressing EzrGFP. Cells over-expressing EzrGFP were fixed with PFA and analyzed under the microscope following three cases: 1 – cells were cultured in usual conditions with serum, 2 – cells were starved in serum-free medium for 5-7 hours, 3 – cells were stimulated with EGF after they were serum-starved. A – EzrGFP, B – actin stained with TRITC-phalloidin, C – merge. Scale bar = 10 µm.

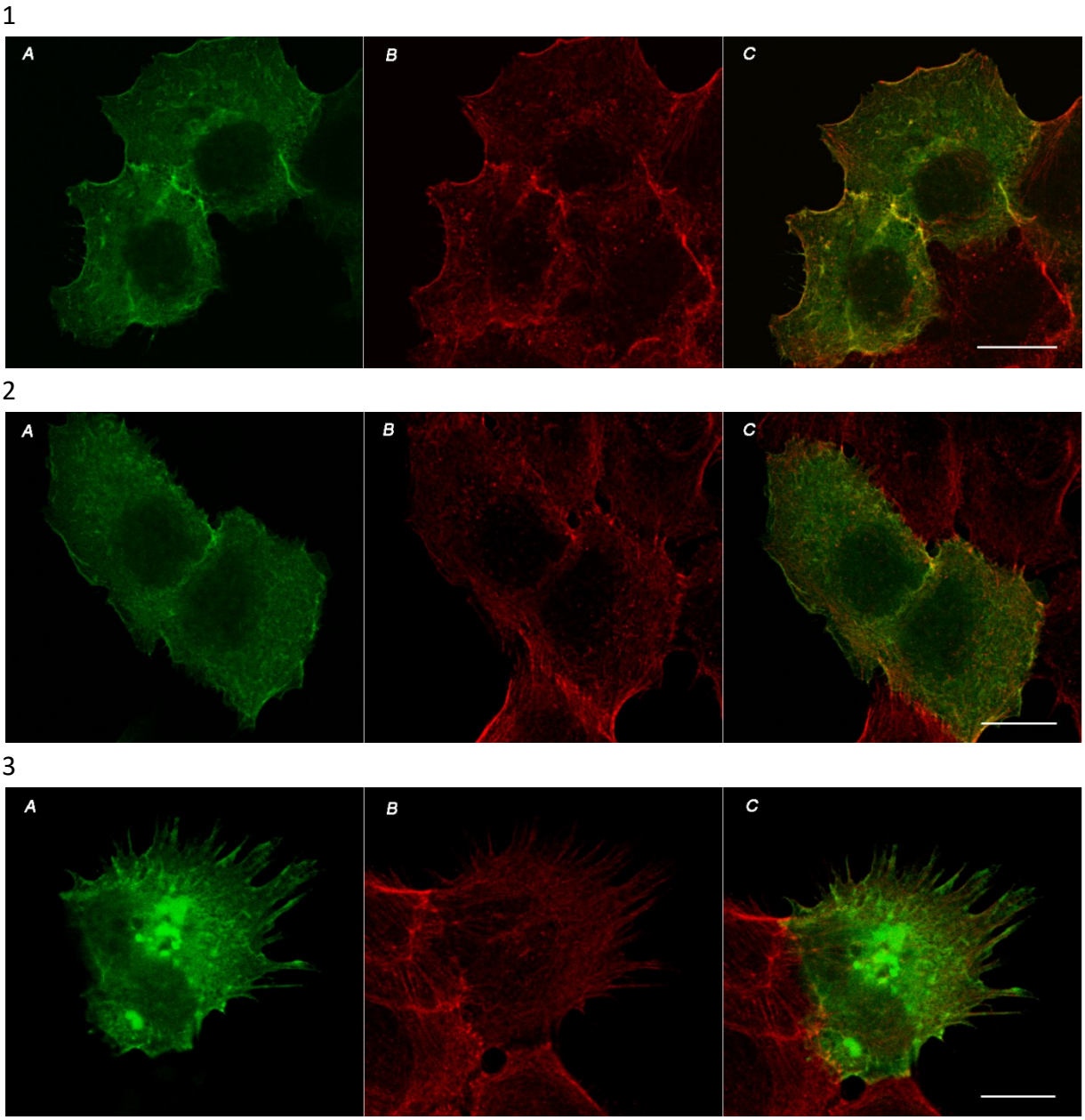

Fig. 14. EGF stimulation of A431 cells over-expressing DGFP. Cells over-expressing DGFP were fixed with PFA and analyzed under the microscope following three cases: 1 – cells were cultured in usual conditions with serum, 2 – cells were starved in serum-free medium for 5-7 hours, 3 – cells were stimulated with EGF after they were serum-starved. A – EzrGFP, B – actin stained with TRITC-phalloidin, C – merge. Scale bar = 10 µm

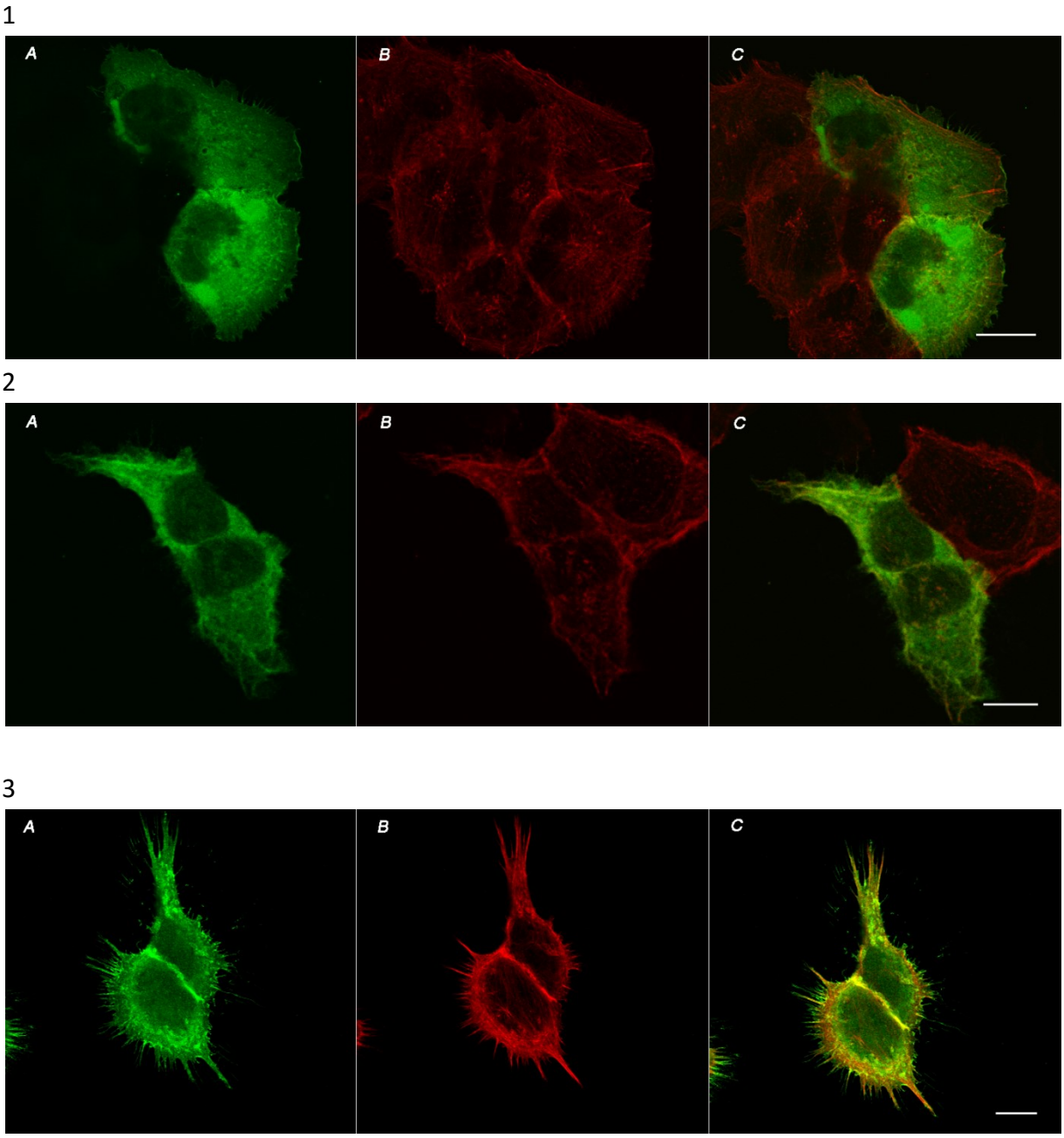

Fig. 15. EGF stimulation of A431 cells expressing ezrin constitutively. Cells expressing endogenous ezrin were fixed with PFA and analyzed under the microscope following three cases: 1 – cells were cultured in usual conditions with serum, 2 – cells were starved in serum-free medium for 5-7 hours, 3 – cells were stimulated with EGF after they were serum-starved. A – endogenous ezrin visualized with Alexa fluor 647, B – actin stained with TRITC-phalloidin, C – merge. Scale bar = 10 µm.

The same analysis was performed with HeLa cells. However, the cells showed a considerable degree of pre-stimulation: they revealed abundant protrusions already before addition of EGF. Thus, the *starved* and *starved-stimulated* cells did show massive protrusion formation, while *non-starved* cells showed, as expected, a phenotype with little protrusions

and a cytosolic distribution of ezrin. Again, no substantial differences between the different constructs and endogenous ezrin were observed, data not shown.

4.4 DyLight405EzrGFP is not suitable for FRET analysis

The fluorescence spectra of the chemical fluorophore DyLight405 (as FRET donor) and eGFP (as FRET acceptor) meet the requirements for FRET (see Introduction 1.7), although this pair was not reported in the literature yet. I used a maleimide modification of DyLight405 to label cysteines of ezrin. It is known that ezrin has two cysteines Cys117 and Cys284, that can be labeled with chemical fluorophores (Bosk et al. 2011). As these cysteins reside in the N-ERMAD, it is likely that FRET can occur between DyLight405, attached to one of the cysteines, and the C-terminal eGFP in the closed conformation of ezrin. DyLight405 labeling was confirmed by UV-illumination of the samples following SDS-PAGE (see Fig.16). Emission spectra of DyLight405EzrGFP showed two peaks in response to excitation at 405 nm with maxima at 425 and 505 nm (Fig. 17). However, experiments with DyLightEzrGFP and DyLightDGFP bound via His-tag to DOGS-Ni-NTA containing SSLB (non-activating condition) showed no FRET, although fluorescent signals of eGFP and DyLight405 in separate channels could be detected (not shown).

Therefore, I switched to another FRET pair for analizing the conformational activation of ezrin.

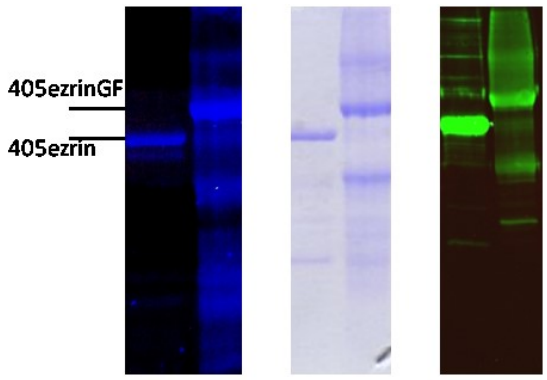

Fig.16. DyLight405 labelling of ezrin and EzrGFP. Purified ezrin and EzrGFP were labeled with DyLight405 as described in Methods. After removing free dye, using size-exclusion chromatography, the labeled proteins were subjected to Western blot for staining with anti-ezrin antibodies (green bands). The Western blot membranes were also analyzed under UV-light to detect the fluorescence of DyLight405 (blue bands on the black background). The blue bands on the light background represent coomassie staining of the SDS-PAGE. Bands on all three pictures coincide, confirming that the label is attached.

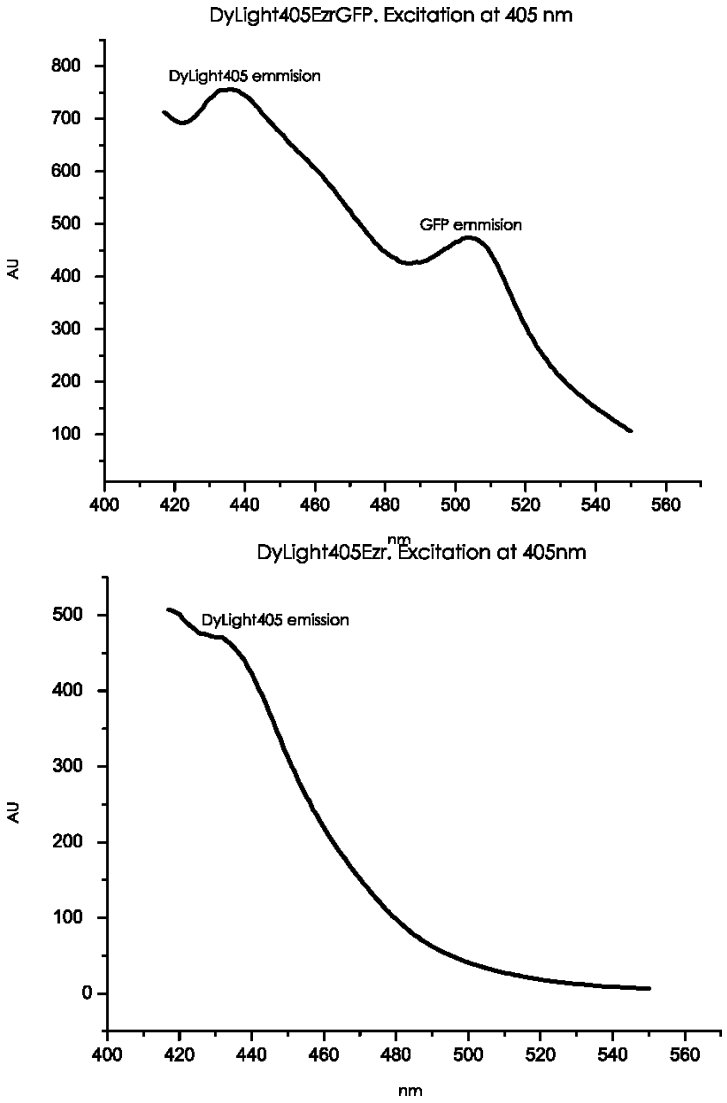

Fig.17. Fluorometric measurements. Emission spectra of DyLight405EzrGFP and DyLight405Ezrin at excitation wavelength of 405 nm (excitation of DyLight405). DyLight405EzrGFP showed two emission maxima: DyLight405 and eGFP. EGFP fluorescence can be attributed to FRET or minor excitation of eGFP at 400 nm. Emission spectra of EzrGFP at 405 nm excitation (molar concentration was close to molar concentration of eGFP moiety in DyLightEzrGFP) was subtracted from depicted spectra using FluoroMax software (Instruments S.A.)

4.5 Cy3EzrGFP shows FRET

EGFP (as FRET donor) and Cy3 (as FRET acceptor) fluorophores are another documented FRET pair (Fessenden, 2009; Parsons et al., 2005; Snapp & Hegde, 2006). Therefore, I attempted to label the EzrGFP construct at a site in the N-ERMAD with the Cy3 dye. I chose a Cy3 NHS ester for labeling, assuming that the position of the cysteines in ezrin might be not optimal for the purpose of effective FRET. NHS esters interact with protein amino

groups by nucleophilic substitution and are often used for modifying proteins. To achieve specific labeling of the N-terminal amino group I established conditions taking into account the chemical characteristics of the reaction and dye manufacturer's recommendations. Values for the pK_a of the α- and ε-amino groups are 8 and 10.54 respectively. Thus, acidic conditions favor labeling of the α-amine but slow down the reaction in general, because at low pH amino groups tend to be protonated and, therefore, have decreased nucleophilic properties. I established the following settings for optimal α-amino group labeling: pH=6.5, low dye to protein molar ratio (1:1) and short reaction time of 4 min.

The success of the labeling was monitored by running the protein samples on SDS-gels and visualizing them with UV-illumination (Fig.18). The efficiency of the labeling (D/P, dye to protein ratio) was calculated as described in 3.2.7.3. Methods, see UV-vis spectra in Supplement materials (Fig. S1). The D/P varied between different protein batches and ranged between 0.7 and 1.1.

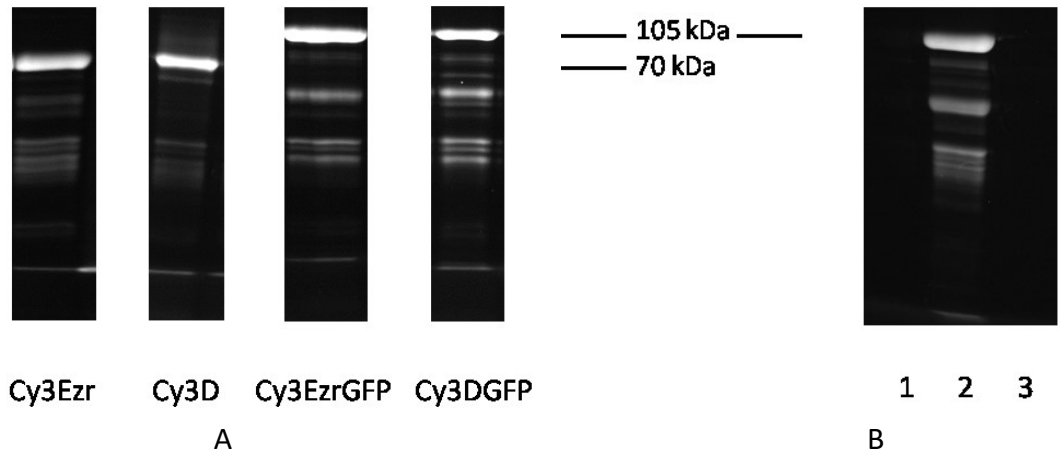

Fig.18. Cy3 labeling. UV-detection. Cy3-labelled eztin, ezrinT567D, EzrGFP and DGFP were run on the SDS-PAGE and the gels were analysed under UV-light to detect the fluorescence of Cy3 dye. A – Cy3-labelled proteins, B – UV-illumination of non labelled and labeled proteins: 1 - EzrGFP, 2 - Cy3EzrGFP, 3 - ezrin. 70 kDa sign indicates Cy3Ezr and Cy3D, 105 kDa sign indicates Cy3EzrGFP and Cy3DGFP. EGFP signal is not detectable here, probably because of denaturating conditions of SDS-PAGE for the fluorophore.

To confirm that Cy3 indeed was cross-linked to the N-terminal amino-group, I conducted an enzymatic digestion of the labeled proteins with chymotrypsin. Chymotrypsin cuts preferably at tryptophan, tyrosine and phenylalanine and is expected to cut 68 times in EzrGFP and DGFP and 40 times in ezrin and ezrinT567D (PeptideCutter ExPASy). Immunodetection of the control and digested samples with antibodies against ezrin, eGFP and the T7-tag, which is present at the very N-terminal part of the constructs (see the plasmid maps in Supplemental materials), visualized the chymotrypsin digestion pattern. It

was compared with the pattern of Cy3 fluorescence observed via exposing the same blot membranes to the UV illumination. This analysis showed that Cy3 dye was bound to two sites in the protein: to the very N-terminal amino acid and a, presumably, very active ε-amino group in the eGFP part, as the Cy3 fluorescence coincided either with anti-T7-tag staining or with anti-GFP antibody staining. In the case of Cy3Ezr and Cy3D the Cy3 fluorescence coincides only with the bands detected with anti-T7-tag antibodies but not with anti-ezrin antibodies (the epitope comprises amino acids 479-498 of the ezrin sequence) (Fig.19). This suggests that the dye was bound to the very N-terminal part only.

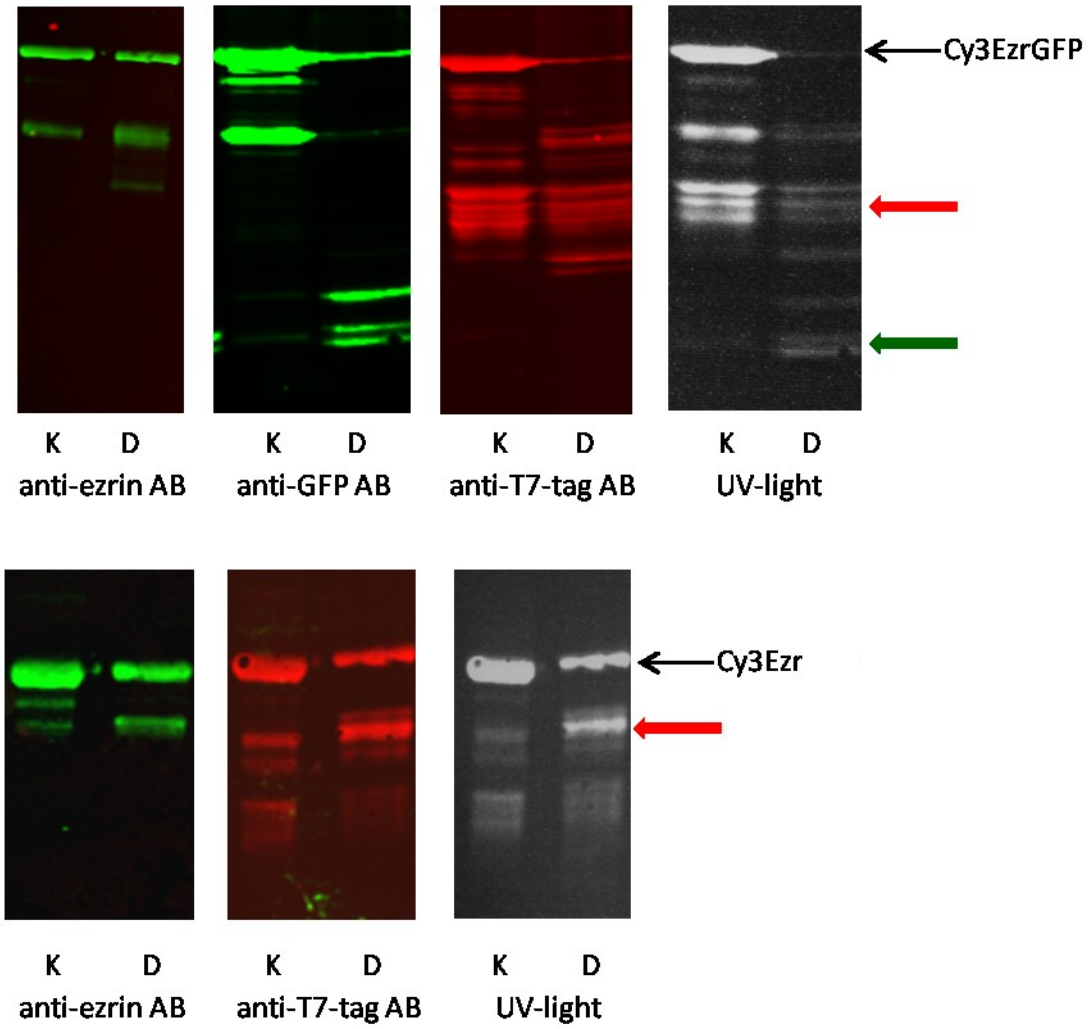

Fig.19. Chymotrypsin digestion of Cy3-labelled proteins. K and D stand for control samples and chymotrypsin digested samples, respectively. The green arrow indicates the bands which were detected in Western blot with anti-GFP antibodies and under UV-light, the red arrow indicates the bands which were detected with anti-T7-tag antibodies and under UV-light. In the control samples: the bands below the Cy3EzrGFP are degradation products. The detection of eGFP and T7-tag with corresponding antibodies was combined in one Western blot membrane, the detection of ezrin were conducted on a separate Western blot membrane.

4.6 Reflectometric Interference Spectroscopy (RIfS) showes binding of the Cy3-labeled ezrin derivatives to PIP_2- and DOGS-Ni-NTA-containing SSLB

RIfS is the physical method for detection of molecular interactions using the interference of white light at the surface. The angle of reflected light beam is dependent on the amount of molecules bound to the surface. Thus the optical thickness of layer bound can be calculated.

A self-assembled RIfS set-up was used in the experiment (see Methods 3.3.11). Briefly, solid supported lipid bilayers (containing 8% PIP_2 or 8% DOGS-Ni-NTA in 92% POPC/DOPC, molar ratios) were formed on hydrophilic wafers in the RIfS flow chamber as described in Methods 3.3.10. The proteins of interest were introduced into the flow system and were circulating until saturation of the receptor lipid was achieved. Fig.20 shows the binding curves at the respectful proteins concentrations. The recordings obtained were similar to the ezrin-wt binding curves (Braunger et al. 2013).

(Fig. 20)

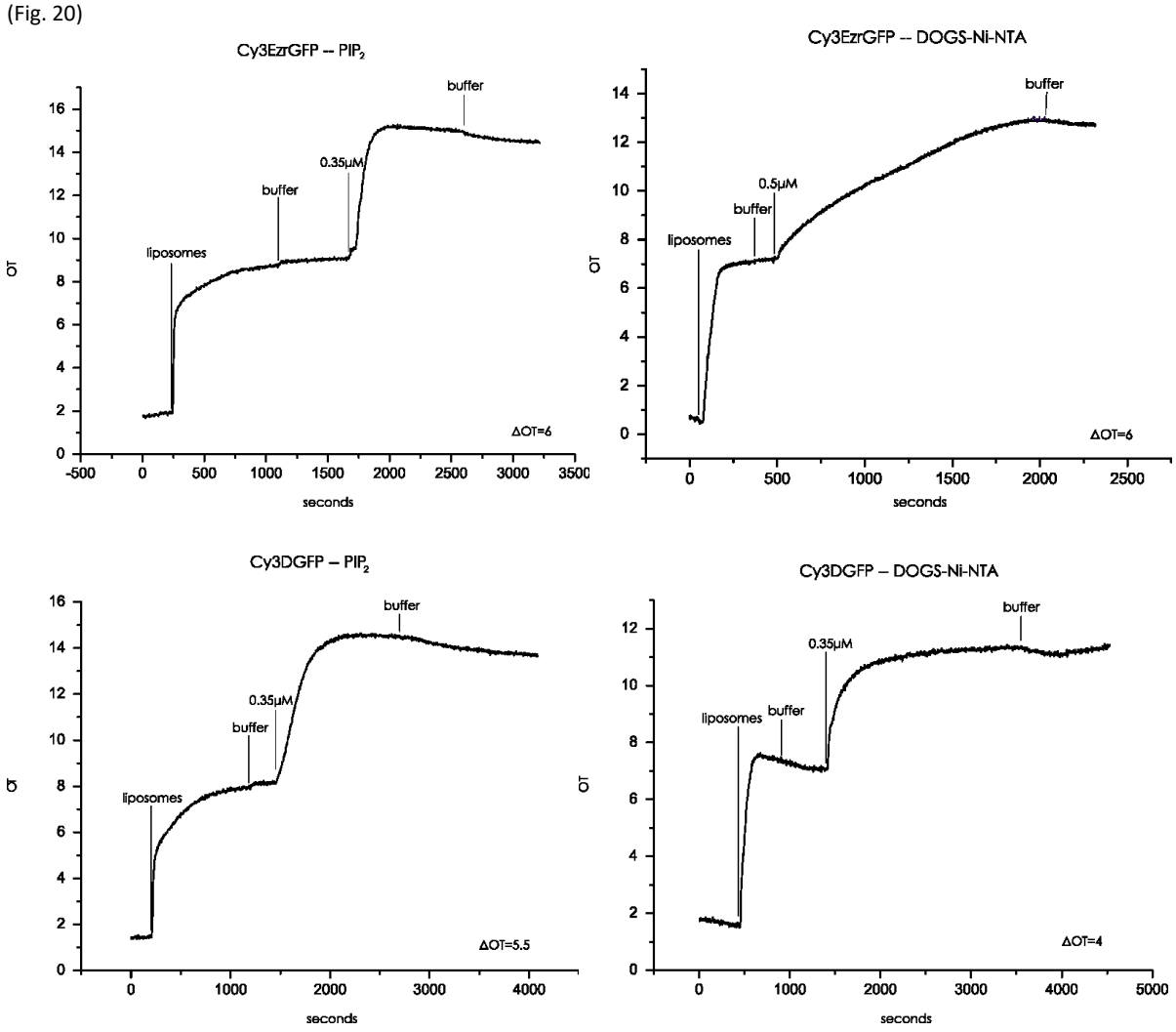

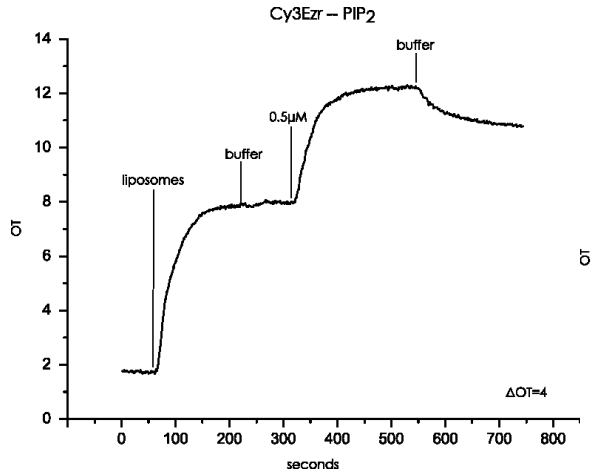
Cy3Ezr – PIP2
buffer
0.5µM
buffer
liposomes
OT
ΔOT=4
seconds

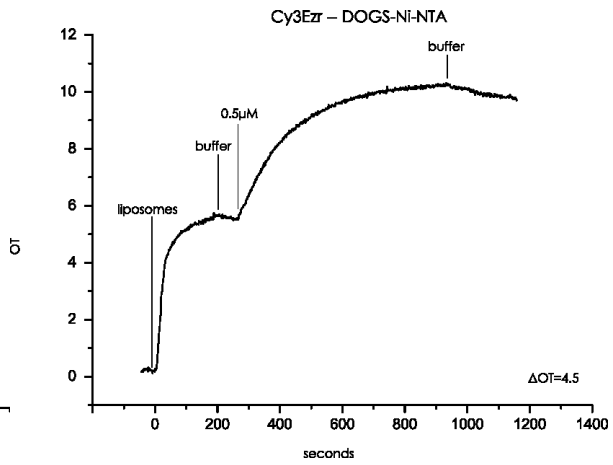
Cy3Ezr – DOGS-Ni-NTA
buffer
0.5µM
buffer
liposomes
OT
ΔOT=4.5
seconds

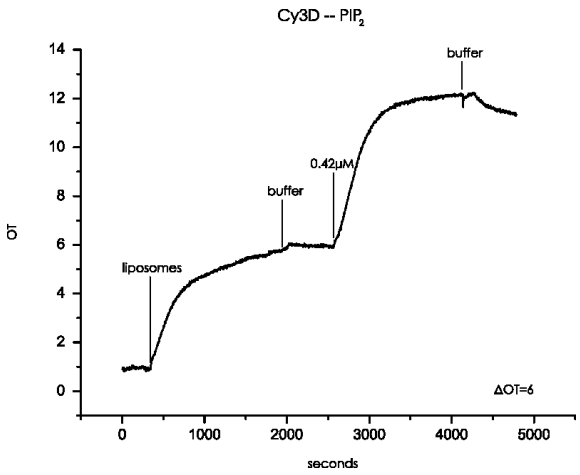
Cy3D -- PIP2
buffer
0.42µM
buffer
liposomes
OT
ΔOT=6
seconds

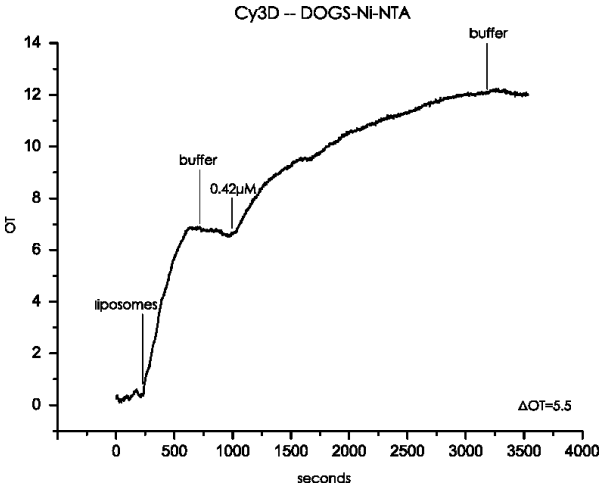
Cy3D -- DOGS-Ni-NTA
buffer
buffer
0.42µM
liposomes
OT
ΔOT=5.5
seconds

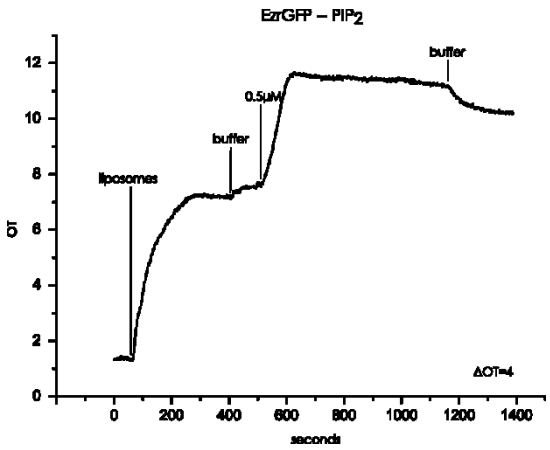
EzrGFP – PIP2
buffer
0.5µM
buffer
liposomes
OT
ΔOT=4
seconds

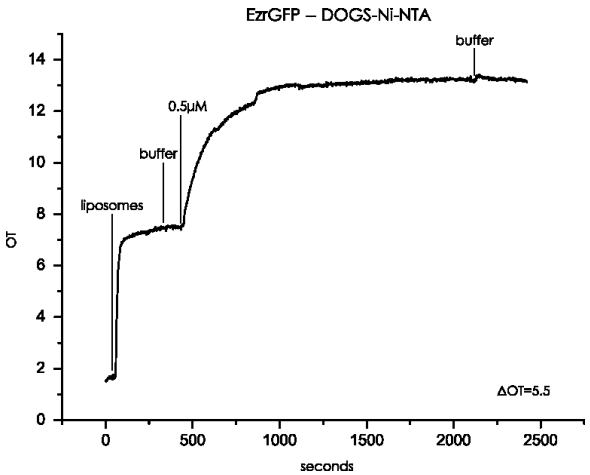
EzrGFP – DOGS-Ni-NTA
buffer
0.5µM
buffer
liposomes
OT
ΔOT=5.5
seconds

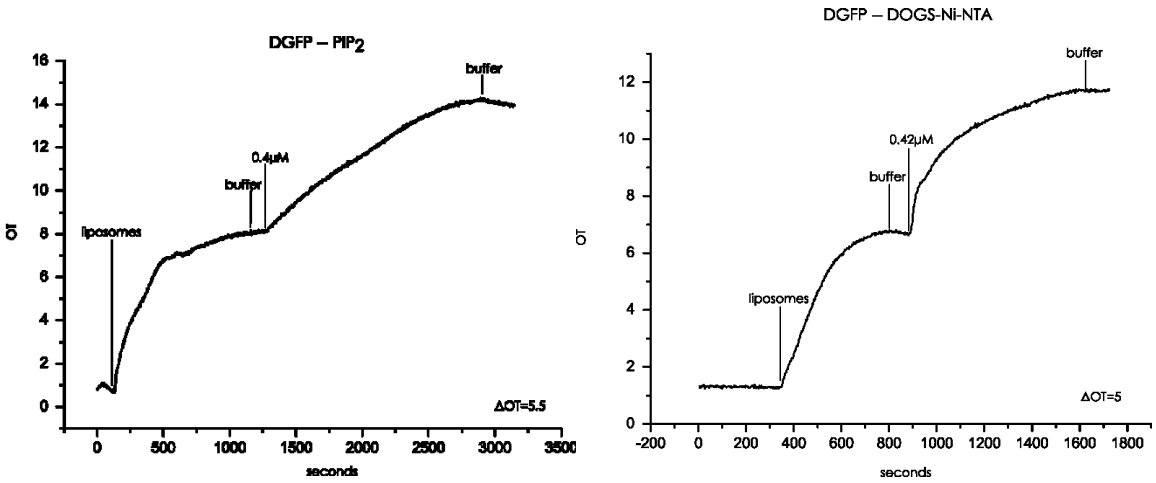

Fig.20. RIfS measurements. Binding of Cy3EzrGFP, Cy3DGFP, Cy3Ezr and CY3D to solid supported POPC/DOPC bilayers containing 8% PIP_2 or 8% DOGS-Ni-NTA. The injection of liposomes into the RIfS flow cell induced formation of a lipid bilayer on silica wafers what is characterized with the first increase of optical thickness, OT, on the graphs. The following addition of the proteins (respective concentrations given) is characterized by the second increase of OT, which showed that the proteins bound to the lipid bilayers.

The binding efficiency, characterized by changes in optical thickness, ΔOT, for all tested constructs ranged from 4 to 6. Cy3DGFP and Cy3Ezr bound to DOGS-Ni-NTA-containing SSLB and Cy3Ezr, EzrGFP bound to PIP_2-containing SSLB showed smaller ΔOT, but the saturation was reached in 200 seconds. The saturation was reached in 1500-2000 seconds in the case of Cy3EzrGFP and Cy3D binding to DOGS-Ni-NTA-containing SSLB and DGFP to PIP_2-containing SSLB. The ΔOT for these constructs was 5.5-6 units. Other binding curves showed fast saturation in 200-500 seconds and ΔOT of 5-6 units (the constructs Cy3EzrGFP, Cy3DGFPCy3D on PIP_2-containing SSLB; EzrGFP, DGFP on DOGS-Ni-NTA-containing SSLB). All Cy3-labeled proteins demonstrated either less steep binding curve or smaller ΔOT on DOGS-Ni-NTA-containing membranes revealing that Cy3 tag might cause the lesser efficiency of the binding to DOGS-Ni-NTA.

4.7 Fluorescent spectra, FRET in solution

To further characterize the fluorescent ezrin derivatives, theirs emissions spectra were recorded on a FluoroMax-2 fluorometer (Instruments S.A.), employing the purified and labeled proteins at the concentration of 0.1 μM.

Cy3Ezr and Cy3D were excited at the excitation maximum of Cy3 – 550 nm, and showed a characteristic Cy3 emission with the main peak at 570 nm and a second minor peak at about

610 nm; EzrGFP and DGFP constructs also showed typical eGFP emission at the excitation at 488 nm, the eGFP excitation maximum (Fig. 21).

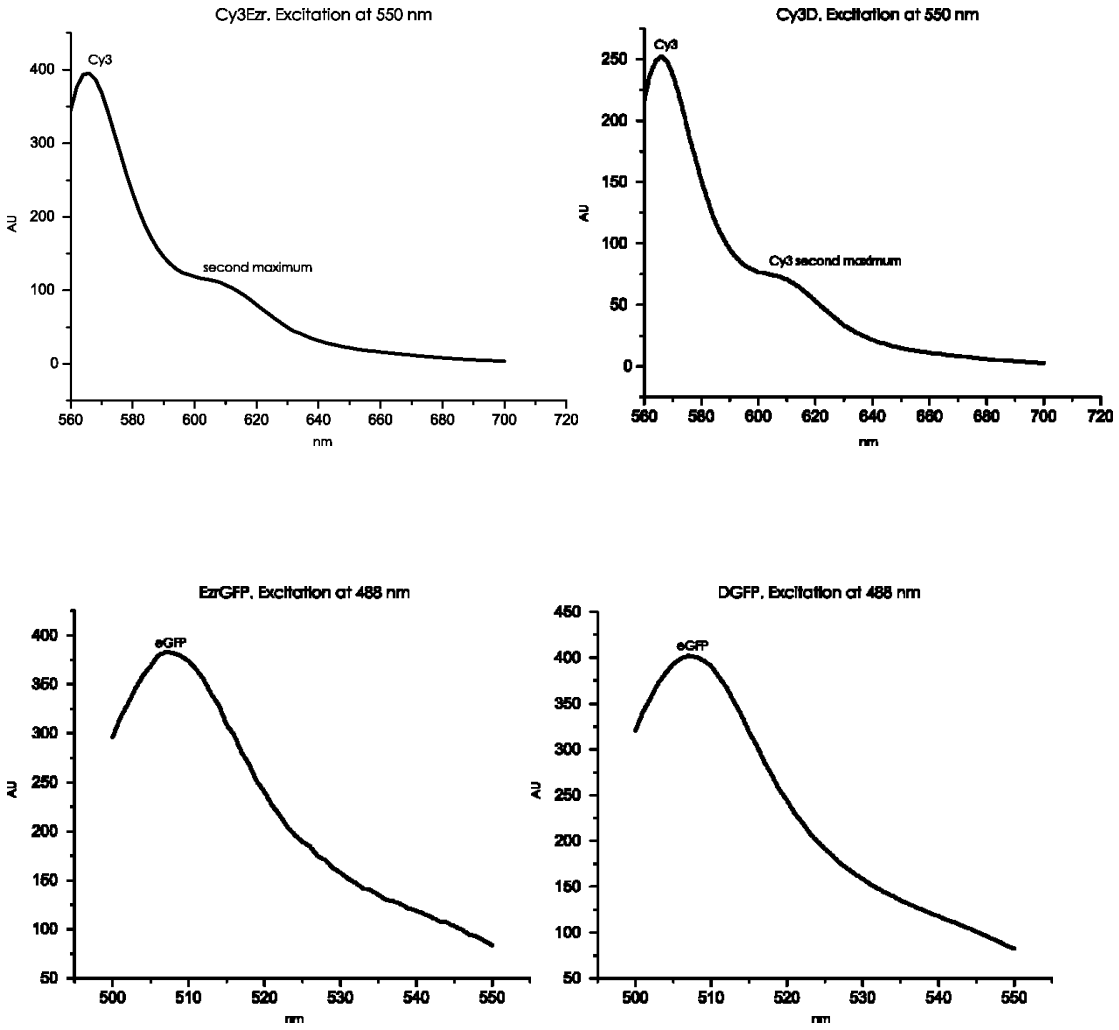

Fig. 21. Fluorometric measurements of the single labeled constructs. Emission spectra of Cy3Ezr and Cy3D, following excitation at 550 nm (excitation of Cy3), and of EzrGFP and DGFP, following excitation at 488 nm (excitation of eGFP) exsibited the characteristic emission peaks for Cy3 and eGFP, respectively.

Cy3EzrGFP and Cy3DGFP samples were excited at eGFP excitation maximum, 488 nm (Fig. 22A). Two emission peaks were detected, corresponding to eGFP emission and Cy3 emission. This Cy3 emission peak corresponded to the FRET signal, although it might also be the result of crossover (or bleed through) due to some minimal Cy3 excitation at 488 nm. Excitation of the same constructs but at the Cy3 excitation wavelength resulted in the much higher Cy3 fluorescence. The emission spectra of Cy3Ezr and Cy3D, excited at 488 nm, were also recorded as controls (Fig. 22B). Detected Cy3 fluorescence was smaller by the factor of

10 than in the double labeled samples, excited at 488 nm. The emission of EzrGFP and DGFP following excitation at 550 nm was not significant (not shown). Therefore, it is likely that some FRET occurs in Cy3EzrGFP and Cy3DGFP in solution, resulting in a Cy3 fluorescence following the excitation of eGFP at 488 nm.

(Fig. 22)

A

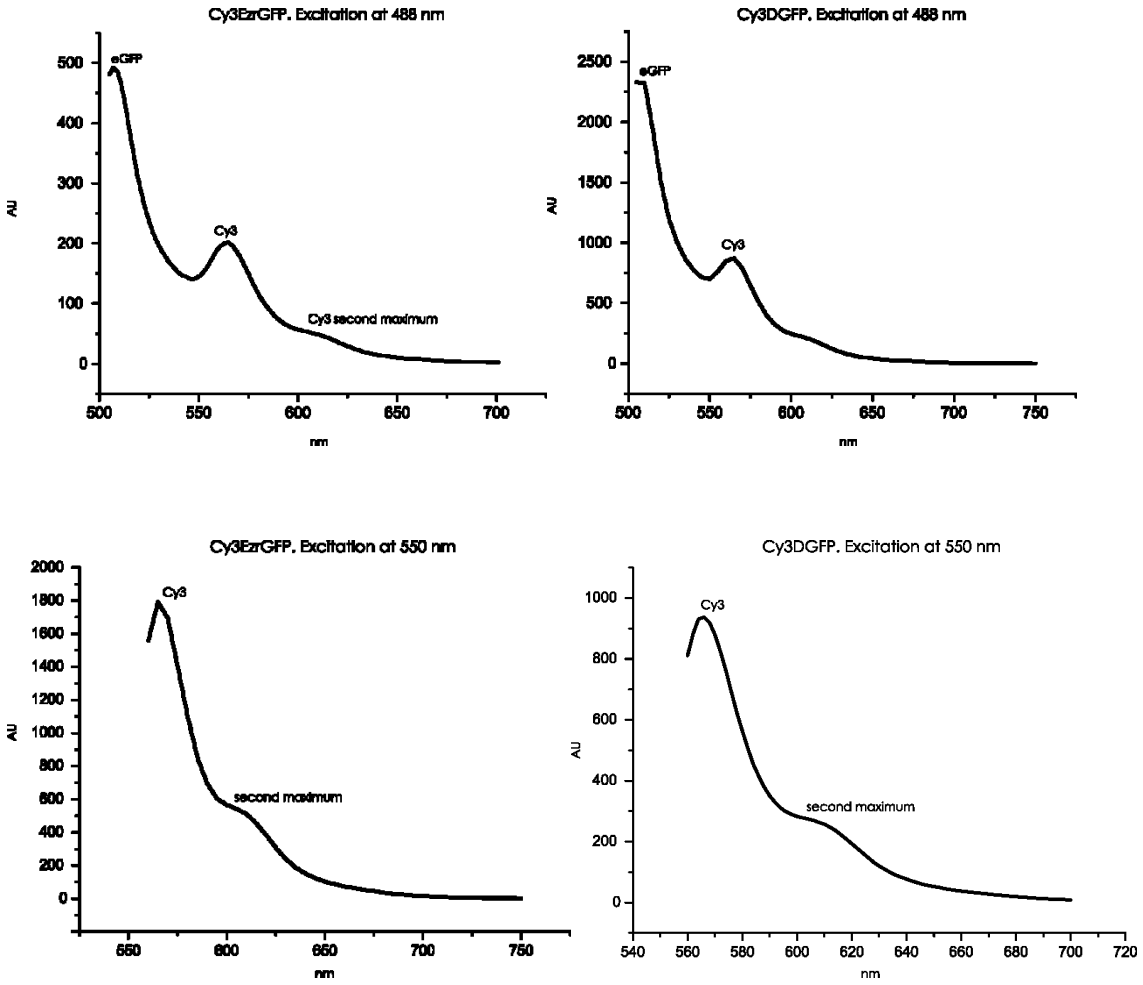

B

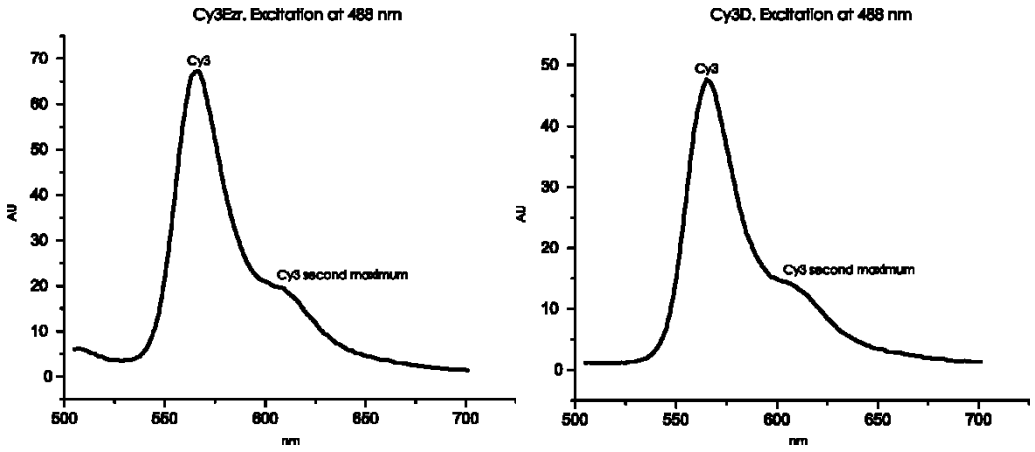

Fig. 22. Fluorometric measurements of FRET. (A) At the excitation at 488 nm Cy3EzrGFP and Cy3DGFP showed two emission maxima that correspond to those of eGFP and Cy3; Cy3 fluorescence detected at the excitation at 550 nm of the same constructs was higher. (B) Cy3 emission of EzrGFP and DGFP following excitation at 488 nm resulted in the minor peaks.

4.8 Analysis of FRET efficiency on solid supported bilayers

The above characterization revealed that ezrin constructs containing a C-terminal eGFP tag and an N-terminal Cy3 label maintain the same properties as wt-ezrin and appear to show FRET between the two fluorophores in solution that suggests the closed conformation. To determine, whether ezrin's conformation changes upon binding to PIP_2 I next performed FRET experiments using fluorescent ezrin constructs bound to artificial lipid membranes spread on silica wafers. The samples were inspected in a LSM 710 microscope (Zeiss). At first, the concentration of 8mol% of PIP_2 in 92% POPC and 8mol% of DOGS-Ni-NTA in 92% DOPC was chosen for the SSLB to achieve full surface coverage of the protein (Herrig et al. 2006). Following protein binding to lipid bilayer FRET was measured by acceptor photobleaching. The increase of donor fluorescence after acceptor photobleaching demonstrates that the donor became "de-quenched" and able to emit light, whilst the acceptor cannot enter the excited state anymore. Fig. 23A shows the typical acceptor bleaching experiment. Here, Cy3EzrGFP was bound to solid a supported membrane containing 8mol% of DOGS-Ni-NTA, therefore the closed conformation and strong FRET were expected. The Region of Interest (ROI) was then subjected to Cy3-acceptor bleaching using laser irradiation at 561 nm. This resulted in decreased red fluorescence (Cy3) and increased green fluorescence of the donor (eGFP) wich gave evidence of acceptor "destruction" and donor being "de-quenched". Thus it appeared that the Cy3EzrGFP construct bound to the DOGS-Ni-NTA-containing SSLB maintained the closed conformation.

The drop in Cy3 fluorescence was calculated as difference between the fluorescence before and after bleaching and given in per-cent of bleaching intensity. In all the measurements the bleaching intensity was kept at 70-80%.

Fig. 23B shows the result of photobleaching Cy3EzrGFP bound to a lipid membrane containing 8mol% PIP_2. As PIP_2 is an activating factor of ezrin and binding to it is expected to lead to conformational changes, a lower FRET intensity was expected. Indeed, the increase of eGFP fluorescence was somewhat reduced when Cy3EzrGFP bound to PIP_2, as compared to DOGS-Ni-NTA. However, FRET still occurred. As ezrin shows high coverage-binding to SSLBs containing 8mol% receptor lipids, FRET could result from inter- as well as from intra-molecular interactions. Therefore, additional controls were included to monitor any inter-molecular FRET. In these experiments two classes of single-labeled ezrin either containing Cy3 ar eGFP label were mixed at a 1:1 molar ratio before binding to a SSLB (Cy3Ezr + EzrGFP or Cy3D + DGFP). When these bound proteins were subjected to the bleaching protocol, an increase of the donor fluorescence after the acceptor bleaching was observed as weel albeit to a lesser extend as compared to experiments employing Cy3EzrGFP (Fig. 24). Thus, the FRET measured in the experiments with double-labeled ezrin molecules (Cy3EzrGFP) most likely consisted of inter- and intra-molecular FRET. To reduce this "background" signal of inter-molecular FRET I switched to lipid membranes containing 4mol% of the receptor lipids, thereby reducing ezrin surface coverage. All further measurements were, therefore, recorded at these new conditions. Five different ROI were randomly chosen on each wafer and FRET was measured by acceptor bleaching. For each of the given conditions the following number of acceptor bleaching experiments was recorded: Cy3EzrGFP/4mol%DOGS-Ni-NTA – 80 scans, Cy3EzrGFP/4mol%PIP_2 – 80 scans, Cy3DGFP/4mol%DOGS-Ni-NTA – 80 scans, Cy3DGFP/4mol%PIP_2 – 50 scans, Cy3Ezr+EzrGFP/DOGS-Ni-NTA – 55 scans, Cy3Ezr+EzrGFP/PIP_2 – 35 scans, Cy3D+DGFP/DOGS-Ni-NTA – 45 scans, Cy3D+DGFP/PIP_2 – 30 scans.

A

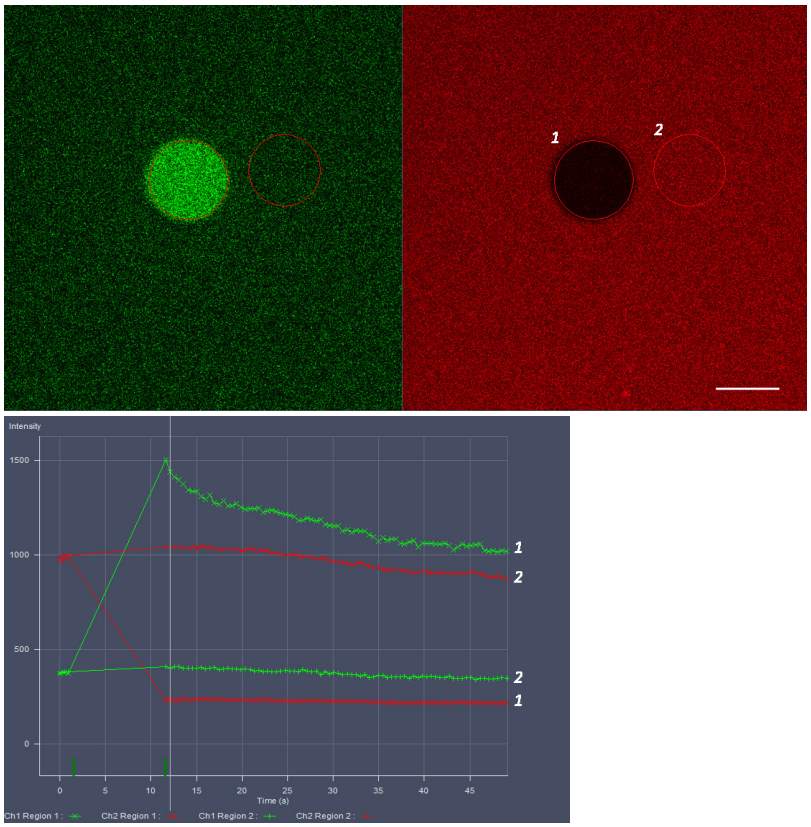

B

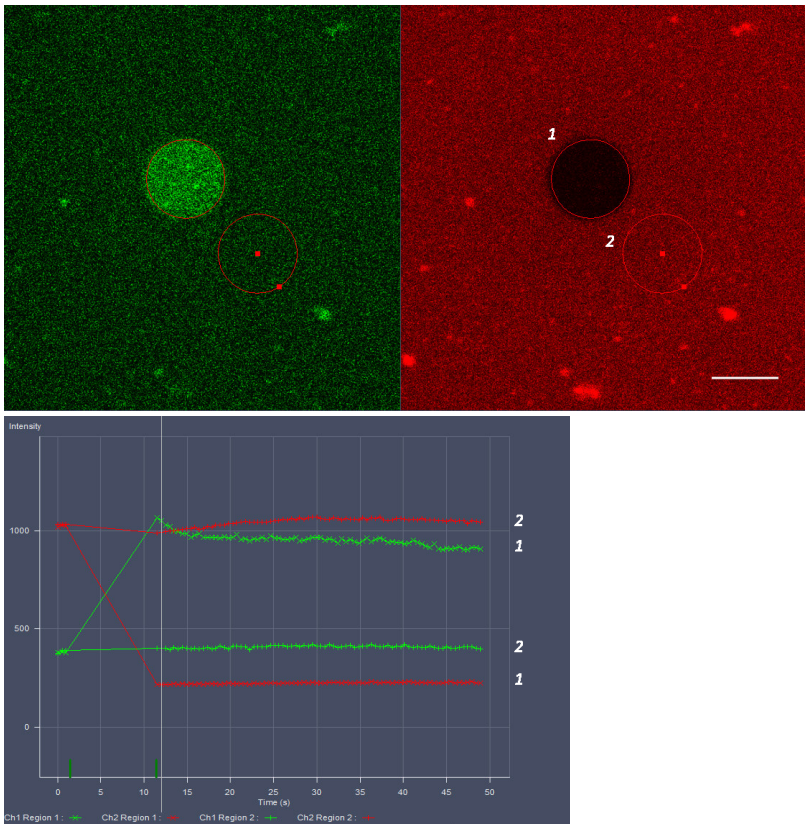

Fig.23. Acceptor bleaching FRET of Cy3EzrGFP, bound to SSLB containing 8mol% receptor lipids. A – Cy3EzrGFP bound to 8mol% DOGS-Ni-NTA-containing SSLB, B – Cy3EzrGFP bound to 8%mol PIP_2-containing SSLB. Circled area 1 is ROI (region of

interest) after CY3 bleaching, circled area 2 is reference area. The diagram depicts the increase of eGFP fluorescence (green line) and the decrease of Cy3 fluorescence (red line), numbers 1 and 2 correspond to ROI and reference area, respectively. The marks at the X axis indicate the start-time and the end-time of the bleach. EGFP fluorescence increase after bleaching of Cy3 appears to be less in case of the protein bound to PIP_2, but a firm conclusion can only be made after statistical analysis of series of experiments. The brighter spots most likely represent aggregates of the protein. ROI avoiding such spots were chosen. Scale bare = 5 μM. Microscope images for other constructs are shown in Supplemental materials, Fig. S2.

A

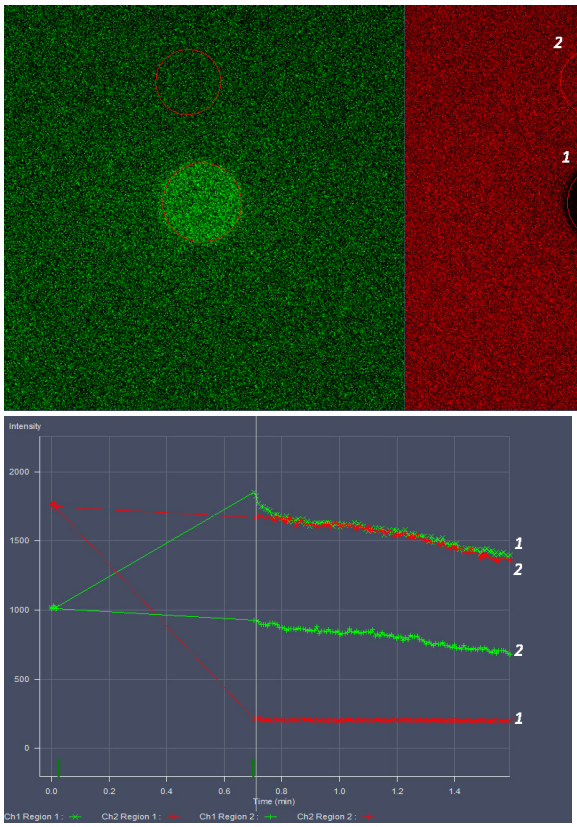

B

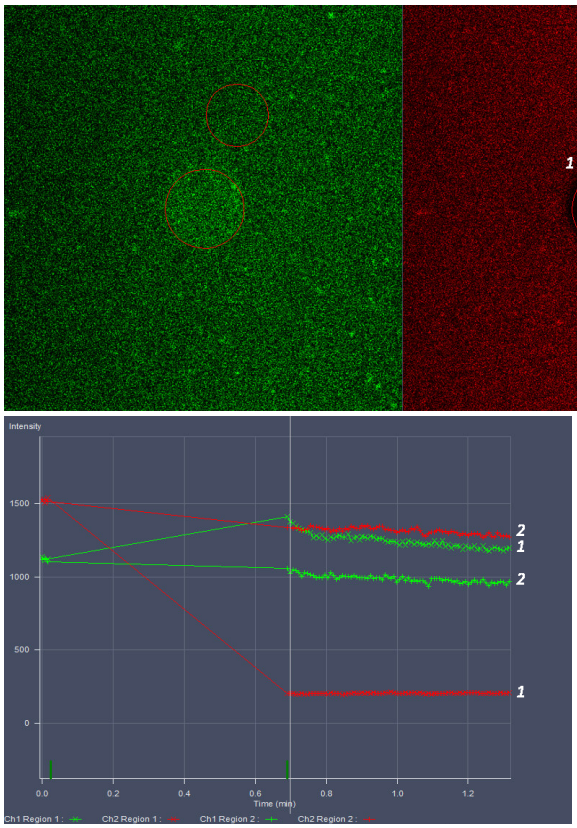

Fig. 24. Acceptor bleaching FRET of the mixture of two single-labeled proteins (Cy3Ezr+EzrGFP), bound to SSLB containing 8mol% receptor lipids. A – Cy3Ezr+EzrGFP bound to 8mol% DOGS-Ni-NTA-containing SSLB, B – Cy3Ezr+EzrGFP

bound to 8%mol PIP_2-containing SSLB. Circled area 1 is ROI (region of interest) after CY3 bleaching, circled area 2 is reference area. The diagram depicts the increase of eGFP fluorescence (green line) and the decrease of Cy3 fluorescence (red line), numbers 1 and 2 correspond to ROI and reference area, respectively. The marks at the X axis indicate the start-time and the end-time of the bleach. EGFP fluorescence increase after bleaching of Cy3 appears to be less in case of the protein bound to PIP_2, but a firm conclusion can only be made after statistical analysis of series of experiments. The brighter spots most likely represent aggregates of the protein. ROI avoiding such spots were chosen. Scale bare = 5 μM. Microscope images for other constructs are shown in Supplemental materials, Fig. S2.

The microscopy scans were processed in ImageJ using FRETcalc plugin which applies pixel-by-pixel analysis and accounts for donor "de-quenching" and bleaching efficiency. Such normalizing allows comparing FRET between samples on different wafers, disregarding minor variations in overall signal intensity and protein binding.

Using this processing tool and analyzing many individual scans on the different wafers, I determined the effect of receptor lipids for all constructs and also compared double-labeled proteins with controls employing the mixture of two single-labeled (Cy3 or GFP) derivatives. The %FRET (FRET efficiency), calculated with FRETcalc-ImageJ, significantly decreased for constructs bound to PIP_2 (mean=18.74879) as compared to contracts bound to DOGS-Ni-NTA (mean= 21.63225), p=9.49e-15. %FRET was almost two times lower for the control samples (Cy3Ezr+EzrGFP and Cy3D+DGFP), mean=12.12861, than for the double-labeled proteins (Cy3EzrGFP and Cy3DGFP), mean=23.93346, p=2.2e-16. P-values were obtained by applying Anova type ll test in R-statistics software on the modeled data which accounts for all conditions of the experiment. The fact that repetitions were carried using proteins with different labeling efficiency was also considered in this modeling by introducing it as another factor in line with the following factors: receptor lipid type, protein type, double labeled/control group.

The box plot in Fig. 25 represents an overview of the series of different experiments. The initial measurements with 8mol% receptor lipids were conducted with a relatively small number of samples. They are included here to demonstrate that %FRET mean values, $\bar{F}$, are similar to those obtained in measurements with 4mol% receptor lipids and, apparently, have great "noise" intra-molecular FRET together with inter-molecular FRET.

A

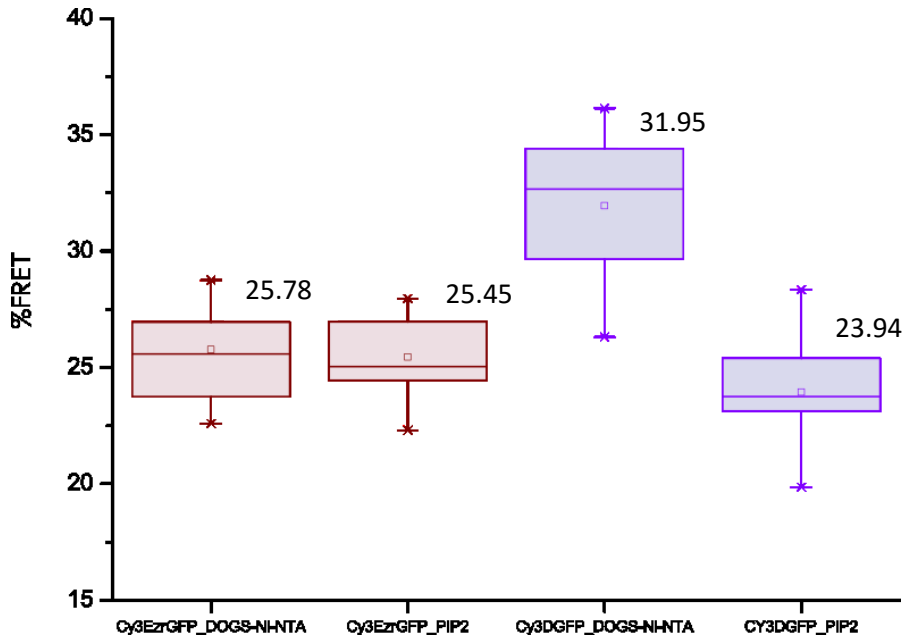

B

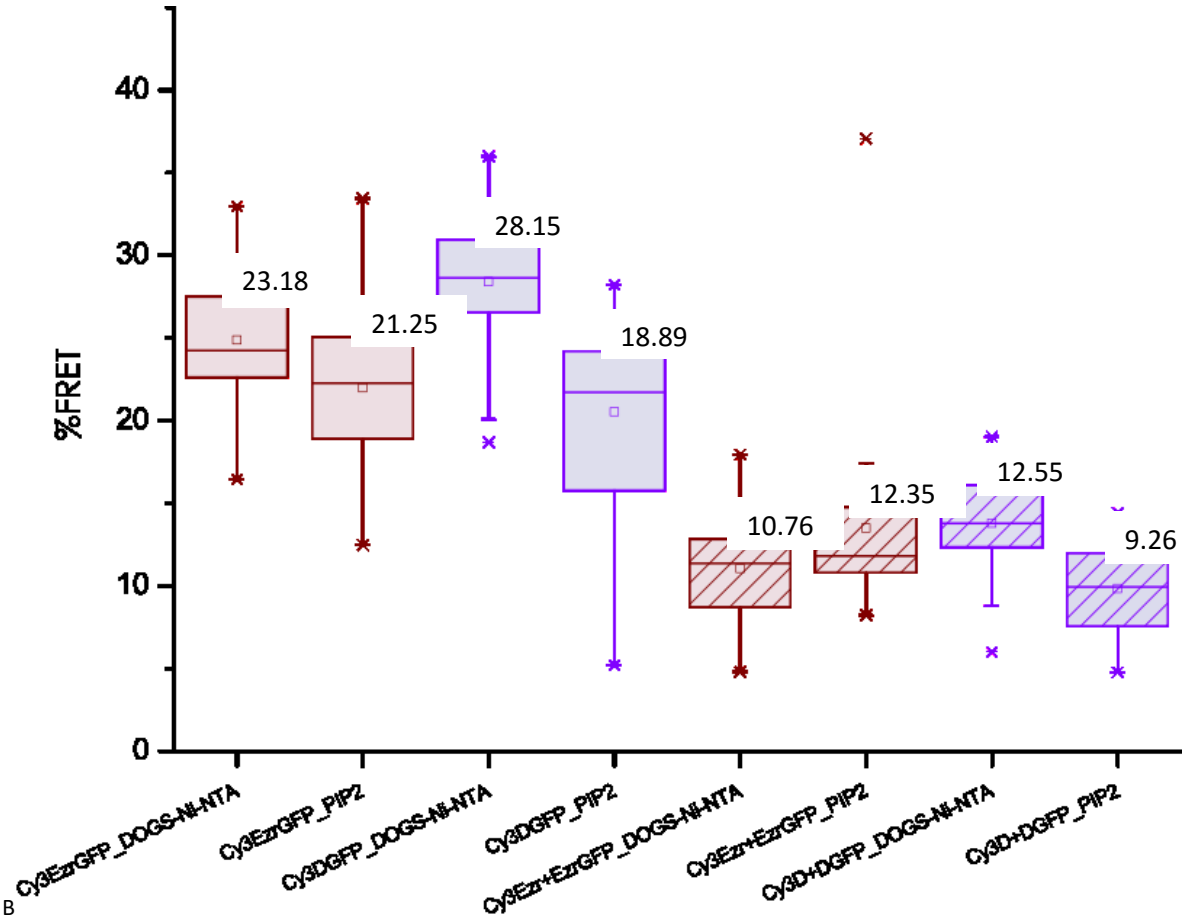

B

Fig. 25. Summary of FRET-CLSM measurements. Mean values are shown next to the boxes. A: Experiments on SSLB comtaining 8mol% receptor lipids. Here, only the Cy3DGFP construct showed a decrease in %FRET when bound to PIP_2, as

compared to the case when bound to DOGS-Ni-NTA. B: Experiments on SSLB with 4mol% receptor lipids. %FRET for control constructs (mixtures of two single-labeled protein species) were significantly lower than for double-labeled proteins, p=2.2e-16. The decrease in FRET upon binding to PIP_2- as compared to DOGS-Ni-NTA-containing lipid membranes was significantly lower in the case of wild type as compared to phosphomimicking constructs.

To estimate the differences between individual groups and compare the wt-constructs to mutant constructs, the delta of mean for each case were calculated using the following formula:

$$\sigma_{Ni-PIP_2} = \bar{F}_{Ni} - \bar{F}_{PIP_2} \pm \sqrt{SE_{Ni}^2 + SE_{PIP_2}^2}$$

where $\delta_{Ni\text{-}PIP2}$ is the difference in %FRET between proteins bound to DOGS-Ni-NTA- and PIP_2-containing lipids bilayers, $\bar{F}_{Ni}$ and $\bar{F}_{PIP2}$ are %FRET averages and SE_{Ni} and SE_{PIP2} represent standard errors. The indexes $_{Ni}$ and $_{PIP2}$ refer to cases where proteins were bound to DOGS-Ni-NTA- and PIP_2-containing lipids bilayers, respectively.
Standard errors were calculated using the following formula:

$$SE = \sqrt{(\frac{\sigma_{Ni}}{\sqrt{n_{Ni}}})^2 + (\frac{\sigma_{PIP_2}}{\sqrt{n_{PIP_2}}})^2}$$

where n_{Ni} and n_{PIP2} are number of measurements for each case.
The $\delta_{Ni\text{-}PIP2}$ value for Cy3EzrGFP is 1.93±0.11 and for Cy3DGFP is 9.26±0.62. For Cy3Ezr+EzrGFP this value is -1.59±0.08 and for Cy3D+DGFP it is 3.29±0.19.
The data analysis suggested that inter-molecular FRET was significantly lower than intra-molecular FRET, interestingly, double-labeled proteins and mixture of single-labeled proteins showed similar tendency towards bigger decrease of %FRET when bound to PIP_2-containing SSLB.

5 Discussion

Ezrin serves in the cells as an intermediary between plasma membrane and cytoskeleton during cells movement, division and formation of apical actin-rich structures. Its disregulation leads to severe consequences, for example, polarity loss in developing embryo, increase of metastatic mobility in cancer cells, and disruption of microvilli arrangement (Fehon, McClatchey, and Bretscher 2010). The transition between the inactive and active state of ezrin, essential for its functioning, is thought to be mediated by PIP_2 binding at the membrane and phosphorylation at the conservative threonine 567. FRET experiments using solid supported lipid bilayers (SSLB) were performed in this work to elucidate the mechanism of ezrin conformational changes and correlation between the two activating factors. These experiments are the first demonstration of FRET with the use of the double-labeled fluorescent ezrin constructs bound to SSLB. The in vitro model applied in this work offers the advantage of tightly controllable activation conditions, as compared to cellular in vivo models. The combination of ezrin-wt and ezrin T567D constructs that were analyzed on PIP_2- and DOGS-Ni-NTA-containing supported membranes were explored here in the FRET studies. It was demonstrated that the phosphomimicking mutation and binding to PIP_2 together caused the most pronounced conformational changes in ezrin.

S100P protein as activation factor of ezrin is not discussed here as it can be considered as analogous to the PIP_2 binding and, supposably, changes the protein conformation in a similar way. The unphosphorylatable ezrin T567A mutant was also excluded from the experiments as it had not shown significant differences to ezrin wild type in any conditions investigated (Bosk et al. 2011; Braunger et al. 2013).

5.1 GFP-tag does not change properties of ezrin in the cells and in in vitro binding assays

Two ezrin constructs fused with different flourescent proteins were generated and used in the thesis: YFPEzrCFP, human ezrin fused with N-terminal YFP and C-terminal CFP tags; and EzrGFP, human ezrin with C-terminal GFP. GFP-tagged ezrin-wt (EzrGFP) and also the T567D mutant (DGFP) could be successfully expressed BL21 strain of E.coli and purified via the His-tag. Recombinant expression and especially purification of the proteins fused with a fluorescent protein is not always a trivial procedure, as GFP (or its variants) can impede folding process and induce protein degradation. This could explain that YFPEzrinCFP was impossible to purify from BL21 bacterial cultures, as only a truncated His-tagged protein could be eluted from the beads functionalized with Ni-NTA. This truncated protein was detected also in immunoblots of E.coli lysates using anti-ezrin and anti-GFP antibodies (that

also recognize YFP and CFP) indicating that the integrity of YFPEzrCFP was already disturbed within the bacterial cells. The possible reason, besides abnormal folding, could be the difference in codon usage between mammalian cells and bacteria. Rosetta strain of E.coli is created to avoid such incompatibility. It has seven tRNAs not typical for E.coli that enables the bacterial translational machinery to recognize amino acids adapted for eukaryotic expression. As eYFP and eCFP sequences used for molecular cloning of the pET28a(+)YFPEzrCFP plasmid were adopted from eukaryotic plasmids, it is possible that YFPEzrCFP can be problematic for the expression in bacteria. (It is important to notice, pE28a(+)ezrin and pE24b(+)eGFP plasmids for prokaryotic expression were used for the design of the pET28a(+)EzrGFP/DGFP plasmid). Therefore, the Rosetta strain was exploited here, but still only the truncated protein could be obtained. The phenomenon of intrinsic transcription termination in prokaryotes could also impede the recombinant expression: specific cytosine-guanine rich RNA spikes followed by several uracils can cause stalling and subsequent dissociation of the RNA polymerase complex. So far, there are no reports of YFP-CFP double-labeled proteins expressed recombinantly in bacteria, although an expression of a YFP-ezrin-CFP construct in HeLa cells was performed successfully by Zhu et al. (Zhu, Liu, and Forte 2005). Therefore mammalian HEK293T cells were chosen for the expression of YFPEzrCFP, as this cell line is often used for recombinant protein expression and purification, the pE-HisTag-YFPEzrCFP plasmid was designed for the purpose. The plasmid carried the G418 antibiotic resistance gene, and HEK293T cells possess the same antibiotic resistance. Nevertheless, it was still possible to obtain stably transfected cell lines with the use of the relatively high G418 concentrations (1.4 μg/ml). For comparison, HEK293 cell line, lacking G418 resistance, are usually killed by 200-500 μg/ml of the antibiotic (http://www.invivogen.com/PDF/G418_TDS.pdf). Although the sensitivity of the selected clones to G418 decreased within 6-8 weeks leading to domination be the plasmid-free cells (monitored by recording the YFP-signal). Repetitive subcloning was necessary to keep the pEYFPEzrinCFP-HEK293T cell line. Intact HisTag-YFPEzrCFP protein was purified, as revealed by its integrity shown in Western blot analysis (Fig. 10). However, the yield was too low for the experiments planned. Therefore, only EzrGFP and DGFP purified from E.coli BL21 strain were used further in this work.

The behavior of EzrGFP and DGFP was tested in the cells. Figures 13 to 15 depict EGF stimulation experiments with A431 cells. Upon stimulation cells formed membrane protrusions and EzrGFP and DGFP demonstrated accumulation at these protrusions; similar behavior was observed for ezrin endogenously expressed by A431 cells. Ezrin labeled with GFP at the C-terminus demonstrated a cell distribution similar to endogenous ezrin also in NIH3T3 fibroblasts and HtTA-1 cells as shown by Amieva et al. and Henry at al. (Amieva et al. 1999; Henry, Gonzalez Agosti, and Solomon 1995). Interestingly, Zhu et al. reported that YFP-ezrin (N-terminal tag) had a tendency of cytoplasmic localization in HeLa cells, while ezrin-CFP (C-terminal tag) and the wild type protein concentrated at the membrane (Zhu, Liu, and Forte 2005). Apparently, the N-terminal fluorescent protein tag, in contrary to the

C-terminal tag, can impede PIP_2-binding. Quantification of EzrGFP and YFPEzrGFP binding to PIP_2, in comparison to DOGS-Ni-NTA binding, was done here by analyzing the results of liposomes pelleting assay. The co-sedimentation tendency suggested that the two fluorescent chimeras and ezrin-wt bind more efficiently to the liposomes containing DOGS-Ni-NTA lipids, than to those containing PIP_2 (Fig. 12). That reflects an easy accessibility of the N-terminal His-tag in all tested proteins. In the case of the binding to PIP_2-containing liposomes approximately 42% of EzrGFP and 50% of ezrin-wt were detected in the pellet fractions, indicating that the GFP tag only slightly inhibits PIP_2 binding of ezrin. In contrast, only approximately 32% of YFPEzrCFP bound to PIP_2-containing liposomes. Thus, the YFP and CFP tags together had more influence on the ability of ezrin to bind PIP_2 but did not supress it completely. In the experiments performed by Zhu et al. in HeLa cells the majority of YFP-ezrin did not bind to the membrane. Such discrepancy could be explained by the higher concentration of the PIP_2 lipid in artificial liposomes than in the cell membrane.

5.2 Properties of Cy3EzrGFP and DyLight405EzrGFP as FRET constructs

Easy accessibility of commercial chemical fluorophores allowed choosing different FRET pairs for eGFP. Two fluorescent dyes, Cy3 NHS ester and DyLight405 maleimide, were tested here. The chemical targets of maleimides are cysteine residues of proteins; molecules functionalized with NHS ester moieties can react with amino-groups. For the design of ezrin-FRET construct it was required to attach the second fluorophore to the N-terminal end of EzrGFP. In the case of Cy3 NHS ester, the preferable labeling of the α-amino group was achieved by performing the reaction at acidic pH: as α-amino group has the properties of a stronger acid than side chain amino groups, it will react with esters in acidic conditions more efficiently than the other. The labeling was confirmed by reading absorption spectra of the resulting products (see Supplemental materials, Fig. S1). To confirm that the label had attached specifically to the N-terminus, the product was digested with chymotrypsin and the resulting fragments were probed with anti-T7-tag antibodies in Western blots (the T7-tag was encoded between the His-tag and ezrin). Illumination of this Western blot membrane with UV-light revealed that Cy3-fluorescent bands coincided with the anti-T7-tag signal indicating that the N-terminal amino group was specifically labeled (Fig. 19). The obtained Cy3EzrGFP and Cy3DGFP constructs were also tested with respect to their binding to PIP_2 and DOGS-Ni-NTA lipids using RIfS (Reflectometric Interference Spectroscopy).

RIfS can estimate amount of proteins bound to solid supported membranes by detection and analysis of multiple reflection of white light from the sample. Fig. 20 shows binding of the Cy3-labeled ezrin derivatives to PIP_2- and DOGS-Ni-NTA-containing SSLB. The binding of EzrGFP and DGFP proteins was also measured to compare the behavior of the double-labeled and the single labeled constructs. The value obtained in this thesis is in the same range with the RIfS measurements performed by Braunger et al. with ezrin-wt (Braunger et

al. 2013). EzrGFP and DGFP showed attenuated binding to PIP_2 lipids, but at the same time Cy3EzrGFP and Cy3DGFP had normal binding curves for PIP_2-containig SSLB. To summarize, Cy3 and GFP tags did not have strong effect on ezrin binding to PIP_2- or DOGS-Ni-NTA-containing solid supported membranes measured by RIfS technique, as all the constructs tested by RIfS could form stable protein layer after 40 minutes maximum. Correspondingly, binding of the proteins to SSLB for the further FRET experiments were performed at incubation time of more than 12 hours to avoid any binding deficiencies. Ezrin wild type and phosphomimicking mutants did not reveal any differences in binding in the RIfS trials.

Ezrin has two cysteins in N-ERMAD at position 117 and 284 that are apparently available for chemical modification (Bosk et al. 2011); they could be potential loci for attachment of DyLight405 for creating a construct for intra-molecular FRET. For that reason the DyLight405EzrGFP construct was also tested in this work. FRET was not detected in experiments with DyLight405EzrGFP bound to SSLB via its His-tag. The explaination could be the unfortunate positioning of the DyLight405-donor on the DyLight405EzrGFP molecule bound to SSLB and/or an exceeding of the Forster distance; or else DyLight405 and GFP do not possess qualities of a FRET pair. FRET measured by fluorometry (Fig. 17) was probably caused by the direct excitation of the acceptor. Moreover, DyLight405-eGFP has not been mentioned anywhere in the literature as the successful FRET pair.

5.3 PIP_2 binding and threonine 567 phosphorylation contribute to conformational change in ezrin simultaneously

FRET experiments with the fluorescent ezrin were first performed in solution. FRET signal was observed at the excitation of Cy3EzrGFP and Cy3DGFP at 488 nm (the donor excitation wavelength). Similar to this, FRET signal in solution was recorded by Zhu et al in the lysates of HeLa cells expressing YFP-ezrin-CFP construct (Zhu, Liu, and Forte 2005). The precise FRET calculations were made during the FRET-LSM experiments with the fluorescent ezrin constructs bound to the solid supported membranes, where FRET was also confirmed by acceptor bleaching. The acceptor bleaching technique was used in this study, as there are no time restrictions; the chosen acceptor, the Cy3 fluorescent dye, is easy to bleach but stable enough for longer measurements.

The first experiments were conducted with 8mol% of the receptor lipids PIP_2 and DOGS-Ni-NTA in the SSLB (Fig. 23, 24). They showed high levels of inter-molecular FRET signals, apparently occurring between neighboring molecules. One ezrin molecule occupies at least 70x70 Å area on the SSLB (the size of the N-ERMAD (K Hamada et al. 2000)) and the area per lipid for PIP_2 equals 70 $Å^2$ (Janke et al. 2008), for DOGS-Ni-NTA it is around 65 $Å^2$ (Körner et al. 2013). Assuming that the protein concentration is large enough to occupy all binding sites on the artificial membranes, it is possible to calculate that at the receptor lipids

concentration of 8mol% at least 6 molecules of PIP_2 or DOGS-Ni-NTA are arranged underneath one ezrin molecule. At a concentration of 4mol% - at least 3 lipid molecules could be associated with the bound ezrin. On practice ezrin showed poor binding to solid supported membranes with PIP_2 concentration less than 3mol% (Herrig et al. 2006). Therefore, the protein density on the lipid surface is high enough for inter-molecular FRET to occur at the available experimental conditions. Thus, 4mol% concentrations of PIP_2 and DOGS-Ni-NTA were accepted as most reasonable for the experiments in this study.

To determine the contribution of inter-molecular FRET signal under these conditions, equimolar mixtures of Cy3Ezr+EzrGFP and Cy3D+DGFP were used as controls. In this case the measured FRET efficiency was by a factor of two lower than that for the double-labeled constructs (Fig. 25). Thus, in the case of the double labeled Cy3EzrGFP and Cy3DGFP the FRET signal measured comprised the sum of intra- and inter-molecular FRET, i.e. FRET between Cy3 and eGFP of a single molecule and of two neighboring molecules. Similarly, inter- and intra-molecular FRET signals were detected by Zhu et al. in HeLa cells expressing YFP-Ezrin-CFP (Zhu, Liu, and Forte 2005). In this paper the level of inter-molecular FRET was significantly smaller than that of intra-molecular FRET, too. The question of conformational changes was not investigated in their experiments, since PIP_2 binding and phosphorylation rate could not be controlled due to complex processes which occur in the cell.

Acceptor bleaching experiments, conducted with ezrin derivatives (wild type and T567D mutant) bound to PIP_2-containing SSLB (thus presumably in a partly activated conformation) and proteins bound to DOGS-Ni-NTA-containing SSLB (thus presumably in a non-activated state) revealed that PIP_2 binding had the most prominent conformational effect on the pseudo-phosphorylated ezrin constructs (T567D constructs). A drop in the FRET signal most likely represents an increase in the distance between N-terminal Cy3 and C-terminal eGFP, i.e. a conformational change caused by the dissociation of ezrin's N-ERMAD and C-ERMAD. The decrease in FRET between Cy3DGFP bound to DOGS-Ni-NTA and to PIP_2 constituted 9.26% ±SE=0.62, whereas Cy3EzrGFP only showed a minor change in FRET efficiency between its PIP_2-bound and DOGS-Ni-NTA bound states, 1.93% ±SE=0.11 (Fig. 24). The decrease in the FRET efficiency for the mixture of Cy3D+DGFP was estimated to be 3.29% ±SE=0.19; and the mixture Cy3Ezr+EzrGFP even demonstrated a slight increase in FRET efficiency when bound to PIP_2-containing membranes, the value was -1.59% ±SE=0.085. These data are in agreament with the study by Bosk et al., in which the ezrin T567D mutant, too, revealed the most stricking increase in acting binding efficiency when immobilized on PIP_2 containing SSLB. In this case actin binding can be veiwed as an indicator of the conformational change as it is only observed in the active state (Bosk et al. 2011). The colloidal probe studies by Braunger et al. (Braunger et al. 2014) showed the different aspect of synergism of the activation factors, in particular, that the ammount of ezrin-actin bonds was strongly increased upon PIP_2 binding, while the phosphomimicking state of the protein caused only minor changes in the ability to bind actin. Interestingly, the strenght of a single

ezrin-actin bond was found equal in all experemintal conditions and estimated around 50 pN (Braunger et al. 2014). Altogether, these findings are in line with the two step ezrin activation model: 1 - PIP_2 binding is required to make the C-terminal threonine accessible for phosphorylation, 2 – threonine phosphorylation induces and/or stabilizes the active state. But it seems that the role of PIP_2 might be expanded, as the conformation of the ezrin phosphomimicking mutant bound to DOGS-Ni-NTA-containing SSLB did not seem to be different from that of the wild type construct in the same conditions, judging from the FRET experiments. Probably that PIP_2 binding, together with the C-terminal threonine phosphorylation, contribute to "pushing" N-ERMAD away from C-ERMAD.

Membrane bound ezrin was characterized to be often present in an oligomeric, non active form (Fritzsche et al., 2014; Zhu et al., 2005). This is in agreement with the report of Coscoy et al. about the excistence of an intermediate ezrin state. They proposed that four ezrin forms excist in the cell: an *inactive cytoplasmic form*; ezrin *bound to the membrane* via PIP_2, this could be present in oligomeric forms; ezrin *bound to the membrane and actin*, i.e. fully activated; and an ezrin *intermediate form* that can transiently interact with actin only for a short time (Coscoy et al., 2002; Fritzsche, Thorogate, & Charras, 2014). This transient interaction is supposed to be maintained by additional acting binding sites which were discovered in the N-ERMAD (Roy, Martin, and Mangeat 1997), see also Fig.26.

The ability of the intermediate, not fully activated form of ezrin to bind actin filaments explains the relatively high actin binding activity of the wild type ezrin in the study of Braunger et al. It is probable that the exploited in their work conditions promoted the formation of actin-ezrin bonds because of the excess of actin filaments and ezrin molecules in the system. Thus, a minor contribution from the wild type form could be overstated at some extend. Thus, even inactive ezrin T567A mutant attached to SSLB was reported to have some actin binding activity (Bosk et al. 2011). The FRET experiemnts performed in this thesis reflect not the binding activity, the quantitative characteristics, but the conformational state of ezrin molecule, a qualitative feature. Although the calculation of FRET efficiency in this work was also complicated because of the high density of the FRET units on the lipid surface. Our data suggest that a fully open ezrin conformation is achievable only in the simultaneous presence of PIP_2 and C-terminal threonine phosphorylation. The ezrin-wt constructs showed little differences between PIP_2-bound and DOGS-Ni-NTA-bound forms, suggesting that PIP_2 binding alone is not sufficient to fully disrupt the N-C association. The observed decrease in FRET for the wild type ezrin bound to PIP_2-containing lipid membranes could also be explained by the excistance of the intermediate ezrin form. The unstaible conformational changes induced by PIP_2 binding could still cause moving the FRET donor away from the FRET acceptor at some extent.

This thesis and other recent studies demonstrated that the activation mechanism of ezrin is a rather complex process regulated by many factors. PIP_2 mediates cell membrane localization of ezrin, its binding makes threonine 567 available for kinases (Rho kinase, PKC)

and the phosphorylation at this residue in turn leads to dissociation of C-ERMAD and N-ERMAD of ezrin. The fully open conformation of ezrin is then stabilized by binding to actin filaments via C-ERMAD and interaction with membrane proteins via N-ERMAD (CD44, PDZK1 ect.). Some membrane proteins may form signalling complexes with ezrin providing highly tuned coordination of membrane-cytoskeleton interactions. Phosphorylation/dephosphorylation cycles at threonine 567 as well as regulation of PIP_2 concentration (e.g. by phospholipase C) in the membrane are also important factors that influence the ezrin activation-deactivation processes. The existance of inactive or partually activated ezrin at the membrane suggests that C-terminal phosphorylation acts as a trigger that switches membrane bound ezrin into an active, membrane-and-actin bound state; this allows regulation of cell cortex organization in a fast and reversible manner. However, further experiments that combine the FRET method established here and AFM technique of measuring adhesion forces of ezrin-actin binding are required to confirm the hypothesis of the intermidiate ezrin state. In particular, protein samples that demonstrated FRET when bound to SSLB could be directly tested on the ability to bind actin. Actin filaments attached to the AFM cantilever would be a convenient model for this. The correlation between FRET efficienies and actin binding efficiencies detected from the same samples could elucidate the question of the correlation between the ezrin conformation and its interaction with actin filaments. Another factor of ezrin activation should be tested in the future: S100P protein that was proposed as the third activation factor and the competitor of PIP_2 (Austermann et al. 2008).

The investigation of factors that recruite ezrin to the membrane is another future direction of research into the ezrin activation mechanism. It is important to know what stimuli initiate and also supress ezrin binding to the membrane and actin as well as to understand the events successive to the interaction of ezrin with its binding partners. For example, there are some evidences suggesting that ezrin may participate in actin polimerization (Crepaldi, Gautreau, Comoglio, Louvard, & Arpin, 1997; Naba, Reverdy, Louvard, & Arpin, 2008). Moreover, many studies showed an involvement of ezrin in cellular signalling via its membrane interactions, but underlying mechanisms is not fully understood. The future investigations in this direction together with additional findings about the mechanism of ezrin activation will provide us with the important knowledge in the field of actin-membrane interaction.

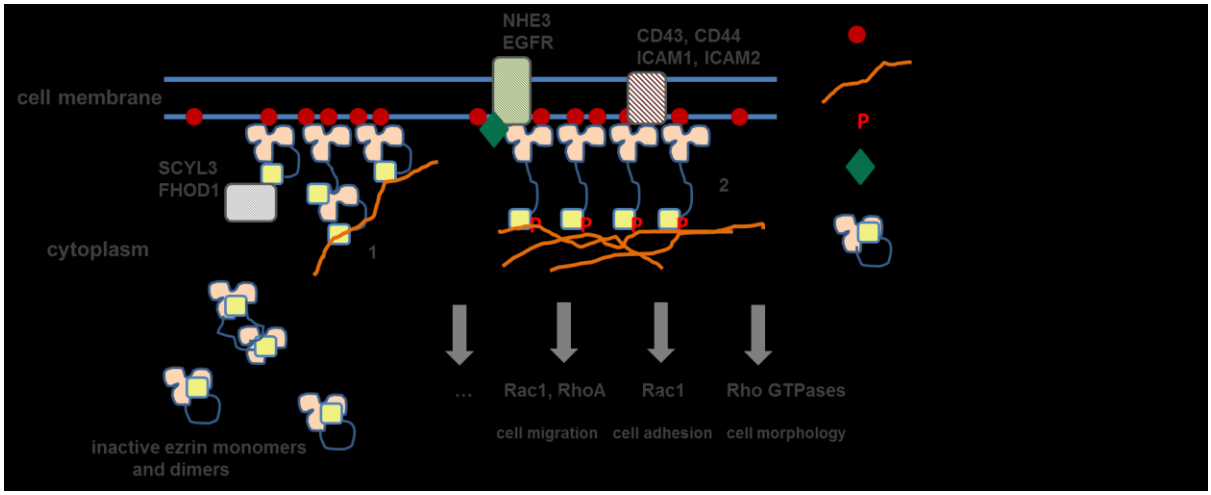

Fig. 26. Proposed scheme for ezrin conformational states in the cell. Inactive ezrin molecules can relocolize from the cytoplasm to the membrane (1), where they bind to PIP_2 molecules and are capable of transient actin binding. Few proteins were shown to bind to C-ERMAD of not fully activated ezrin, for example SCYL3 and FHOD1. Ezrin can then transit to a membrane-and-actin bound state (2) which is characterized by threonine 567 phosphorylation in ezrin and its interactions with membrane proteins via N-ERMAD and actin filaments via C-ERMAD. Membrane proteins can bind directly to ezrin or via the EBP50 protein. Arrows indicate other processes with ezrin participation.

References

Adada, Mohamad M, Daniel Canals, Nara Jeong, Ashwin D Kelkar, Maria Hernandez-Corbacho, Michael J Pulkoski-Gross, Jane C Donaldson, Yusuf A Hannun, and Lina M Obeid. 2015. "Intracellular Sphingosine Kinase 2-Derived Sphingosine-1-Phosphate Mediates Epidermal Growth Factor-Induced Ezrin-Radixin-Moesin Phosphorylation and Cancer Cell Invasion." *FASEB Journal : Official Publication of the Federation of American Societies for Experimental Biology*, July. doi:10.1096/fj.15-274340.

Algrain, M, O Turunen, A Vaheri, D Louvard, and M Arpin. 1993. "Ezrin Contains Cytoskeleton and Membrane Binding Domains Accounting for Its Proposed Role as a Membrane-Cytoskeletal Linker." *The Journal of Cell Biology* 120 (1): 129–39. http://www.pubmedcentral.nih.gov/articlerender.fcgi?artid=2119498&tool=pmcentrez&rendertype=abstract.

Amieva, M R, P Litman, L Huang, E Ichimaru, and H Furthmayr. 1999. "Disruption of Dynamic Cell Surface Architecture of NIH3T3 Fibroblasts by the N-Terminal Domains of Moesin and Ezrin: In Vivo Imaging with GFP Fusion Proteins." *Journal of Cell Science* 112 (Pt 1 (January): 111–25. http://www.ncbi.nlm.nih.gov/pubmed/9841908.

Arpin, M, M Algrain, and D Louvard. 1994. "Membrane-Actin Microfilament Connections: An Increasing Diversity of Players Related to Band 4.1." *Current Opinion in Cell Biology* 6 (1): 136–41. http://www.ncbi.nlm.nih.gov/pubmed/8167019.

Arpin, Monique, Dafne Chirivino, Alexandra Naba, and Ingrid Zwaenepoel. 2011. "Emerging Role for ERM Proteins in Cell Adhesion and Migration." *Cell Adhesion & Migration* 5 (2): 199–206. doi:10.4161/cam.5.2.15081.

Austermann, Judith, Ali Reza Nazmi, Carsten Müller-Tidow, and Volker Gerke. 2008. "Characterization of the Ca2+-Regulated Ezrin-S100P Interaction and Its Role in Tumor Cell Migration." *Journal of Biological Chemistry* 283 (43): 29331–40. doi:10.1074/jbc.M806145200.

Autero, Matti, Leena Heiska, Lars Rönnstrand, Antti Vaheri, Carl G Gahmberg, and Olli Carpén. 2003. "Ezrin Is a Substrate for Lck in T Cells." *FEBS Letters* 535 (1-3): 82–86. http://www.ncbi.nlm.nih.gov/pubmed/12560083.

Auvinen, Eeva, Niina Kivi, and Antti Vaheri. 2007. "Regulation of Ezrin Localization by Rac1 and PIPK in Human Epithelial Cells." *Experimental Cell Research* 313 (4): 824–33. doi:10.1016/j.yexcr.2006.12.002.

Barret, Cécile, Christian Roy, Philippe Montcourrier, Paul Mangeat, and Verena Niggli. 2000. "Mutagenesis of the Phosphatidylinositol 4 , 5-Bisphosphate (PIP 2) Binding Site in the NH 2 -Terminal Domain of Ezrin Correlates with Its Altered Cellular Distribution." *The Journal of Cell Biology* 151 (5): 1067–79.

Baumgartner, Martin, Amy L Sillman, Elizabeth M Blackwood, Jyoti Srivastava, Nikki Madson, James W Schilling, Jocelyn H Wright, and Diane L Barber. 2006. "The Nck-Interacting Kinase Phosphorylates ERM Proteins for Formation of Lamellipodium by Growth Factors." *Proceedings of the National Academy of Sciences of the United States of America* 103 (36): 13391–96. doi:10.1073/pnas.0605950103.

Ben-Aissa, Khadija, Genaro Patino-Lopez, Natalya V. Belkina, Ofelia Maniti, Tilman Rosales, Jian Jiang Hao, Michael J. Kruhlak, Jay R. Knutson, Catherine Picart, and Stephen Shaw. 2012. "Activation of Moesin, a Protein That Links Actin Cytoskeleton to the Plasma Membrane, Occurs by Phosphatidylinositol 4,5-Bisphosphate (PIP2) Binding Sequentially to Two Sites and Releasing an Autoinhibitory Linker." *Journal of Biological Chemistry* 287 (20): 16311–23. doi:10.1074/jbc.M111.304881.

Berryman, M, Z Franck, and A Bretscher. 1993. "Ezrin Is Concentrated in the Apical Microvilli of a Wide Variety of Epithelial Cells Whereas Moesin Is Found Primarily in Endothelial Cells." *Journal of Cell Science* 105 (Pt 4 (August): 1025–43. http://www.ncbi.nlm.nih.gov/pubmed/8227193.

Blin, Guillaume, Emmanuel Margeat, Kévin Carvalho, Catherine a Royer, Christian Roy, and Catherine Picart. 2008. "Quantitative Analysis of the Binding of Ezrin to Large Unilamellar Vesicles Containing Phosphatidylinositol 4,5 Bisphosphate." *Biophysical Journal* 94 (3): 1021–33. doi:10.1529/biophysj.107.110213.

Bok, D. 1993. “The Retinal Pigment Epithelium: A Versatile Partner in Vision.” *Journal of Cell Science. Supplement* 17 (January): 189–95. http://www.ncbi.nlm.nih.gov/pubmed/8144697.

Bonilha, Vera L, Mary E Rayborn, Ichiko Saotome, Andrea I McClatchey, and Joe G Hollyfield. 2006. “Microvilli Defects in Retinas of Ezrin Knockout Mice.” *Experimental Eye Research* 82 (4): 720–29. doi:10.1016/j.exer.2005.09.013.

Bonilha, Vera Lúcia, Silvia C. Finnemann, and Enrique Rodriguez-Boulan. 1999. “Ezrin Promotes Morphogenesis of Apical Microvilli and Basal Infoldings in Retinal Pigment Epithelium.” *Journal of Cell Biology* 147 (7): 1533–47. doi:10.1083/jcb.147.7.1533.

Bosk, Sabine, Julia a. Braunger, Volker Gerke, and Claudia Steinem. 2011. “Activation of F-Actin Binding Capacity of Ezrin: Synergism of PIP2 Interaction and Phosphorylation.” *Biophysical Journal* 100 (7). Biophysical Society: 1708–17. doi:10.1016/j.bpj.2011.02.039.

Braunger, Julia a., Bastian R. Bruckner, Stefan Nehls, Anna Pietuch, Volker Gerke, Ingo Mey, Andreas Janshoff, and Claudia Steinem. 2014. “Phosphatidylinositol 4,5-Bisphosphate Alters the Number of Attachment Sites between Ezrin and Actin Filaments: A Colloidal Probe Study.” *Journal of Biological Chemistry* 289 (14): 9833–43. doi:10.1074/jbc.M113.530659.

Braunger, Julia a., Corinna Kramer, Daniela Morick, and Claudia Steinem. 2013. “Solid Supported Membranes Doped with PIP2: Influence of Ionic Strength and pH on Bilayer Formation and Membrane Organization.” *Langmuir* 29 (46): 14204–13. doi:10.1021/la402646k.

Bretscher, A. 1983. “Purification of an 80,000-Dalton Protein That Is a Component of the Isolated Microvillus Cytoskeleton, and Its Localization in Nonmuscle Cells.” *The Journal of Cell Biology* 97 (2): 425–32. http://www.pubmedcentral.nih.gov/articlerender.fcgi?artid=2112519&tool=pmcentrez&rendertype=abstract.

———. 1989. “Rapid Phosphorylation and Reorganization of Ezrin and Spectrin Accompany Morphological Changes Induced in A-431 Cells by Epidermal Growth Factor.” *The Journal of Cell Biology* 108 (3): 921–30. http://www.pubmedcentral.nih.gov/articlerender.fcgi?artid=2115383&tool=pmcentrez&rendertype=abstract.

Bretscher, A, R Gary, and M Berryman. 1995. “Soluble Ezrin Purified from Placenta Exists as Stable Monomers and Elongated Dimers with Masked C-Terminal Ezrin-Radixin-Moesin Association Domains.” *Biochemistry* 34 (51): 16830–37. http://www.ncbi.nlm.nih.gov/pubmed/8527459.

Bretscher, a, D Reczek, and M Berryman. 1997. “Ezrin: A Protein Requiring Conformational Activation to Link Microfilaments to the Plasma Membrane in the Assembly of Cell Surface Structures.” *Journal of Cell Science* 110 (Pt 2: 3011–18.

Bretscher, Anthony, Kevin Edwards, and Richard G Fehon. 2002. “ERM Proteins and Merlin: Integrators at the Cell Cortex.” *Nature Reviews. Molecular Cell Biology* 3 (8): 586–99. doi:10.1038/nrm882.

Brown, D A, and E London. 2000. “Structure and Function of Sphingolipid- and Cholesterol-Rich Membrane Rafts.” *The Journal of Biological Chemistry* 275 (23): 17221–24. doi:10.1074/jbc.R000005200.

Brown, Martin J, Ruchika Nijhara, John A Hallam, Michelle Gignac, Kenneth M Yamada, Stanley L Erlandsen, Jerome Delon, Michael Kruhlak, and Stephen Shaw. 2003. “Chemokine Stimulation of Human Peripheral Blood T Lymphocytes Induces Rapid Dephosphorylation of ERM Proteins, Which Facilitates Loss of Microvilli and Polarization.” *Blood* 102 (12): 3890–99. doi:10.1182/blood-2002-12-3807.

Charrin, Stephanie, and Andres Alcover. 2006. “Role of ERM (ezrin-Radixin-Moesin) Proteins in T Lymphocyte Polarization, Immune Synapse Formation and in T Cell Receptor-Mediated Signaling.” *Frontiers in Bioscience : A Journal and Virtual Library* 11 (January): 1987–97. http://www.ncbi.nlm.nih.gov/pubmed/16368573.

Chen, F, L Ma, M C Parrini, X Mao, M Lopez, C Wu, P W Marks, et al. 2000. “Cdc42 Is Required for PIP(2)-Induced Actin Polymerization and Early Development but Not for Cell Viability.” *Current Biology : CB* 10 (13): 758–65. http://www.ncbi.nlm.nih.gov/pubmed/10898977.

Chen, J., J. A. Cohn, and L. J. Mandel. 1995. “Dephosphorylation of Ezrin as an Early Event in Renal Microvillar Breakdown and Anoxic Injury.” *Proceedings of the National Academy of Sciences* 92 (16): 7495–99. doi:10.1073/pnas.92.16.7495.

Chen, X, U Vinkemeier, Y Zhao, D Jeruzalmi, J E Darnell, and J Kuriyan. 1998. “Crystal Structure of a Tyrosine Phosphorylated STAT-1 Dimer Bound to DNA.” *Cell* 93 (5): 827–39. http://www.ncbi.nlm.nih.gov/pubmed/9630226.

Chishti, A H, A C Kim, S M Marfatia, M Lutchman, M Hanspal, H Jindal, S C Liu, et al. 1998. “The FERM Domain: A Unique Module Involved in the Linkage of Cytoplasmic Proteins to the Membrane.” *Trends in Biochemical Sciences* 23 (8): 281–82. http://www.ncbi.nlm.nih.gov/pubmed/9757824.

Cohen, P. 2001. “The Role of Protein Phosphorylation in Human Health and Disease. The Sir Hans Krebs Medal Lecture.” *European Journal of Biochemistry / FEBS* 268 (19): 5001–10. http://www.ncbi.nlm.nih.gov/pubmed/11589691.

Conboy, J, Y W Kan, S B Shohet, and N Mohandas. 1986. “Molecular Cloning of Protein 4.1, a Major Structural Element of the Human Erythrocyte Membrane Skeleton.” *Proceedings of the National Academy of Sciences of the United States of America* 83 (24): 9512–16. http://www.pubmedcentral.nih.gov/articlerender.fcgi?artid=387170&tool=pmcentrez&rendertype=abstract.

Coscoy, Sylvie, François Waharte, Alexis Gautreau, Marianne Martin, Daniel Louvard, Paul Mangeat, Monique Arpin, and Françis Amblard. 2002. “Molecular Analysis of Microscopic Ezrin Dynamics by Two-Photon FRAP.” *Proceedings of the National Academy of Sciences of the United States of America* 99 (20): 12813–18. doi:10.1073/pnas.192084599.

Crepaldi, T, A Gautreau, P M Comoglio, D Louvard, and M Arpin. 1997. “Ezrin Is an Effector of Hepatocyte Growth Factor-Mediated Migration and Morphogenesis in Epithelial Cells.” *The Journal of Cell Biology* 138 (2): 423–34. http://www.pubmedcentral.nih.gov/articlerender.fcgi?artid=2138186&tool=pmcentrez&rendertype=abstract.

Cullinan, Patrick, Anne I Sperling, and Janis K Burkhardt. 2002. “The Distal Pole Complex: A Novel Membrane Domain Distal to the Immunological Synapse.” *Immunological Reviews* 189 (November): 111–22. http://www.ncbi.nlm.nih.gov/pubmed/12445269.

Curto, Marcello, and Andrea I McClatchey. 2004. “Ezrin...a Metastatic detERMinant?” *Cancer Cell* 5 (2): 113–14. http://www.ncbi.nlm.nih.gov/pubmed/14998486.

Czech, M P. 2000. “PIP2 and PIP3: Complex Roles at the Cell Surface.” *Cell* 100 (6): 603–6. http://www.ncbi.nlm.nih.gov/pubmed/10761925.

D’Angelo, Romina, Sandra Aresta, Anne Blangy, Laurence Del Maestro, Daniel Louvard, and Monique Arpin. 2007. “Interaction of Ezrin with the Novel Guanine Nucleotide Exchange Factor PLEKHG6 Promotes RhoG-Dependent Apical Cytoskeleton Rearrangements in Epithelial Cells.” *Molecular Biology of the Cell* 18 (12): 4780–93. doi:10.1091/mbc.E06-12-1144.

Delon, J, K Kaibuchi, and R N Germain. 2001. “Exclusion of CD43 from the Immunological Synapse Is Mediated by Phosphorylation-Regulated Relocation of the Cytoskeletal Adaptor Moesin.” *Immunity* 15 (5): 691–701. http://www.ncbi.nlm.nih.gov/pubmed/11728332.

Diederichs, Sven, Etmar Bulk, Björn Steffen, Ping Ji, Lara Tickenbrock, Kerstin Lang, Kurt S Zänker, et al. 2004. “S100 Family Members and Trypsinogens Are Predictors of Distant Metastasis and Survival in Early-Stage Non-Small Cell Lung Cancer.” *Cancer Research* 64 (16): 5564–69. doi:10.1158/0008-5472.CAN-04-2004.

Doi, Y, M Itoh, S Yonemura, S Ishihara, H Takano, T Noda, and S Tsukita. 1999. “Normal Development of Mice and Unimpaired Cell Adhesion/cell Motility/actin-Based Cytoskeleton without Compensatory up-Regulation of Ezrin or Radixin in Moesin Gene Knockout.” *The Journal of Biological Chemistry* 274 (4): 2315–21. http://www.ncbi.nlm.nih.gov/pubmed/9890997.

Dorner, C, T Ciossek, S Müller, P H Møller, A Ullrich, and R Lammers. 1998. “Characterization of KIF1C, a New Kinesin-like Protein Involved in Vesicle Transport from the Golgi Apparatus to the Endoplasmic Reticulum.” *The Journal of Biological Chemistry* 273 (32): 20267–75. http://www.ncbi.nlm.nih.gov/pubmed/9685376.

Drucker, P., M. Pejic, H.-J. Galla, and V. Gerke. 2013. “Lipid Segregation and Membrane Budding Induced by the Peripheral Membrane Binding Protein Annexin A2.” *Journal of Biological Chemistry* 288 (34): 24764–76. doi:10.1074/jbc.M113.474023.

Edwards, S D, and N H Keep. 2001. “The 2.7 A Crystal Structure of the Activated FERM Domain of Moesin: An Analysis of Structural Changes on Activation.” *Biochemistry* 40 (24): 7061–68. http://www.ncbi.nlm.nih.gov/pubmed/11401550.

Fehon, Richard G, Andrea I McClatchey, and Anthony Bretscher. 2010. “Organizing the Cell Cortex: The Role of ERM Proteins.” *Nature Reviews. Molecular Cell Biology* 11 (4): 276–87. doi:10.1038/nrm2866.

Fessenden, James D. 2009. “Förster Resonance Energy Transfer Measurements of Ryanodine Receptor Type 1 Structure Using a Novel Site-Specific Labeling Method.” *PloS One* 4 (10): e7338. doi:10.1371/journal.pone.0007338.

Fiévet, Bruno, Daniel Louvard, and Monique Arpin. 2007. “ERM Proteins in Epithelial Cell Organization and Functions.” *Biochimica et Biophysica Acta* 1773 (5): 653–60. doi:10.1016/j.bbamcr.2006.06.013.

Fievet, Bruno T, Alexis Gautreau, Christian Roy, Laurence Del Maestro, Paul Mangeat, Daniel Louvard, and Monique Arpin. 2004. “Phosphoinositide Binding and Phosphorylation Act Sequentially in the Activation Mechanism of Ezrin.” *The Journal of Cell Biology* 164 (5): 653–59. doi:10.1083/jcb.200307032.

Finnerty, Casey M, David Chambers, Janet Ingraffea, H Richard Faber, P Andrew Karplus, and Anthony Bretscher. 2004. “The EBP50-Moesin Interaction Involves a Binding Site Regulated by Direct Masking on the FERM Domain.” *Journal of Cell Science* 117 (Pt 8): 1547–52. doi:10.1242/jcs.01038.

FISCHER, E H, and E G KREBS. 1955. “Conversion of Phosphorylase B to Phosphorylase a in Muscle Extracts.” *The Journal of Biological Chemistry* 216 (1): 121–32. http://www.ncbi.nlm.nih.gov/pubmed/13252012.

Fritzsche, Marco, Richard Thorogate, and Guillaume Charras. 2014. “Quantitative Analysis of Ezrin Turnover Dynamics in the Actin Cortex.” *Biophysical Journal* 106 (2). The Authors: 343–53. doi:10.1016/j.bpj.2013.11.4499.

Funayama, N, A Nagafuchi, N Sato, and S Tsukita. 1991. “Radixin Is a Novel Member of the Band 4.1 Family.” *The Journal of Cell Biology* 115 (4): 1039–48. http://www.pubmedcentral.nih.gov/articlerender.fcgi?artid=2289953&tool=pmcentrez&rendertype=abstract.

Garbett, Damien, and Anthony Bretscher. 2012. “PDZ Interactions Regulate Rapid Turnover of the Scaffolding Protein EBP50 in Microvilli.” *Journal of Cell Biology* 198 (2): 195–203. doi:10.1083/jcb.201204008.

Gary, R, and A Bretscher. 1995. “Ezrin Self-Association Involves Binding of an N-Terminal Domain to a Normally Masked C-Terminal Domain That Includes the F-Actin Binding Site.” *Molecular Biology of the Cell* 6 (8): 1061–75. http://www.pubmedcentral.nih.gov/articlerender.fcgi?artid=301263&tool=pmcentrez&rendertype=abstract.

Gautreau, A, D Louvard, and M Arpin. 2000. “Morphogenic Effects of Ezrin Require a Phosphorylation-Induced Transition from Oligomers to Monomers at the Plasma Membrane.” *The Journal of Cell Biology* 150 (1): 193–203. http://www.pubmedcentral.nih.gov/articlerender.fcgi?artid=2185562&tool=pmcentrez&rendertype=abstract.

Gillooly, D J, and H Stenmark. 2001. “Cell Biology. A Lipid Oils the Endocytosis Machine.” *Science (New York, N.Y.)* 291 (5506): 993–94. http://www.ncbi.nlm.nih.gov/pubmed/11232585.

Goldenberg, Neil M, and Benjamin E Steinberg. 2010. “Surface Charge: A Key Determinant of Protein Localization and Function.” *Cancer Research* 70 (4): 1277–80. doi:10.1158/0008-5472.CAN-09-2905.

Gould, K L, A Bretscher, F S Esch, and T Hunter. 1989. “cDNA Cloning and Sequencing of the Protein-Tyrosine Kinase Substrate, Ezrin, Reveals Homology to Band 4.1.” *The EMBO Journal* 8 (13): 4133–42. http://www.pubmedcentral.nih.gov/articlerender.fcgi?artid=401598&tool=pmcentrez&rendertype=abstract.

Grakoui, A, S K Bromley, C Sumen, M M Davis, A S Shaw, P M Allen, and M L Dustin. 1999. “The Immunological Synapse: A Molecular Machine Controlling T Cell Activation.” *Science (New York, N.Y.)* 285 (5425): 221–27. http://www.ncbi.nlm.nih.gov/pubmed/10398592.

Hamada, K, T Shimizu, T Matsui, S Tsukita, and T Hakoshima. 2000. “Structural Basis of the Membrane-Targeting and Unmasking Mechanisms of the Radixin FERM Domain.” *The EMBO Journal* 19 (17): 4449–62. doi:10.1093/emboj/19.17.4449.

Hamada, Keisuke, Toshiyuki Shimizu, Shigenobu Yonemura, Shoichiro Tsukita, Sachiko Tsukita, and Toshio Hakoshima. 2003. “Structural Basis of Adhesion-Molecule Recognition by ERM Proteins Revealed by the Crystal Structure of the Radixin-ICAM-2 Complex.” *EMBO Journal* 22 (3): 502–14. doi:10.1093/emboj/cdg039.

Hao, Jian Jiang, Yin Liu, Michael Kruhlak, Karen E. Debell, Barbara L. Rellahan, and Stephen Shaw. 2009. “Phospholipase C - Mediated Hydrolysis of PIP2 Releases ERM Proteins from Lymphocyte Membrane.” *Journal of Cell Biology* 184 (3): 451–62. doi:10.1083/jcb.200807047.

Hatzoglou, Anastassia, Isabelle Ader, Anne Splingard, James Flanders, Evelyne Saade, Ingrid Leroy, Sabine Traver, Sandra Aresta, and Jean de Gunzburg. 2007. “Gem Associates with Ezrin and Acts via the Rho-GAP Protein Gmip to down-Regulate the Rho Pathway.” *Molecular Biology of the Cell* 18 (4): 1242–52. doi:10.1091/mbc.E06-06-0510.

Hebert, A. M., B. DuBoff, J. B. Casaletto, A. B. Gladden, and A. I. McClatchey. 2012. “Merlin/ERM Proteins Establish Cortical Asymmetry and Centrosome Position.” *Genes & Development* 26 (24): 2709–23. doi:10.1101/gad.194027.112.

Heiska, Leena, and Olli Carpén. 2005. “Src Phosphorylates Ezrin at Tyrosine 477 and Induces a Phosphospecific Association between Ezrin and a Kelch-Repeat Protein Family Member.” *The Journal of Biological Chemistry* 280 (11): 10244–52. doi:10.1074/jbc.M411353200.

Helander, T S, O Carpén, O Turunen, P E Kovanen, A Vaheri, and T Timonen. 1996. “ICAM-2 Redistributed by Ezrin as a Target for Killer Cells.” *Nature* 382 (6588): 265–68. doi:10.1038/382265a0.

Henry, M D, C Gonzalez Agosti, and F Solomon. 1995. “Molecular Dissection of Radixin: Distinct and Interdependent Functions of the Amino- and Carboxy-Terminal Domains.” *The Journal of Cell Biology* 129 (4): 1007–22. http://www.pubmedcentral.nih.gov/articlerender.fcgi?artid=2120491&tool=pmcentrez&rendertype=abstract.

Herrig, Alexander, Matthias Janke, Judith Austermann, Volker Gerke, Andreas Janshoff, and Claudia Steinem. 2006. “Cooperative Adsorption of Ezrin on PIP 2 -Containing Membranes †.” *Society*, no. 20: 13025–34.

Hoeflich, Klaus P, Sachiko Tsukita, Leslie Hicks, Cyril M Kay, Shoichiro Tsukita, and Mitsuhiko Ikura. 2003. “Insights into a Single Rod-like Helix in Activated Radixin Required for Membrane-Cytoskeletal Cross-Linking.” *Biochemistry* 42 (40): 11634–41. doi:10.1021/bi0350497.

Honda, A, M Nogami, T Yokozeki, M Yamazaki, H Nakamura, H Watanabe, K Kawamoto, et al. 1999. “Phosphatidylinositol 4-Phosphate 5-Kinase Alpha Is a Downstream Effector of the Small G Protein ARF6 in Membrane Ruffle Formation.” *Cell* 99 (5): 521–32. http://www.ncbi.nlm.nih.gov/pubmed/10589680.

Hoskin, Victoria, Alvin Szeto, Abdi Ghaffari, Peter A Greer, Graham P Côté, and Bruce E Elliott. 2015. “Ezrin Regulates Focal Adhesion and Invadopodia Dynamics by Altering Calpain Activity to Promote Breast Cancer Cell Invasion.” *Molecular Biology of the Cell*, August. doi:10.1091/mbc.E14-12-1584.

Huang, L, T Y Wong, R C Lin, and H Furthmayr. 1999. “Replacement of Threonine 558, a Critical Site of Phosphorylation of Moesin in Vivo, with Aspartate Activates F-Actin Binding of Moesin. Regulation by Conformational Change.” *The Journal of Biological Chemistry* 274 (18): 12803–10. http://www.ncbi.nlm.nih.gov/pubmed/10212266.

Hughes, Sarah C, and Richard G Fehon. 2007. “Understanding ERM Proteins--the Awesome Power of Genetics Finally Brought to Bear.” *Current Opinion in Cell Biology* 19 (1): 51–56. doi:10.1016/j.ceb.2006.12.004.

Ivetic, Aleksandar, and Anne J Ridley. 2004. “Ezrin/radixin/moesin Proteins and Rho GTPase Signalling in Leucocytes.” *Immunology* 112 (2): 165–76. doi:10.1111/j.1365-2567.2004.01882.x.

Janke, Matthias, Alexander Herrig, Judith Austermann, Volker Gerke, Claudia Steinem, and Andreas Janshoff. 2008. "Actin Binding of Ezrin Is Activated by Specific Recognition of PIP2-Functionalized Lipid Bilayers." *Biochemistry* 47 (12): 3762–69. doi:10.1021/bi702542s.

Johnson, L N, and D Barford. 1993. "The Effects of Phosphorylation on the Structure and Function of Proteins." *Annual Review of Biophysics and Biomolecular Structure* 22 (January): 199–232. doi:10.1146/annurev.bb.22.060193.001215.

Johnson, Louise N. 2009. "The Regulation of Protein Phosphorylation." *Biochemical Society Transactions* 37 (Pt 4): 627–41. doi:10.1042/BST0370627.

Khanna, Chand, Xiaolin Wan, Seuli Bose, Ryan Cassaday, Osarenoma Olomu, Arnulfo Mendoza, Choh Yeung, Richard Gorlick, Stephen M Hewitt, and Lee J Helman. 2004. "The Membrane-Cytoskeleton Linker Ezrin Is Necessary for Osteosarcoma Metastasis." *Nature Medicine* 10 (2): 182–86. doi:10.1038/nm982.

Kikuchi, Shojiro, Masaki Hata, Kanehisa Fukumoto, Yukari Yamane, Takeshi Matsui, Atsushi Tamura, Shigenobu Yonemura, et al. 2002. "Radixin Deficiency Causes Conjugated Hyperbilirubinemia with Loss of Mrp2 from Bile Canalicular Membranes." *Nature Genetics* 31 (3): 320–25. doi:10.1038/ng905.

Kim, J, T Shishido, X Jiang, A Aderem, and S McLaughlin. 1994. "Phosphorylation, High Ionic Strength, and Calmodulin Reverse the Binding of MARCKS to Phospholipid Vesicles." *The Journal of Biological Chemistry* 269 (45): 28214–19. http://www.ncbi.nlm.nih.gov/pubmed/7961759.

Kitajiri, Shin-ichiro, Kanehisa Fukumoto, Masaki Hata, Hiroyuki Sasaki, Tatsuya Katsuno, Takayuki Nakagawa, Juichi Ito, Shoichiro Tsukita, and Sachiko Tsukita. 2004. "Radixin Deficiency Causes Deafness Associated with Progressive Degeneration of Cochlear Stereocilia." *The Journal of Cell Biology* 166 (4): 559–70. doi:10.1083/jcb.200402007.

Kivelä, T, J Jääskeläinen, A Vaheri, and O Carpén. 2000. "Ezrin, a Membrane-Organizing Protein, as a Polarization Marker of the Retinal Pigment Epithelium in Vertebrates." *Cell and Tissue Research* 301 (2): 217–23. http://www.ncbi.nlm.nih.gov/pubmed/10955717.

Koltzscher, Max, Claudia Neumann, Simone König, and Volker Gerke. 2003. "Ca2+-Dependent Binding and Activation of Dormant Ezrin by Dimeric S100P." *Molecular Biology of the Cell* 14 (6): 2372–84. doi:10.1091/mbc.E02-09-0553.

Körner, Alexander, Christina Deichmann, Fernanda F Rossetti, Almut Köhler, Oleg V Konovalov, Doris Wedlich, and Motomu Tanaka. 2013. "Cell Differentiation of Pluripotent Tissue Sheets Immobilized on Supported Membranes Displaying Cadherin-11." *PloS One* 8 (2): e54749. doi:10.1371/journal.pone.0054749.

Krieg, J, and T Hunter. 1992. "Identification of the Two Major Epidermal Growth Factor-Induced Tyrosine Phosphorylation Sites in the Microvillar Core Protein Ezrin." *The Journal of Biological Chemistry* 267 (27): 19258–65. http://www.ncbi.nlm.nih.gov/pubmed/1382070.

Lamb, R F, B W Ozanne, C Roy, L McGarry, C Stipp, P Mangeat, and D G Jay. 1997. "Essential Functions of Ezrin in Maintenance of Cell Shape and Lamellipodial Extension in Normal and Transformed Fibroblasts." *Current Biology : CB* 7 (9): 682–88. http://www.ncbi.nlm.nih.gov/pubmed/9285722.

Lankes, W, A Griesmacher, J Grünwald, R Schwartz-Albiez, and R Keller. 1988. "A Heparin-Binding Protein Involved in Inhibition of Smooth-Muscle Cell Proliferation." *The Biochemical Journal* 251 (3): 831–42. http://www.pubmedcentral.nih.gov/articlerender.fcgi?artid=1149078&tool=pmcentrez&rendertype=abstract.

Lankes, W T, and H Furthmayr. 1991. "Moesin: A Member of the Protein 4.1-Talin-Ezrin Family of Proteins." *Proceedings of the National Academy of Sciences of the United States of America* 88 (19): 8297–8301. http://www.pubmedcentral.nih.gov/articlerender.fcgi?artid=52495&tool=pmcentrez&rendertype=abstract.

Lee, Jong-Hwan, Tomoya Katakai, Takahiro Hara, Hiroyuki Gonda, Manabu Sugai, and Akira Shimizu. 2004. "Roles of P-ERM and Rho-ROCK Signaling in Lymphocyte Polarity and Uropod Formation." *The Journal of Cell Biology* 167 (2): 327–37. doi:10.1083/jcb.200403091.

Lemmon, M A, and K M Ferguson. 2000. “Signal-Dependent Membrane Targeting by Pleckstrin Homology (PH) Domains.” *The Biochemical Journal* 350 Pt 1 (August): 1–18. http://www.pubmedcentral.nih.gov/articlerender.fcgi?artid=1221219&tool=pmcentrez&rendertype=abstract.

Li, Qianzhi, Mark R. Nance, Rima Kulikauskas, Kevin Nyberg, Richard Fehon, P. Andrew Karplus, Anthony Bretscher, and John J G Tesmer. 2007. “Self-Masking in an Intact ERM-Merlin Protein: An Active Role for the Central A-Helical Domain.” *Journal of Molecular Biology* 365 (5): 1446–59. doi:10.1016/j.jmb.2006.10.075.

Lo Vasco, Vincenza Rita, Martina Leopizzi, Caterina Chiappetta, Chiara Puggioni, Claudio Di Cristofano, and Carlo Della Rocca. 2013. “Expression of Phosphoinositide-Specific Phospholipase C Enzymes in Human Osteosarcoma Cell Lines.” *Journal of Cell Communication and Signaling* 7 (2): 141–50. doi:10.1007/s12079-013-0194-6.

Loebrich, Sven, Robert Bähring, Tatsuya Katsuno, Sachiko Tsukita, and Matthias Kneussel. 2006. “Activated Radixin Is Essential for GABAA Receptor alpha5 Subunit Anchoring at the Actin Cytoskeleton.” *The EMBO Journal* 25 (5): 987–99. doi:10.1038/sj.emboj.7600995.

Louvet, S, J Aghion, A Santa-Maria, P Mangeat, and B Maro. 1996. “Ezrin Becomes Restricted to Outer Cells Following Asymmetrical Division in the Preimplantation Mouse Embryo.” *Developmental Biology* 177 (2): 568–79. doi:10.1006/dbio.1996.0186.

Martin, T F. 2001. “PI(4,5)P(2) Regulation of Surface Membrane Traffic.” *Current Opinion in Cell Biology* 13 (4): 493–99. http://www.ncbi.nlm.nih.gov/pubmed/11454457.

Matsui, T, M Maeda, Y Doi, S Yonemura, M Amano, K Kaibuchi, and S Tsukita. 1998. “Rho-Kinase Phosphorylates COOH-Terminal Threonines of Ezrin/radixin/moesin (ERM) Proteins and Regulates Their Head-to-Tail Association.” *The Journal of Cell Biology* 140 (3): 647–57. http://www.pubmedcentral.nih.gov/articlerender.fcgi?artid=2140160&tool=pmcentrez&rendertype=abstract.

Matsui, T, S Yonemura, and S Tsukita. 1999. “Activation of ERM Proteins in Vivo by Rho Involves Phosphatidyl-Inositol 4-Phosphate 5-Kinase and Not ROCK Kinases.” *Current Biology : CB* 9 (21): 1259–62. http://www.ncbi.nlm.nih.gov/pubmed/10556088.

McClatchey, a. I. 2014. “ERM Proteins at a Glance.” *Journal of Cell Science*, no. June: 1–6. doi:10.1242/jcs.098343.

McLaughlin, Stuart, Jiyao Wang, Alok Gambhir, and Diana Murray. 2002. “PIP(2) and Proteins: Interactions, Organization, and Information Flow.” *Annual Review of Biophysics and Biomolecular Structure* 31: 151–75. doi:10.1146/annurev.biophys.31.082901.134259.

Menager, C, J Vassy, C Doliger, Y Legrand, and A Karniguian. 1999. “Subcellular Localization of RhoA and Ezrin at Membrane Ruffles of Human Endothelial Cells: Differential Role of Collagen and Fibronectin.” *Experimental Cell Research* 249 (2): 221–30. doi:10.1006/excr.1999.4481.

Naba, Alexandra, Céline Reverdy, Daniel Louvard, and Monique Arpin. 2008. “Spatial Recruitment and Activation of the Fes Kinase by Ezrin Promotes HGF-Induced Cell Scattering.” *The EMBO Journal* 27 (1): 38–50. doi:10.1038/sj.emboj.7601943.

Nakamura, F, L Huang, K Pestonjamasp, E J Luna, and H Furthmayr. 1999. “Regulation of F-Actin Binding to Platelet Moesin in Vitro by Both Phosphorylation of Threonine 558 and Polyphosphatidylinositides.” *Molecular Biology of the Cell* 10 (8): 2669–85. http://www.pubmedcentral.nih.gov/articlerender.fcgi?artid=25498&tool=pmcentrez&rendertype=abstract.

Niggli, V, C Andréoli, C Roy, and P Mangeat. 1995. “Identification of a Phosphatidylinositol-4,5-Bisphosphate-Binding Domain in the N-Terminal Region of Ezrin.” *FEBS Letters* 376 (3): 172–76. http://www.ncbi.nlm.nih.gov/pubmed/7498535.

Niggli, Verena, and Jérémie Rossy. 2008. “Ezrin/radixin/moesin: Versatile Controllers of Signaling Molecules and of the Cortical Cytoskeleton.” *International Journal of Biochemistry and Cell Biology* 40 (3): 344–49. doi:10.1016/j.biocel.2007.02.012.

Nunomura, W, Y Takakuwa, R Tokimitsu, S W Krauss, M Kawashima, and N Mohandas. 1997. "Regulation of CD44-Protein 4.1 Interaction by Ca2+ and Calmodulin. Implications for Modulation of CD44-Ankyrin Interaction." *The Journal of Biological Chemistry* 272 (48): 30322–28. http://www.ncbi.nlm.nih.gov/pubmed/9374519.

Oshiro, N, Y Fukata, and K Kaibuchi. 1998. "Phosphorylation of Moesin by Rho-Associated Kinase (Rho-Kinase) Plays a Crucial Role in the Formation of Microvilli-like Structures." *The Journal of Biological Chemistry* 273 (52): 34663–66. http://www.ncbi.nlm.nih.gov/pubmed/9856983.

Pace, C N, F Vajdos, L Fee, G Grimsley, and T Gray. 1995. "How to Measure and Predict the Molar Absorption Coefficient of a Protein." *Protein Science : A Publication of the Protein Society* 4 (11): 2411–23. doi:10.1002/pro.5560041120.

Pakkanen, R, K Hedman, O Turunen, T Wahlström, and A Vaheri. 1987. "Microvillus-Specific Mr 75,000 Plasma Membrane Protein of Human Choriocarcinoma Cells." *The Journal of Histochemistry and Cytochemistry : Official Journal of the Histochemistry Society* 35 (8): 809–16. http://www.ncbi.nlm.nih.gov/pubmed/3298422.

Parameswaran, Neetha, Ken Matsui, and Neetu Gupta. 2011. "Conformational Switching in Ezrin Regulates Morphological and Cytoskeletal Changes Required for B Cell Chemotaxis." *Journal of Immunology (Baltimore, Md. : 1950)* 186 (7): 4088–97. doi:10.4049/jimmunol.1001139.

Parsons, Maddy, James Monypenny, Simon M Ameer-Beg, Thomas H Millard, Laura M Machesky, Marion Peter, Melanie D Keppler, et al. 2005. "Spatially Distinct Binding of Cdc42 to PAK1 and N-WASP in Breast Carcinoma Cells." *Molecular and Cellular Biology* 25 (5): 1680–95. doi:10.1128/MCB.25.5.1680-1695.2005.

Pearson, M a, D Reczek, a Bretscher, and P a Karplus. 2000. "Structure of the ERM Protein Moesin Reveals the FERM Domain Fold Masked by an Extended Actin Binding Tail Domain." *Cell* 101 (3): 259–70. doi:10.1016/S0092-8674(00)80836-3.

Prehoda, K E, J A Scott, R D Mullins, and W A Lim. 2000. "Integration of Multiple Signals through Cooperative Regulation of the N-WASP-Arp2/3 Complex." *Science (New York, N.Y.)* 290 (5492): 801–6. http://www.ncbi.nlm.nih.gov/pubmed/11052943.

Raucher, D, T Stauffer, W Chen, K Shen, S Guo, J D York, M P Sheetz, and T Meyer. 2000. "Phosphatidylinositol 4,5-Bisphosphate Functions as a Second Messenger That Regulates Cytoskeleton-Plasma Membrane Adhesion." *Cell* 100 (2): 221–28. http://www.ncbi.nlm.nih.gov/pubmed/10660045.

Roumier, A, J C Olivo-Marin, M Arpin, F Michel, M Martin, P Mangeat, O Acuto, A Dautry-Varsat, and A Alcover. 2001. "The Membrane-Microfilament Linker Ezrin Is Involved in the Formation of the Immunological Synapse and in T Cell Activation." *Immunity* 15 (5): 715–28. http://www.ncbi.nlm.nih.gov/pubmed/11728334.

Roy, C, M Martin, and P Mangeat. 1997. "A Dual Involvement of the Amino-Terminal Domain of Ezrin in F- and G-Actin Binding." *The Journal of Biological Chemistry* 272 (32): 20088–95. http://www.ncbi.nlm.nih.gov/pubmed/9242682.

Rubin, Seth M, Anne-Laure Gall, Ning Zheng, and Nikola P Pavletich. 2005. "Structure of the Rb C-Terminal Domain Bound to E2F1-DP1: A Mechanism for Phosphorylation-Induced E2F Release." *Cell* 123 (6): 1093–1106. doi:10.1016/j.cell.2005.09.044.

Saotome, Ichiko, Marcello Curto, and Andrea I McClatchey. 2004. "Ezrin Is Essential for Epithelial Organization and Villus Morphogenesis in the Developing Intestine." *Developmental Cell* 6 (6): 855–64. doi:10.1016/j.devcel.2004.05.007.

Sato, N, N Funayama, A Nagafuchi, S Yonemura, and S Tsukita. 1992. "A Gene Family Consisting of Ezrin, Radixin and Moesin. Its Specific Localization at Actin Filament/plasma Membrane Association Sites." *Journal of Cell Science* 103 (Pt 1 (September): 131–43. http://www.ncbi.nlm.nih.gov/pubmed/1429901.

Shcherbina, Anna, Anthony Bretscher, Dianne M. Kenney, and Eileen Remold-O'Donnell. 1999. "Moesin, the Major ERM Protein of Lymphocytes and Platelets, Differs from Ezrin in Its Insensitivity to Calpain." *FEBS Letters* 443 (1): 31–36. doi:10.1016/S0014-5793(98)01674-3.

Shi, Xiaoshan, Yunchen Bi, Wei Yang, Xingdong Guo, Yan Jiang, Chanjuan Wan, Lunyi Li, et al. 2013. “Ca2+ Regulates T-Cell Receptor Activation by Modulating the Charge Property of Lipids.” *Nature* 493 (7430): 111–15. doi:10.1038/nature11699.

Simons, P C, S F Pietromonaco, D Reczek, A Bretscher, and L Elias. 1998. “C-Terminal Threonine Phosphorylation Activates ERM Proteins to Link the Cell’s Cortical Lipid Bilayer to the Cytoskeleton.” *Biochemical and Biophysical Research Communications* 253 (3): 561–65. doi:10.1006/bbrc.1998.9823.

Simonsen, A, A E Wurmser, S D Emr, and H Stenmark. 2001. “The Role of Phosphoinositides in Membrane Transport.” *Current Opinion in Cell Biology* 13 (4): 485–92. http://www.ncbi.nlm.nih.gov/pubmed/11454456.

Smith, William James, Nicolas Nassar, Anthony Bretscher, Richard a. Cerione, and P. Andrew Karplus. 2003. “Structure of the Active N-Terminal Domain of Ezrin: Conformational and Mobility Changes Identify Keystone Interactions.” *Journal of Biological Chemistry* 278 (7): 4949–56. doi:10.1074/jbc.M210601200.

Snapp, Erik L, and Ramanujan S Hegde. 2006. “Rational Design and Evaluation of FRET Experiments to Measure Protein Proximities in Cells.” *Current Protocols in Cell Biology / Editorial Board, Juan S. Bonifacino ... [et Al.]* Chapter 17 (October): Unit 17.9. doi:10.1002/0471143030.cb1709s32.

Spertini, Caroline, Bénédicte Baïsse, and Olivier Spertini. 2012. “Ezrin-Radixin-Moesin-Binding Sequence of PSGL-1 Glycoprotein Regulates Leukocyte Rolling on Selectins and Activation of Extracellular Signal-Regulated Kinases.” *The Journal of Biological Chemistry* 287 (13): 10693–702. doi:10.1074/jbc.M111.318022.

Srivastava, J, B E Elliott, D Louvard, and M Arpin. 2005. “Src-Dependent Ezrin Phosphorylation in Adhesion-Mediated Signaling.” *Molecular Biology of the Cell* 16 (3): 1481–90. doi:10.1091/mbc.E04-08-0721.

Stephan, Milena, Corinna Kramer, Claudia Steinem, and Andreas Janshoff. 2014. “Binding Assay for Low Molecular Weight Analytes Based on Reflectometry of Absorbing Molecules in Porous Substrates.” *The Analyst* 139 (8): 1987–92. doi:10.1039/c4an00009a.

Takeuchi, K, a Kawashima, a Nagafuchi, and S Tsukita. 1994. “Structural Diversity of Band 4.1 Superfamily Members.” *Journal of Cell Science* 107 (Pt 7: 1921–28.

Takeuchi, Kosei, Naruki Sato, Hideko Kasahara, Noriko Funayama, Akira Nagafuchi, Shigenobu Yonemura, Sachiko Tsukita, and Shoichiro Tsukita. 1994. “Perturbation of Cell Adhesion and Microvilli Formation by Antisense Oligonucleotides to ERM Family Members.” *Journal of Cell Biology* 125 (6): 1371–84. doi:10.1083/jcb.125.6.1371.

Tall, E G, I Spector, S N Pentyala, I Bitter, and M J Rebecchi. 2000. “Dynamics of Phosphatidylinositol 4,5-Bisphosphate in Actin-Rich Structures.” *Current Biology : CB* 10 (12): 743–46. http://www.ncbi.nlm.nih.gov/pubmed/10873804.

Tamura, Atsushi, Shojiro Kikuchi, Masaki Hata, Tatsuya Katsuno, Takeshi Matsui, Hisayoshi Hayashi, Yuichi Suzuki, Tetsuo Noda, Shoichiro Tsukita, and Sachiko Tsukita. 2005. “Achlorhydria by Ezrin Knockdown: Defects in the Formation/expansion of Apical Canaliculi in Gastric Parietal Cells.” *The Journal of Cell Biology* 169 (1): 21–28. doi:10.1083/jcb.200410083.

Tsukita, S, and Y Hieda. 1989. “A New 82-kD Barbed End-Capping Protein (radixin) Localized in the Cell-to-Cell Adherens Junction: Purification and Characterization.” *The Journal of Cell Biology* 108 (6): 2369–82. http://www.pubmedcentral.nih.gov/articlerender.fcgi?artid=2115614&tool=pmcentrez&rendertype=abstract.

Turunen, O, T Wahlström, and A Vaheri. 1994. “Ezrin Has a COOH-Terminal Actin-Binding Site That Is Conserved in the Ezrin Protein Family.” *The Journal of Cell Biology* 126 (6): 1445–53. http://www.pubmedcentral.nih.gov/articlerender.fcgi?artid=2290954&tool=pmcentrez&rendertype=abstract.

Van den Ent, Fusinita, and Jan Löwe. 2006. “RF Cloning: A Restriction-Free Method for Inserting Target Genes into Plasmids.” *Journal of Biochemical and Biophysical Methods* 67 (1): 67–74. doi:10.1016/j.jbbm.2005.12.008.

Van Fürden, Daniela, Kevin Johnson, Christoph Segbert, and Olaf Bossinger. 2004. "The C. Elegans Ezrin-Radixin-Moesin Protein ERM-1 Is Necessary for Apical Junction Remodelling and Tubulogenesis in the Intestine." *Developmental Biology* 272 (1): 262–76. doi:10.1016/j.ydbio.2004.05.012.

Vanhaesebroeck, B, S J Leevers, K Ahmadi, J Timms, R Katso, P C Driscoll, R Woscholski, P J Parker, and M D Waterfield. 2001. "Synthesis and Function of 3-Phosphorylated Inositol Lipids." *Annual Review of Biochemistry* 70 (January): 535–602. doi:10.1146/annurev.biochem.70.1.535.

Viswanatha, Raghuvir, Patrice Y Ohouo, Marcus B Smolka, and Anthony Bretscher. 2012. "Local Phosphocycling Mediated by LOK/SLK Restricts Ezrin Function to the Apical Aspect of Epithelial Cells." *The Journal of Cell Biology* 199 (6): 969–84. doi:10.1083/jcb.201207047.

Viswanatha, Raghuvir, Jessica Wayt, Patrice Y. Ohouo, Marcus B. Smolka, and Anthony Bretscher. 2013. "Interactome Analysis Reveals Ezrin Can Adopt Multiple Conformational States." *The Journal of Biological Chemistry* 288 (49): 35437–51. doi:10.1074/jbc.M113.505669.

Yan, H, K Krishnan, J T Lim, L G Contillo, and J J Krolewski. 1996. "Molecular Characterization of an Alpha Interferon Receptor 1 Subunit (IFNaR1) Domain Required for TYK2 Binding and Signal Transduction." *Molecular and Cellular Biology* 16 (5): 2074–82. http://www.pubmedcentral.nih.gov/articlerender.fcgi?artid=231194&tool=pmcentrez&rendertype=abstract.

Yao, Xuebiao, Leon Cheng, John G Forte, and J G Mol Biol Cell. 1996. "Biochemical Characterization of Ezrin-Actin Interaction *" 271 (12): 7224–29.

Yonemura, S, M Hirao, Y Doi, N Takahashi, T Kondo, and S Tsukita. 1998. "Ezrin/radixin/moesin (ERM) Proteins Bind to a Positively Charged Amino Acid Cluster in the Juxta-Membrane Cytoplasmic Domain of CD44, CD43, and ICAM-2." *The Journal of Cell Biology* 140 (4): 885–95. http://www.pubmedcentral.nih.gov/articlerender.fcgi?artid=2141743&tool=pmcentrez&rendertype=abstract.

Yonemura, S, and S Tsukita. 1999. "Direct Involvement of Ezrin/radixin/moesin (ERM)-Binding Membrane Proteins in the Organization of Microvilli in Collaboration with Activated ERM Proteins." *The Journal of Cell Biology* 145 (7): 1497–1509. http://www.pubmedcentral.nih.gov/articlerender.fcgi?artid=2133160&tool=pmcentrez&rendertype=abstract.

Yonemura, Shigenobu, Takeshi Matsui, Shoichiro Tsukita, and Sachiko Tsukita. 2002. "Rho-Dependent and -Independent Activation Mechanisms of Ezrin/radixin/moesin Proteins: An Essential Role for Polyphosphoinositides in Vivo." *Journal of Cell Science* 115 (Pt 12): 2569–80. http://www.ncbi.nlm.nih.gov/pubmed/12045227.

Yu, J, D A Fischman, and T L Steck. 1973. "Selective Solubilization of Proteins and Phospholipids from Red Blood Cell Membranes by Nonionic Detergents." *Journal of Supramolecular Structure* 1 (3): 233–48. doi:10.1002/jss.400010308.

Zhu, Lixin, Yuechueng Liu, and John G Forte. 2005. "Ezrin Oligomers Are the Membrane-Bound Dormant Form in Gastric Parietal Cells." *American Journal of Physiology. Cell Physiology* 288 (6): C1242–54. doi:10.1152/ajpcell.00521.2004.

Zhu, Lixin, Rihong Zhou, Shelley Mettler, Tim Wu, Aennes Abbas, Joseph Delaney, and John G Forte. 2007. "High Turnover of Ezrin T567 Phosphorylation: Conformation, Activity, and Cellular Function." *American Journal of Physiology. Cell Physiology* 293 (3): C874–84. doi:10.1152/ajpcell.00111.2007.

Supplemental materials

S1. Absorbtion spectra of ezrin fluorescent constructs

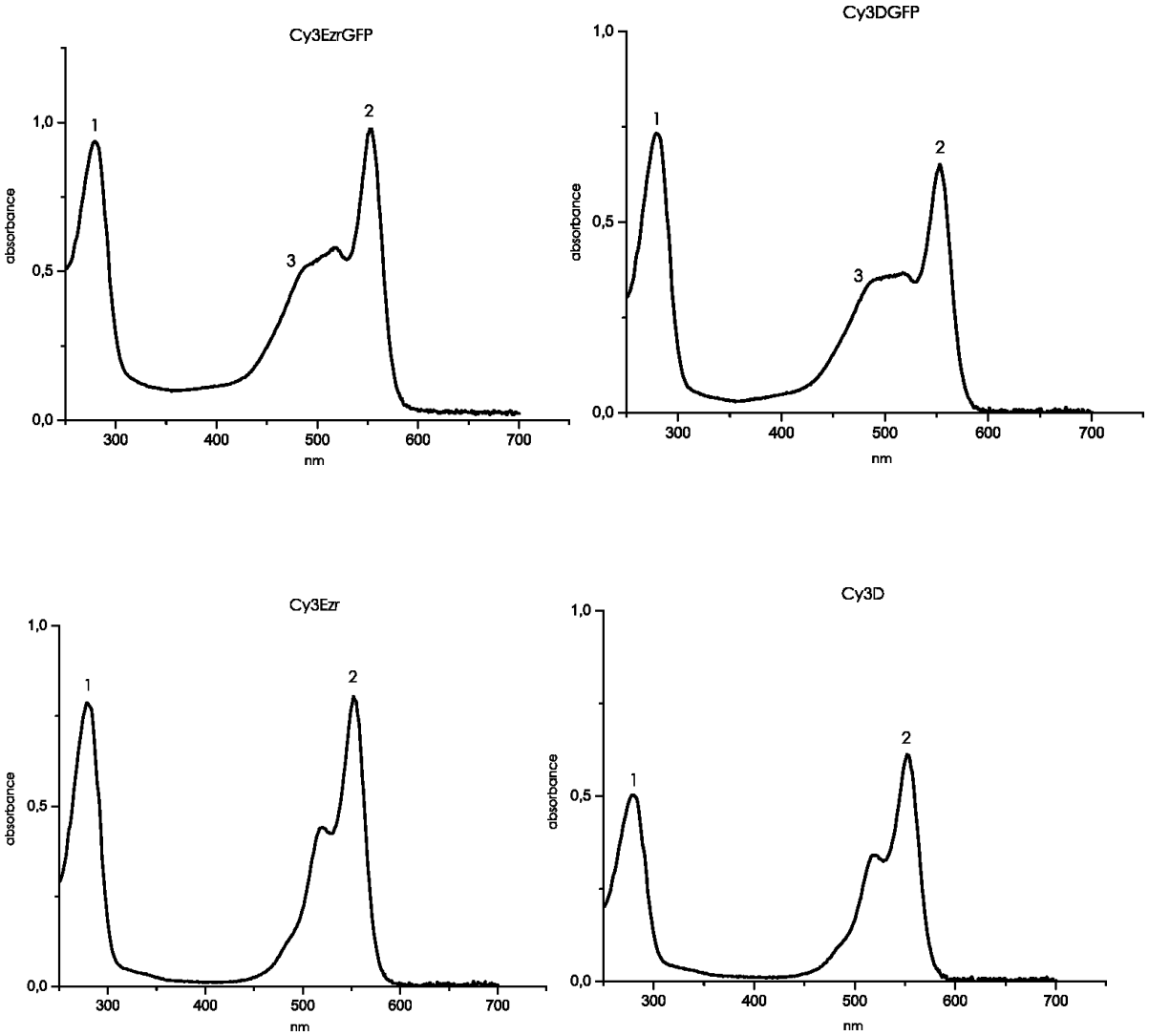

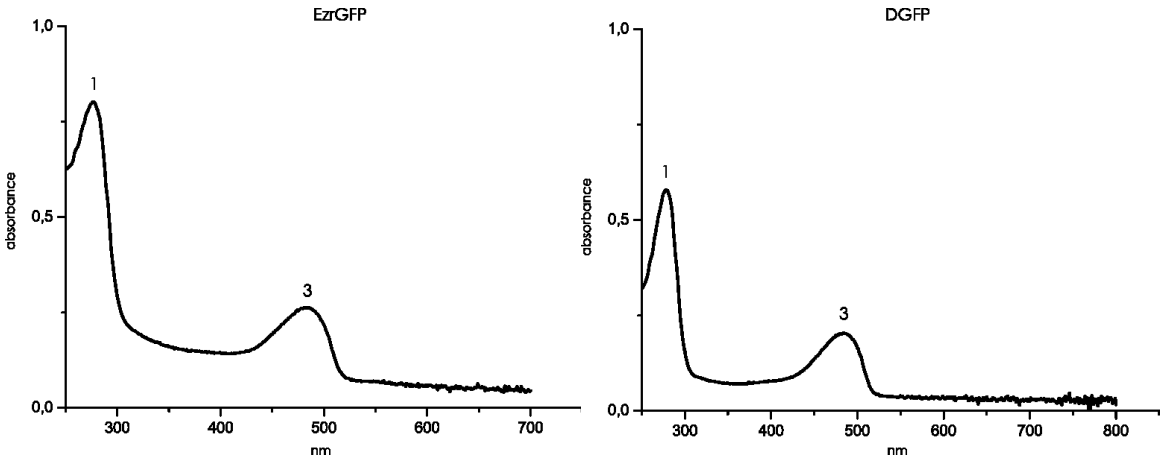

Fig. S1. Absorption spectra of Cy3EzrGFP, Cy3DGFP, Cy3Ezr, Cy3D and EzrGFP, DGFP. 1 – maximum absorption peak of aromatic amino acids of the proteins at 280 nm, 2 – maximum absorption peak of Cy3 dye at 550 nm, 3 – maximum absorption peak of eGFP at 488 nm. The spectra were read using spectrophotometer UV-visible 50scan Varian.

S2. Fluorescent images of acceptor bleaching FRET

Fig S2A. Acceptor bleaching FRET of the proteins bound to SSLB containing 8mol% receptor lipids. Circled area 1 is ROI (region of interest) after Cy3 bleaching, circled area 2 is reference area. The diagram depicts the increase of eGFP fluorescence (green line) and the decrease of Cy3 fluorescence (red line), numbers 1 and 2 correspond to ROI and reference area, respectively. The marks at the X axis indicate the start-time and the end-time of the bleach. The brighter spots most likely represent aggregates of the protein. ROI avoiding such spots were chosen. Scale bare = 5 µM.

Cy3EzrGFP bound to SSLB containing 8mol% DOGS-Ni-NTA

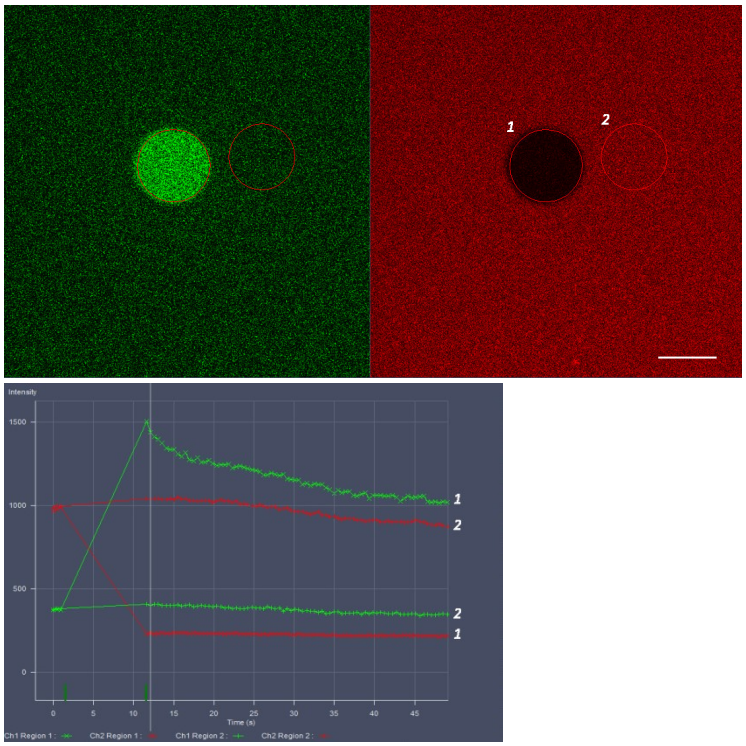

Cy3EzrGFP bound to SSLB containing 8mol% PIP_2

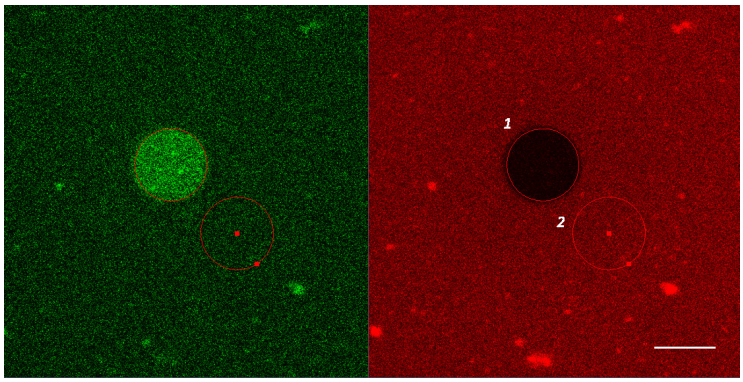

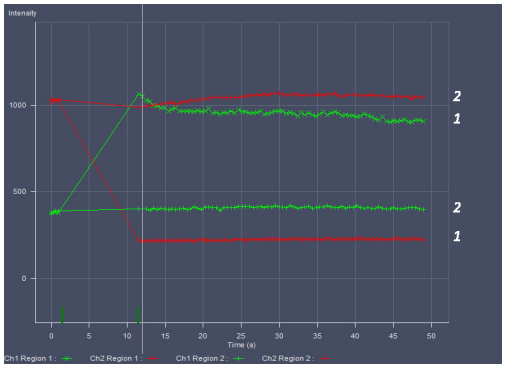

Cy3DGFP bound to SSLB containing 8mol% DOGS-Ni-NTA

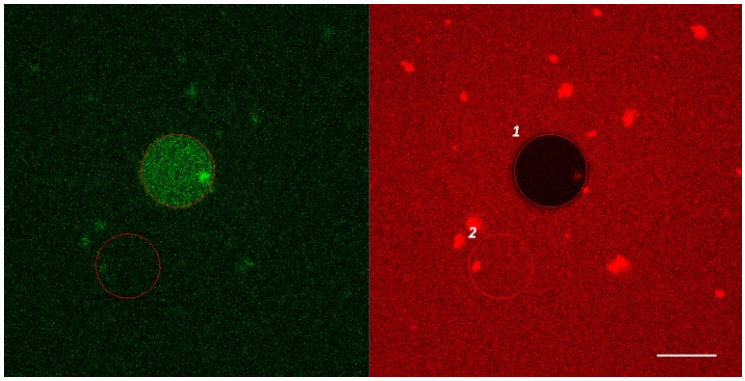

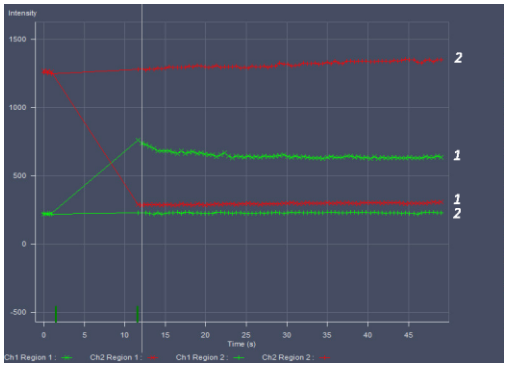

Cy3DGFP bound to SSLB containing 8mol% PIP_2

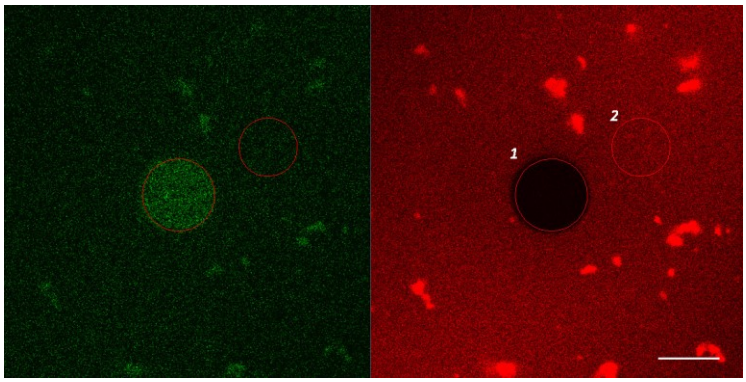

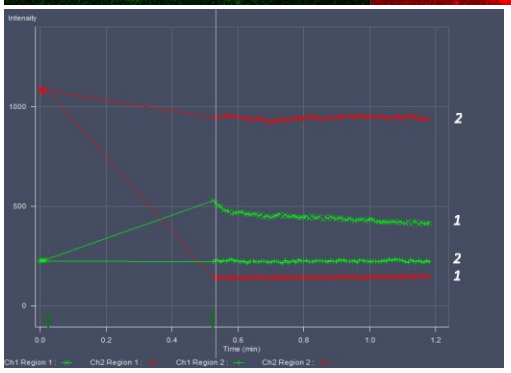

Cy3Ezr+EzrGFP bound to SSLB containing 8mol% DOGS-Ni-NTA

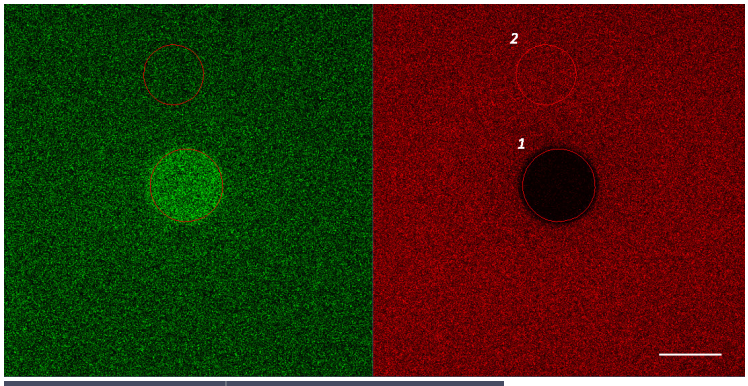

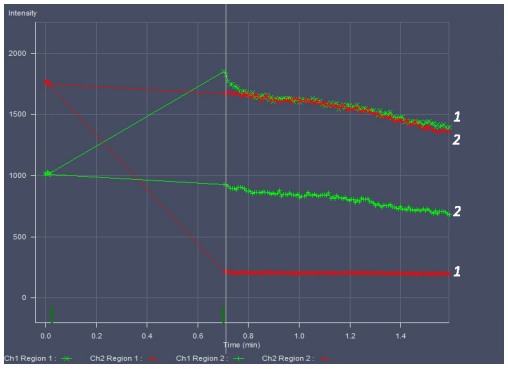

Cy3Ezr+EzrGFP bound to SSLB containing 8mol% PIP_2

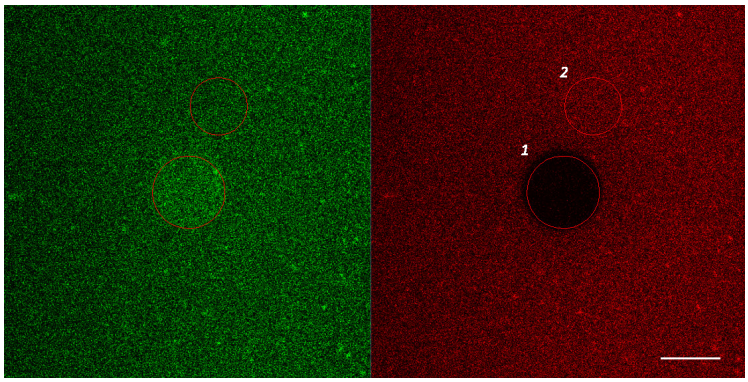

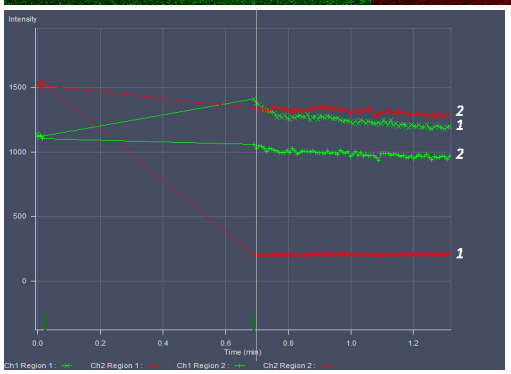

Cy3D+DGFP bound to SSLB containing 8mol% DOGS-Ni-NTA

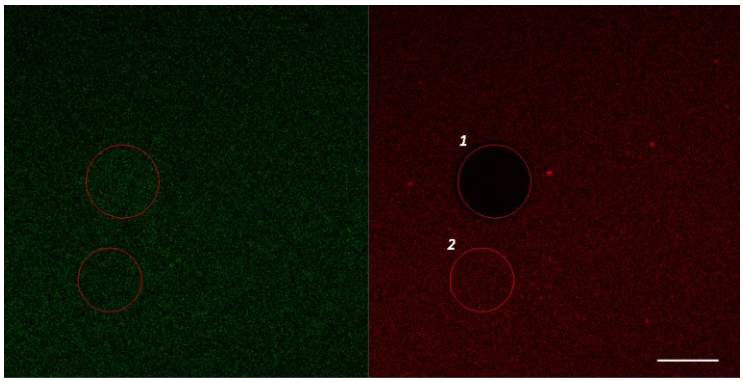

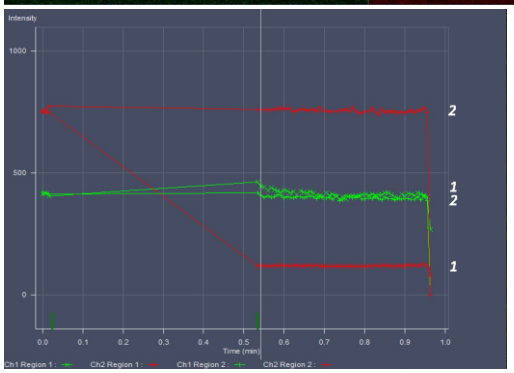

Cy3D+DGFP bound to SSLB containing 8mol% PIP_2

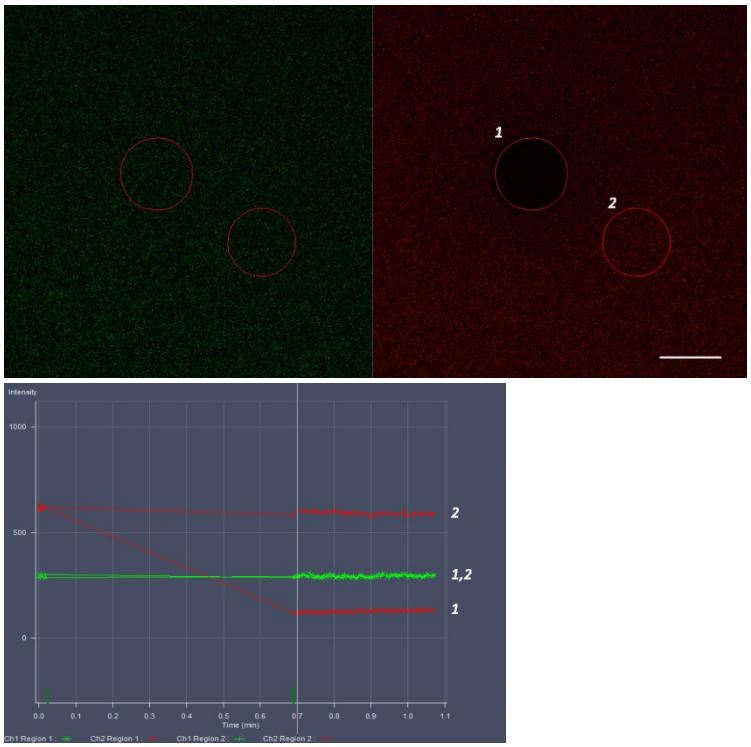

Fig S2A. Acceptor bleaching FRET of the proteins bound to SSLB containing 8mol% receptor lipids. Circled area 1 is ROI (region of interest) after Cy3 bleaching, circled area 2 is reference area. The diagram depicts the increase of eGFP fluorescence (green line) and the decrease of Cy3 fluorescence (red line), numbers 1 and 2 correspond to ROI and reference area, respectively. The marks at the X axis indicate the start-time and the end-time of the bleach. The brighter spots most likely represent aggregates of the protein. ROI avoiding such spots were chosen. Scale bare = 5 μM.

Next:

Fig S2B. Acceptor bleaching FRET of the proteins bound to SSLB containing 4mol% receptor lipids. Circled area 1 is ROI (region of interest) after Cy3 bleaching, circled area 2 is reference area. The diagram depicts the increase of eGFP fluorescence (green line) and the decrease of Cy3 fluorescence (red line), numbers 1 and 2 correspond to ROI and reference area, respectively. The marks at the X axis indicate the start-time and the end-time of the bleach. The brighter spots most likely represent aggregates of the protein. ROI avoiding such spots were chosen. Scale bare = 5 μM.

Cy3EzrGFP bound to SSLB containing 4mol% DOGS-Ni-NTA

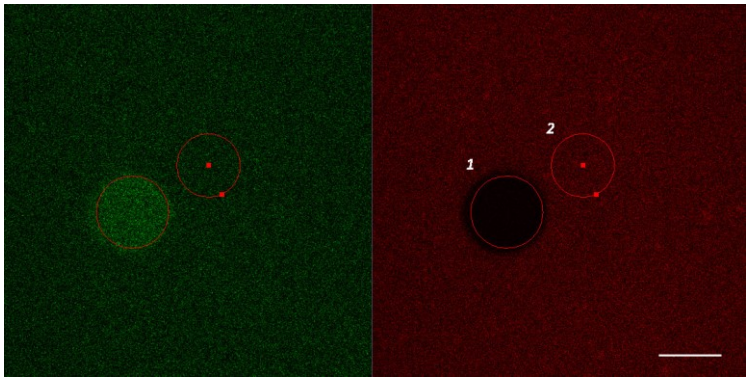

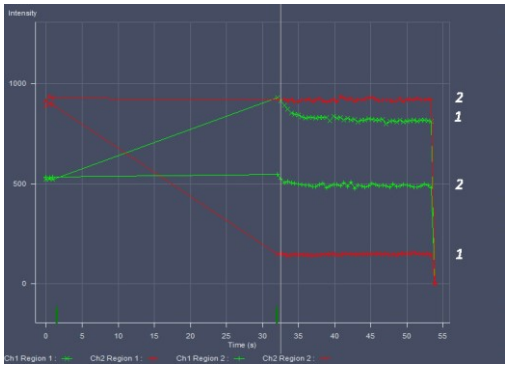

Cy3EzrGFP bound to SSLB containing 4mol% PIP_2

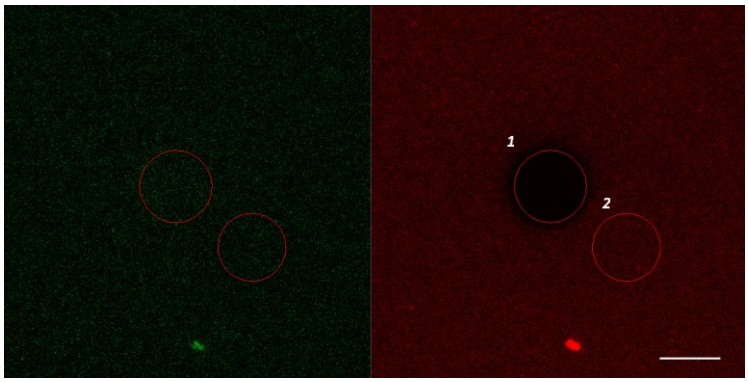

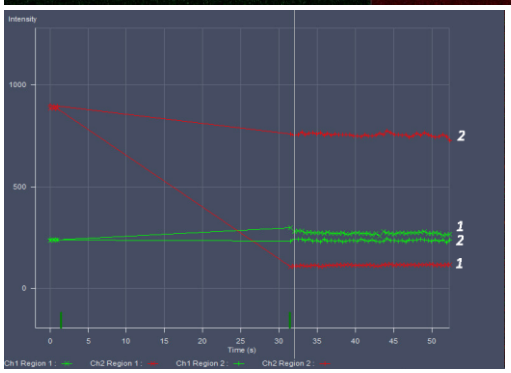

Cy3DGFP bound to SSLB containing 4mol% DOGS-Ni-NTA

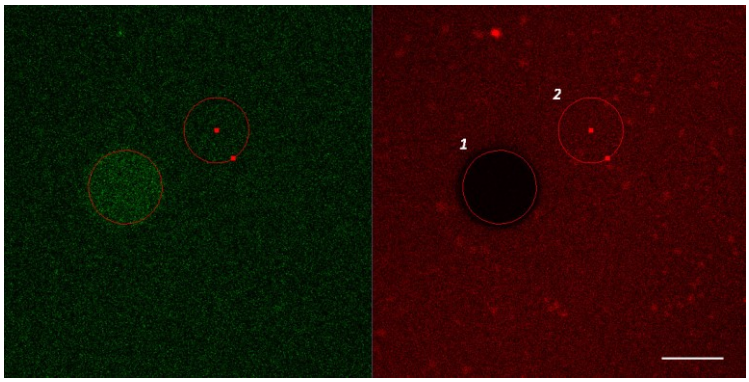

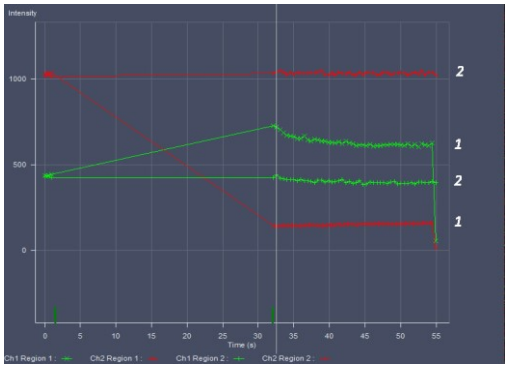

Cy3DGFP bound to SSLB containing 4mol% PIP_2

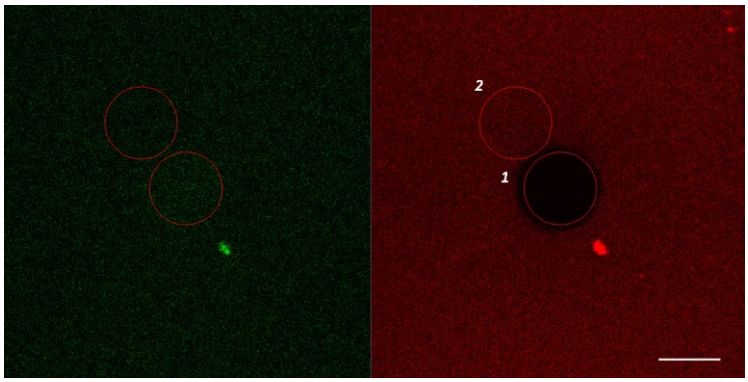

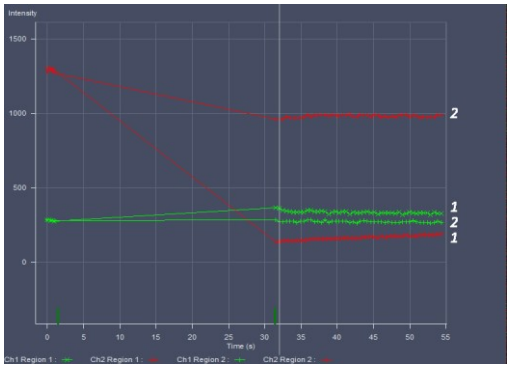

Cy3Ezr+EzrGFP bound to SSLB containing 4mol% DOGS-Ni-NTA

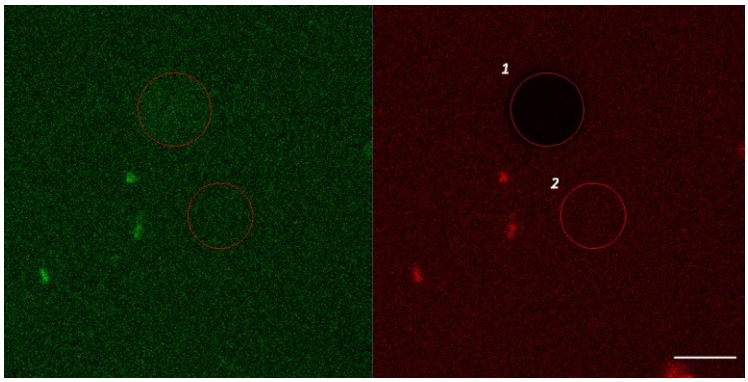

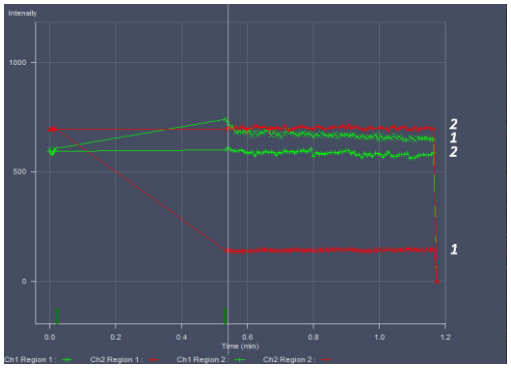

Cy3Ezr+EzrGFP bound to SSLB containing 4mol% PIP_2

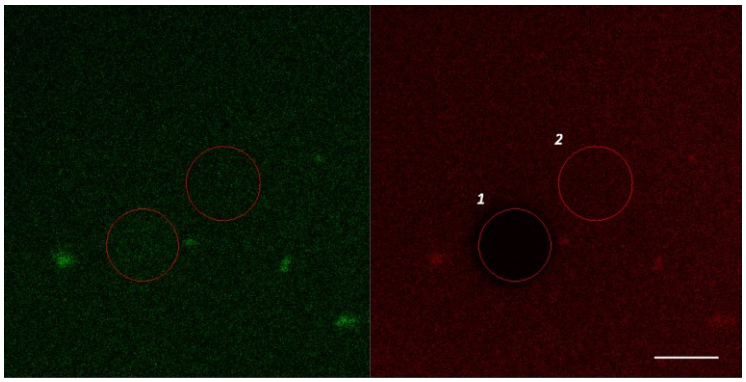

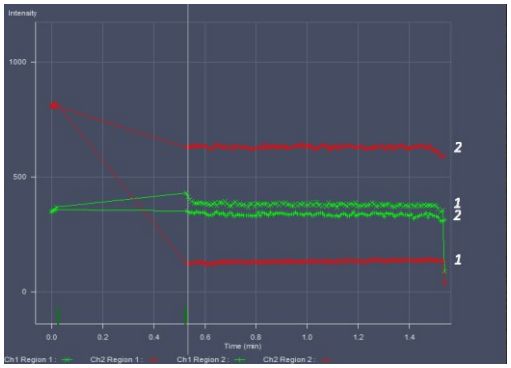

Cy3D+DGFP bound to SSLB containing 4mol% DOGS-Ni-NTA

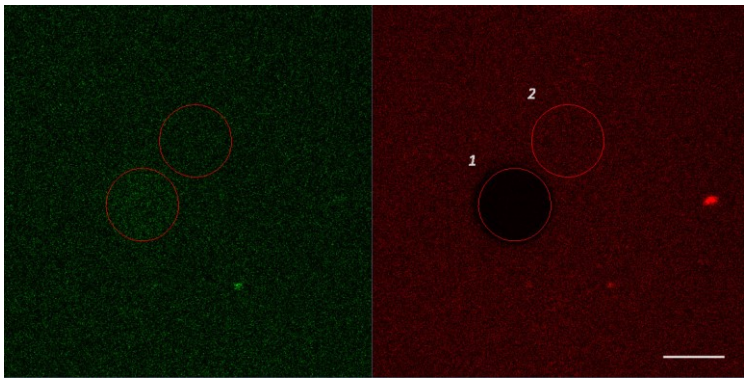

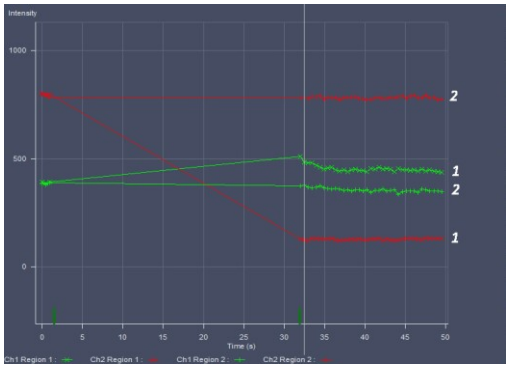

Cy3D+DGFP bound to SSLB containing 4mol% PIP_2

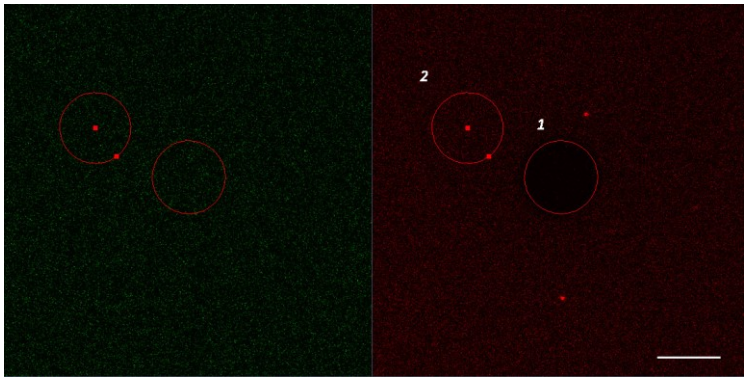

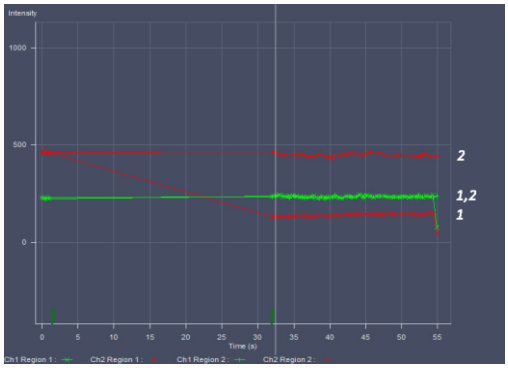

Fig S2B. Acceptor bleaching FRET of the proteins bound to SSLB containing 4mol% receptor lipids. Circled area 1 is ROI (region of interest) after Cy3 bleaching, circled area 2 is reference area. The diagram depicts the increase of eGFP

fluorescence (green line) and the decrease of Cy3 fluorescence (red line), numbers 1 and 2 correspond to ROI and reference area, respectively. The marks at the X axis indicate the start-time and the end-time of the bleach. The brighter spots most likely represent aggregates of the protein. ROI avoiding such spots were chosen. Scale bare = 5 μM.

S3. Plasmid maps **(next)**

S3. Plasmid maps

pE-ezrin-CFP(N1)

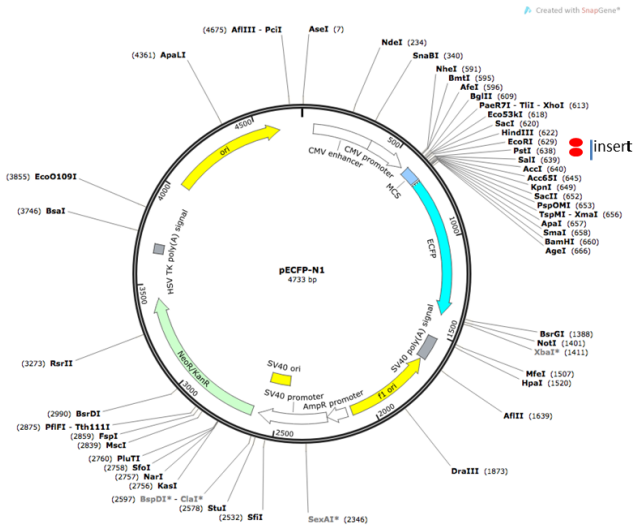

Vector name pE-ezrin-CFP(n1)
Plasmid type pECFP-N1
Exact description of the insert
-hunam ezrin wt (1759bp)
-EcoR1/Sal1 cut ezrin cDNA fragment was integrated into EcoR1/Sal1 linearized pECFP-N1 plasmid
Host bacteria E.coli
Size of the construct 6490 bp

ezrin

G CTA GCG CTA CCG GAC TCA GAT CTC GAG CTC AAG CTT CGA ATT Ct ***ATGCCG……CCCTGTt*** G TCG ACG

Nhe I Eco47 III Bgl II Xho I Sac I Ec/136 II Hind III EcoR I Sal I

GTA CCG CGG GCC CGG GAT CCA CCG GTG GCC ACC ***ATGGTG***

Kpn I Asp718 I Sac II Apa I Bsp120 I Xma I Sma I BamH I Age I ECFP

pE-his-YFP(C1)-ezrinCFP(N1)

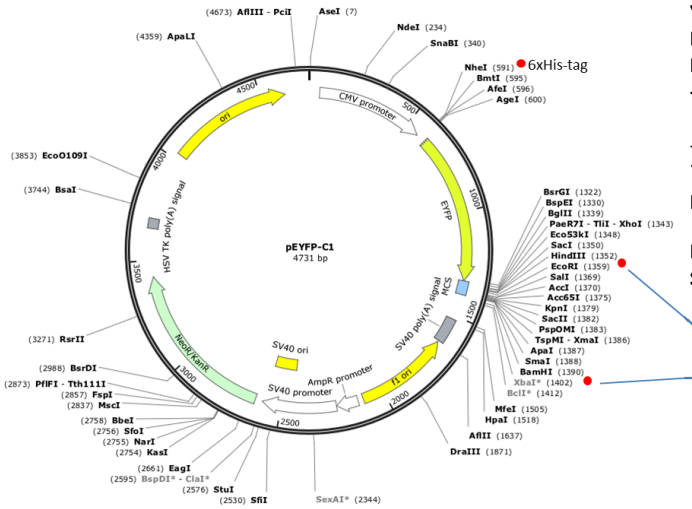

Vector name pE-his-YFP(C1)-ezrinCFP(N1)
Plasmid type pEYFP-C1
Exact description of the insert
-hunam ezrin wt (1759bp) +CFP (710bp) from E.victoria
- 1.EcoR1/Xba1 cut ezrin-CFP cDNA fragment was integrated into EcoR1/Xba1 linearized pEYFP-C1 plasmid. 2.via PCR 6xHis-tag was introduced after Nhe1, before YFP sequence
Host bacteria E.coli
Size of the construct 7244 bp

6xHis-tag region ezrin

GATCC GCTAGC GGAGCCGCC **ATG** CATCATCATCATCATCAT GGAGGA **GTGAGCAAGGGCG**…

Nhe1 6xHis codones

EYFP ezrin

TACAAG TCC GGA CTC AGA TCT CGA GCT CAA GCT TCG AAT TC **tATGCCG**…*-SalI-ECFP*…

ECFP BspEI BglII XhoI SacI Ec/136II HindIII EcoRI

CGCGAC TCT AGA TAA CTG ATC A

XbaI BclI

pET28a(+)ezrin-GFP

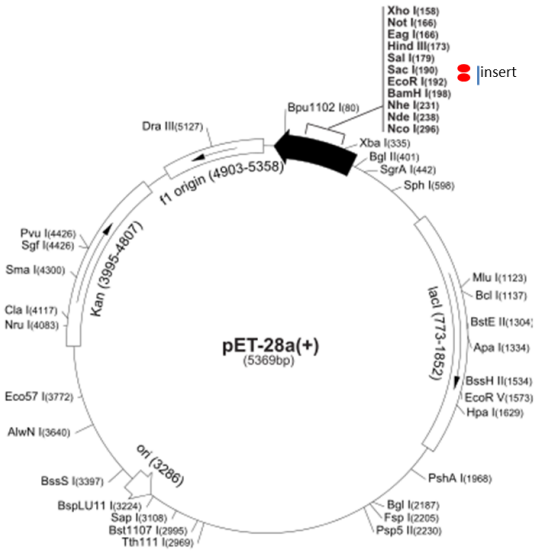

Vector name pET28a(+)ezrinGFP
Plasmid type pET28a(+)
Exact description of the insert
-hunam ezrin wt (1759 bp)
-eGFP from pET24a(+)eGFP plasmid (693 bp)
-eGFP cDNA fragment was integrated in pET28a(+)ezrin plasmid (M. Koltzscher, ezrin was integrated between EcoRI and SalI) by restriction free cloning
Host bacteria E.coli
Size of the construct 7836 bp

Forward cloning primer

ezrin → eGFP →

*GGATCCGAATTC*ATGCCG....TTCGAGGCCCTGTtAAAGCTTGCGGATGGGTCG*GGATCC*AGTAAAGGAGA....

BamH I EcoR I BamH I

GCTGCTGGGGTTACACATGGCTAA*GTCGAC*AAGCTTGCGGCCGCACTCG

Sal I

Reverse cloning primer

pET28a(+)ezrinT567D-GFP

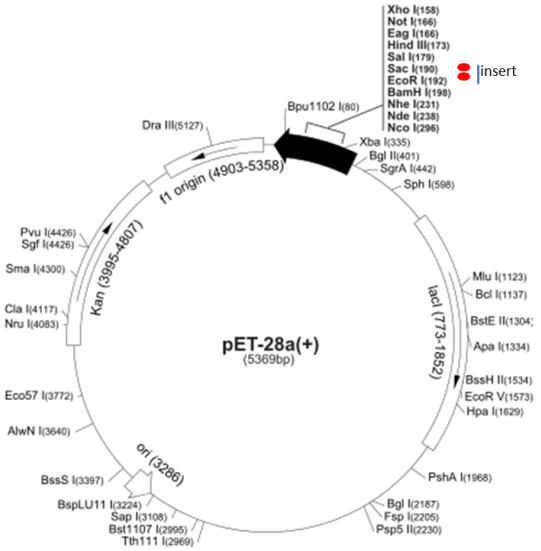

Vector name pET28a(+)ezrinT567D-GFP
Plasmid type pET28a(+)
Exact description of the insert
-hunam ezrinT567D (1759 bp)
-eGFP from pET24a(+)eGFP plasmid (693 bp)
-eGFP cDNA fragment was integrated in pET28a(+)ezrinT567D plasmid (J. Austermann, ezrin insert is between EcoRI and SalI) by restriction free cloning
Host bacteria E.coli
Size of the construct 7836 bp

Forward cloning primer

ezrinT567D → eGFP →

*GGATCCGAATTC*ATGCCG....TTCGAGGCCCTGTtAAAGCTTGCGGATGGGTCG*GGATCC*AGTAAAGGAGA....

BamH I EcoR I BamH I

GCTGCTGGGGTTACACATGGCTAA*GTCGAC*AAGCTTGCGGCCGCACTCG

Sal I

Reverse cloning primer

Abbreviations

A	Ampere
AB	Antibody
ABS	Actin binding site
AFM	Atomic force microscopy
APC	Antigen presenting cell
AU	Arbitrary unit
Ca^{2+}	Calcium ion
C-ERMAD	C-terminal ERM association domain
CLSM	Confocal laser scanning microscopy
C-N association	Association between C-terminus and N-terminus of a protein
Cy3EzrGFP	Cy3 crosslinked EzrGFP
Cy3DGFP	Cy3 crosslinked DGFP
ddH2O	Double-destilled H2O (Millipore filtered and autoclaved)
DGFP	EzrinT567D-eGFP, phosphomimicking ezrin mutant T567D fused with C-terminal eGFP
DOGS-NTA-Ni	1,2-dioleoyl-*sn*-glycero-3-[(N-(5-amino-1-carboxypentyl)iminodiacetic acid)succinyl] Ni salt
DOPC	1,2-dioleoyl-*sn*-glycero-3-phosphocholine
e.g.	Exempli gratia (for example)
EGF	Epidermal growth factor
eGFP	Enhanced green fluorescent protein
ERM	Ezrin, radixin, moesin protein group
EzrGFP	Ezrin fused with C-terminal eGFP
EzrinT567D	Ezrin phosphomimicking mutant
Ezrin-wt	Wild type ezrin
F-actin	Filamentous actin
FERM	Four-point-one-ERM
FLIM	Fluorescence-lifetime imaging microscopy
FRAP	Fluorescence recovery after photobleaching
FRET	Förster resonance energy transfer
G418	Geneticin, antibiotic
h	hour

IF	Immunofluorescence
IS	Immunological synapse
kDa	kilo Dalton
LSM	Laser scanning microscope
m	milli (thousandths)
M	molar
min	minute
n	nano (billionth)
N-ERMAD	N-terminal ERM association domain
OD	Optical density
PH domain	Pleckstrin homology domain
PI	Phosphatidylinositol
PIP_2	Phosphatidylinositol-4,5-bisphosphate
POPC	1-Palmitoyl-2-oleoyl-sn-glycero-3-phosphocholine
QCM	Quartz crystal microbalance
RIfS	Reflectometric interference spectroscopy
rpm	Rounds per minute
RT	Room temperature
SDS-PAGE	Sodium dodecyl sulfate polyacrylamide gel electrophoresis
SE	Standard error (statistics)
SSLB	Solid supported lipid bilayers
T567A	Ezrin unphosphorylatable mutant
T567D, T567E	Ezrin phosphomimicking muatnts
TCR	T cell receptor
tRNA	Transfer ribonucleic acid
UV	Ultraviolet light
UV-vis	Ultraviolet-visible
V	Volt
YFPEzrCFP	Ezrin fused with N-terminal eYFP and C-terminal eCFP
µ	micro (millionth)
°C	Degree Celsius

Acknowledgements

I would like to thank my advisor Prof. Dr. Volker Gerke for the leading me through the project, teaching about scientific reserach and for patiently pointing to my mistakes and helping to correct them. I also would like to thank Prof. Dr. Claudia Steinem for the advices and discussions during the experimental work at her laboratory.
Working in the friendly and kind atmosphere of my group was a happy experience. And, of course, I thank my collegues in Münster for the help in the lab-work and for many advices. I appreciate the assistance of the collegues from the Institue of Biomolecular Chemistry, University of Göttingen, especially Julia Braunger and Corinna Kramer.
The big Danke to Dr. Randy Benedict for the writing corrections.
I am gratefull for the opportunity to conduct my thesis work in the Münster scientific society to CiM IMPRS Graduate Program and Prof.Dr. Martin Wild for the administrative help and his kind support to the students from the Graduate Program.
And I thank my familiy and my dear Münster friends for being with me.